Signaling mechanisms modulating neuron-glia interactions following axonal injury

By

Petra Richer

A DISSERTATION

Presented to the Neuroscience Graduate Program

and the Oregon Health & Science University

School of Medicine

In partial fulfillment of the requirements for the degree of

Doctor of Philosophy

February 16, 2022

TABLE OF CONTENTS

LIST OF FIGURES

Chapter 1: Introduction

Chapter 2: Examining the role of neuronal DCV release in the glial injury response

Chapter 3: FLARIM v2.0, an adapted method to quantify transcript-interactions *in vivo* in the adult *Drosophila* brain

Chapter 4: Discussion & Future Directions

Appendix

LIST OF ABBREVIATIONS

Aß: amyloid-beta

AD: Alzheimer's disease

AL: antennal lobe

ALS: amyotrophic lateral sclerosis

ANF: atrial natriuretic factor

AP-1: activator protein 1

ATP: adenosine triphosphate

BBB: blood-brain barrier

BDNF: brain-derived neurotrophic factor

ß-gal or beta-gal: beta galactosidase

Brp: bruchpilot

C1q: complement component 1q

Ca^{2+}: calcium

Caps: calcium-activated protein for secretion

CNS: central nervous system

DCR-2: dicer 2

DCV: dense core vesicle

Dilp: *Drosophila* insulin-like peptide

dnInR: dominant negative insulin receptor

Dpe: days post-eclosion

Dpi: days post-injury

Drpr: draper

ECM: extracellular matrix

ER: endoplasmic reticulum

FAP: fluorogen activating protein

FGF: fibroblast growth factor

FISH: fluorescence *in situ* hybridization

FLARIM: fluorescence assay to detect ribosome interactions with mRNA

FUS: fused in sarcoma

GA: Golgi apparatus

GFAP: glial fibrillary acidic protein

GFP: green fluorescent protein

GPCR: G-protein coupled receptor

GRASP: GFP reconstitution across synaptic partners

HCR: hybridization chain reaction

HD: Huntington's disease

HL-3: hemolymph-like HL3 saline

Hpi: hours post-injury

HRP: horseradish peroxidase

Htt: Huntingtin

Ilp: insulin-like peptide

ILS: insulin-like signaling

InR: insulin receptor

JAK: janus kinase

JNK: c-Jun N-terminal kinase

K: potassium

KO: knock out

L1: longitudinal vein 1

lncRNA: long non-coding RNA

LSM: laser scanning microscope

MARCM: mosaic analysis with repressible cell marker

Mbp: myelin basic protein

MEGF10: multiple EGF-like domains 10

MERTK: MER proto-oncogene tyrosine kinase

MG: malachite green

Mito: mitochondria

MIP: maximum intensity projection

miRNA: micro RNA

Mmp: matrix metalloproteinase

Mpi: minutes post-injury

Mps: minutes post-stimulation

mRNA: messenger RNA

MS: multiple sclerosis

mTOR: mammalian target of rapamycin

NA: numerical aperture

NAD+: nicotinamide adenine dinucleotide

ncRNA: non-coding RNA

NGF: nerve growth factor

NLS: nuclear localization signal

NMDA: N-methyl D-aspartate

NMJ: neuromuscular junction

Nmnat: nicotinamide mononucleotide adenylyltransferase

NPY: neuropeptide Y

NT: neurotransmitter

OPC: oligodendrocyte precursor cell

oPool: oligo Pool

ORN: olfactory receptor neuron

PBS: phosphate buffered saline

PC2: proprotein convertase 2

PCR: polymerase chain reaction

PD: Parkinson’s disease

PFA: paraformaldehyde

PG: perineurial glia

PI3K: phosphatidylinositol-3-kinase

PNS: peripheral nervous system

polyQ: polyglutamine

PtdSer: phosphatidyl serine

qPCR: quantitative PCR

RNAi: RNA interference

RNAseq: RNA sequencing

ROI: region of interest

rRNA: ribosomal RNA

RT: room temperature

S6K: ribosomal protein p-70-S6

Sarm: sterile alpha and armadillo motif

Shark: SH2 ankyrin repeat kinase

SIM: structured illumination microscopy

smFISH: single molecule FISH

smiFISH: single molecule inexpensive FISH

SNARE: soluble N-ethylmaleimide-sensitive factor attachment protein receptor

snoRNA: small nucleolar RNA

SPG: subperineurial glia

spGFP: split GFP

SSC: saline sodium citrate

STAT: signal transducer and activator of transcription

SV: synaptic vesicle

TBI: traumatic brain injury

TDP-43: TAR DNA binding protein 43

TeTXLC: tetanus toxin light chain

TGF-ß: transforming growth factor beta

TGN: trans Golgi network

TOR: target of rapamycin

TRAP: translating ribosome affinity purification

TREM2: triggering receptor expressed on myeloid cells 2

ts: temperature sensitive

tub-Gal80: tubulin Gal80

TX: Triton X-100

UAS: upstream activation sequence

UTR: untranslated region

VNC: ventral nerve cord

WD: Wallerian degeneration

Wlds: Wallerian degeneration slow

WT: wild type

ACKNOWLEDGEMENTS

This work would not have been possible without the mentorship and guidance of my advisor, Mary Logan. Inside and outside of the lab, Mary has been extremely supportive and has helped me develop as an independent researcher. I am also grateful for the mentorship I have received from Sean Speese. The scientific and technical discussions over the years have been invaluable. Also, many thanks to Mary and Sean for sharing dog pictures and stories back and forth over the years.

I extend my gratitude to members of the Logan and Speese labs, past and present: Jolanda Muenzel, Arpita Ray, Brian Jenkins, Matt Boisvert, and Cole Brashaw, who have been wonderful colleagues to work with in lab and have taught me so much. I also want to thank my dissertation committee: Kelly Monk, Anusha Mishra, Ian Martin, and Philip Copenhaver for their helpful insight, expertise, and willingness to troubleshoot difficult aspects of my project – even lending a helping hand with experiments. Their comments and guidance in committee meetings and seminars have contributed greatly to the progression of this work. I would also like the thank the members of the Neuroscience Graduate Program, the Jungers Center for Neurosciences Research, the Advanced Light Microscopy Core, and Jessica Parks for their help and support.

The journey to graduate school would not have been possible without the help I have received from Tony Gooch and Florence Davis through the Klein Family Scholarship. To get the chance to complete my undergraduate studies in the United States has been a life changing experience and I am eternally grateful for the opportunity.

I would like to thank my parents, Andrea and László, my brother, Márk, and my grandparents for their love and encouragement during graduate school. They have always patiently listened to presentations, stories about failed experiments, and my excitement about science. I also owe my deepest gratitude to my Chinese family (the Xus) and my Florida family (the Morans) for their kindness and for giving me a home away from home, and for my friends for

keeping me sane and laughing through this journey. Finally, I want to thank Shane Xu, whose humor, support, and love has made graduate school, and life outside of it, really wonderful.

This work was supported by National Institutes of Health grants (R21 NS084112, R21 NS107771, and R01 NS117934), the Ken and Ginger Term Professor Award (M.A.L.), and the Tartar Trust Fellowship at Oregon Health and Sciences University (P.R.).

ABSTRACT

Glial cells perform paramount functions within the nervous system, closely monitoring and regulating neurons. Indispensable roles for glia have been elucidated in most aspects of proper brain function, while they are gaining more interest in the context of neurological diseases. Glia shape synapses in the developing brain and modulate neuronal firing in mature circuits to maintain homeostatic conditions, while they also become activated in response to different brain insults. Glia serve as the resident immune cells of the brain, reacting to pathogens, cellular debris, and neuronal injury through the upregulation of specific transcripts, changes in morphology, and phagocytic ability. As our understanding of glial cells has grown over the past decades, it has become increasingly clear that glial responses within the brain are often context-dependent, ranging from the neuroprotective to the neurotoxic. Recent work, along with research described in this dissertation, has focused on uncovering the signaling mechanisms that are employed by glia to combat neuronal injury. Unraveling the molecular underpinnings of glial responses in varying contexts can help us understand the functional consequences of glial activation in the brain following injury. In this dissertation, I utilize the genetically powerful model system *Drosophila melanogaster* to examine injury signaling between transected neurons and the responding glia. I demonstrate that neuronal dense core vesicles and the insulin-like signaling pathway are regulators of glial phagocytic function following injury. Moreover, I utilize a novel fluorescence *in situ* hybridization method to investigate the role of transcriptional and translational control of glial immune genes in the injury response. The findings in this dissertation provide evidence for novel mechanisms involved in glial function following neuronal axotomy.

CHAPTER 1: INTRODUCTION

Glia

Over the past couple of decades, the study of glial biology has taught us that the "glue" definition coined by Rudolf Virchow in the 1860s is largely a misnomer for these dynamic and complex cells of the brain(1). Today, we recognize that although the word "glia" derives from the Greek for "glue", these cells are not merely the connective tissue that holds the brain together, but an indispensable counterpart to neurons. Glia play paramount roles in brain development, homeostasis, signaling, and disease, among other vital functions in the nervous system(2). Therefore, elucidating how these cells function in a variety of contexts is essential to our understanding of the brain as a complete system. The major types of glia within the central nervous system (CNS) of mammals are astrocytes, oligodendrocytes, and microglia, while the peripheral nervous system (PNS) houses Schwann cells(2). The model system utilized in this dissertation, *Drosophila melanogaster*, also contains glial cells in the brain and the periphery that closely associate with neurons and carry out functions similar to mammalian glia(3). This conservation across species also strengthens the argument for studying neuron-glia signaling in a tractable model system. As much of this dissertation examines the responses of glial cells to neuronal injury events, I will begin by providing a background on what scientists have uncovered about glial cells thus far.

Functional roles in mammals and *Drosophila*

Astrocytes

Astrocytes are aptly named for their star-like morphology. Their processes are highly ramified, which allows them to tile the brain and interact with numerous other cell types. Among these interaction partners are neurons, other glia, and blood vessels(4, 5). Astrocytes can modulate neuronal activity through their presence at the synaptic cleft, deemed the tripartite synapse(6). Astrocytes associate with pre- and post-synaptic neurons to remove

neurotransmitters (NTs) from the synapse to maintain homeostasis and can also impact neuronal signaling through the release of neuroactive substances(7, 8). Moreover, astrocytes maintain the blood-brain barrier (BBB) through connections of their end feet to the circulatory system. This neurovascular interface is vital for the control of blood flow, transfer of nutrients, and metabolic support to neurons(9, 10). Astrocytes also communicate to one another via calcium (Ca^{2+}) signaling through gap junctions(11). In *Drosophila*, astrocytes have a similar star-like, or tufted, morphology and occupy dense neuronal networks (neuropil regions) to play a role in modulating synaptic signaling(12). *Drosophila* astrocytes do not, however, maintain the BBB. This function is performed by two distinct glial cells: perineurial (PG) and subperineurial glia (SPG), which separate the central and peripheral nervous system from the circulating hemolymph(13).

Microglia

Microglia are the resident immune cells of the brain, constantly surveying their environment for the presence of pathogens, apoptotic and degenerating cells, as well as misfolded proteins(14-16). The dynamic behavior of microglia was elegantly demonstrated by Davalos and colleagues (2005) in an *in vivo* experiment that labeled microglia in the mouse brain with GFP and imaged them through a thinned skull using two-photon microscopy(17). In striking videos from this experiment, ramified microglial processes can be seen as highly motile as they extend and retract their projections under basal conditions. However, when the researchers induce an injury in the brain using a laser, microglia rapidly extend their processes to the site of injury and sequester the area. In the context of neuronal injury and degeneration, microglia have been shown to phagocytose and degrade material that would otherwise be neurotoxic(18). Additionally, microglia are vital in the context of development, where they prune weak synaptic connections, supporting a mantra of neuroscience: “use it or lose it” – by way of microglia(19). In the *Drosophila* brain, immune and phagocytic functions are carried out by astrocytes and ensheathing glia(20). The work in this dissertation is largely focused on the immune response

role of ensheathing glia in the adult olfactory system, specifically in response to axonal injury of the olfactory receptor neurons (ORNs). Ensheathing glia are present at the border of the antennal lobes (ALs), project through discrete nerves into the antennal lobes (ALs) of the central brain. Ensheathing glia extend their processes to divide the synapse-rich glomeruli of the ALs and closely enwrap projections(21).

Oligodendrocytes and Schwann cells

In order to communicate with their targets, neurons transform chemical information (NTs) into electrical information (action potentials), which travels down the axon to propagate signals to secondary targets. Insulation is vital for the efficient conduction of electricity down any wire, and the same holds true for axons. Oligodendrocytes are the glial cell type in the CNS that are responsible for wrapping their sheaths around axons to produce a lipid-rich substance called myelin(22). A single oligodendrocyte can wrap multiple axons, which allows for neurons to undergo saltatory conduction and increases the conduction velocity of action potentials. Myelination continues throughout the life of the animal, into adulthood, and is vital for cognitive development, as well as learning and synaptic plasticity(23). Pools of oligodendrocyte precursor cells (OPCs) also exist in the brain, which retain the capacity to differentiate into oligodendrocytes in the event of cell death or injury(24). Within the PNS, Schwann cells perform similar functions as oligodendrocytes: they myelinate peripheral projections and provide trophic support to neurons(25). Schwann cells also perform immune-like functions, engulfing degenerating axonal and synaptic material during development and post-injury in adult animals(26, 27). *Drosophila* do not have myelin; however, ensheathing glia within the central brain and wrapping glia in the periphery closely associate with and enwrap axonal projections to provide trophic support and respond to injury(28).

Other glia

A *Drosophila* glial subtype not yet discussed are the cortex glia, which surround neuronal cell bodies in the cortical regions of the brain(29). They are perhaps the most understudied glial cell type in the fruit fly; however, they are important for the support of neuronal firing and interact with SPGs to potentially play a role in nutrient transfer from the hemolymph to neurons(3, 30). Mammalian satellite glia in the PNS have a similar localization, as they surround neuronal cell bodies in peripheral ganglia and play a role in maintaining homeostasis in their microenvironment and contribute to pain following nerve damage(31). As a field, we are continuously uncovering new information about glial biology and glial subtypes. Using single cell RNA sequencing (RNAseq) technology, we have been able to gain new insights into the differing biological profiles and functions of glial cells, and how they might change under different contexts, in response to stimuli, or across brain regions(32-35). Although I have described major types of glia, new definitions are constantly emerging, and we will undoubtedly be able to subdivide glia even further.

Neuron-glia interactions within the brain: Astrocytes & microglia

Glial cells play essential roles in the developing brain by guiding neural circuit formation, supporting neuronal survival, and modulating neuronal signaling. Astrocytes and microglia are the primary glial cells performing these functions(36). During the development of the nervous system, neurons and synapses are over-produced(26). Neurons that are unable to form adequate connections undergo programmed cell death, resulting in apoptotic debris. An example of a site of robust neurogenesis in the brain is the developing hippocampus, where microglia have been observed near apoptotic cells(37). Microglia are largely responsible for adopting a phagocytic phenotype to clear dying neurons and a microglial receptor, triggering receptor expressed on myeloid cells 2 (TREM2), has been implicated in synapse elimination in mice(38). As the principal phagocytic glia of the brain, microglia have also been shown to prune neurons in the visual thalamus through the classical complement cascade(39). In this cascade, complement component 1q (C1q) tags synapses, while microglia detect these opsonized neurons and

transform into a pro-inflammatory and phagocytic state. Astrocytes also feed into this synaptic pruning pathway, as they secrete transforming growth factor beta (TGF-ß), which induces C1q expression in neurons(40, 41). Furthermore, astrocytes are able to prune synapses through a complement-independent mechanism during development, whereby the activation of scavenger receptors multiple EGF-like domains 10 (MEGF10) and MER proto-oncogene tyrosine kinase (MERTK) results in phagocytosis of phosphatidyl-serine (PtdSer)-tagged synapses and dying cells(42-44).

Astrocytes and microglia also support neuronal development and function. Studies have posited that microglial secretion of neurotrophic factors, such as nerve growth factor (NGF), brain-derived neurotrophic factor (BDNF), and fibroblast growth factor (FGF), among others, promote axon elongation(45). Additionally, astrocytes stimulate neural circuit formation through the release of Glypicans 4 and 6, Thrombospondin 1, and Hevin(46). Following development, glia are crucial for maintaining homeostatic conditions within the brain. Through their presence at the tripartite synapse, astrocytes support neurotransmission through removing excess glutamate to prevent neuronal over-excitation. They are also able to influence synaptic activity and plasticity through the release of gliotransmitters, such as glutamate, D-serine, and adenosine triphosphate (ATP)(6, 47). Within the developing and mature CNS, neurons and glia are inextricably connected.

In response to injury, degeneration, and disease

I have described some of the indispensable functions carried out by astrocytes and microglia within a healthy CNS, but how do these cells respond to brain insults? Several mechanisms employed by astrocytes and microglia in neuronal development and maintenance are re-engaged in injury and disease, and with prolonged activation can often become aberrant. Following acute brain injury, microglia transform from their ramified state to a hypertrophic and ameboid phenotype in order to phagocytose cellular debris(48). Microglia are able to detect dsDNA, RNA, and proteins from dying cells through cell surface receptors, which serve as an

activation signal for microglia to adopt a pro-inflammatory state(18, 49, 50). Through the release of cytokines, microglia are also able to recruit immune cells from the periphery for the removal of damaged neurons, myelin, and other glial cells(36). These functions are necessary to prevent the spread of damage from the injured brain region to healthy cells. In multiple sclerosis (MS), a disease characterized by demyelinating lesions, myelin debris is cleared away by glia(51, 52). Studies have shown that microglia are able to remove myelin debris, with MERTK and TREM2 receptors implicated in myelin phagocytosis(53-55). In Alzheimer's disease (AD), amyloid-beta (Aß) plaques and neurofibrillary tangles are hallmarks of disease pathogenesis and can be identified in postmortem brains(56, 57). Microglia and astrocytes have been observed surrounding Aß plaques in AD brains, while studies have demonstrated that microglia engage the complement pathway to tag and remove these inclusions of aggregated protein(58, 59).

In response to traumatic brain injury (TBI), astrocytes, along with microglia, make up the glial scar, which physically sequesters areas of damage(60). Astrocytes also adopt a "reactive" phenotype following TBI, leading to the production of cytokines, chemokines, along with matrix metalloproteinases (Mmps). Expression of Mmps functions to remodel the extracellular matrix (ECM) surrounding the lesion, which can create a permissive environment for neurite outgrowth(49). Mmps have also been shown to promote glial migration and infiltration following spinal cord injury, as well as contribute to glial scar formation(61). Astrocyte production of trophic factors (e.g., NGF, BDNF, FGF, TGF-ß) can also serve to promote neurogenesis following brain injury(62). Although the glial functions described above promote restoration of brain homeostasis and function, the responses of glial cells to injury and disease do not always have a neuroprotective outcome. Reactive gliosis, or the activation of astrocytes and microglia following injury, is a highly diverse process depending on the context, and can lead to neuronal damage and even death.

Neuroprotection vs. Neurotoxicity

Even as the glial scar can sequester an area of damage in instances of brain injury, some studies have suggested that this physical barrier may inhibit regrowth and regeneration of neurons(63). This is just one example of a glial response where the neuroprotective vs. neurotoxic function of glia has been called into question. In a mouse model of AD, for example, activation of the complement pathway can also lead to the opsonization of not only Aß, but synapses, which can become aberrantly phagocytosed(64). Some researchers have hinted that this process may lead to the cognitive decline observed in the disease(65). In the case of brain injury, chronic activation of microglia and astrocytes can lead to persistent inflammation, even at sites removed from the initial injury(18). This can create an environment that promotes neuronal degeneration.

The role of aging has been extensively studied in how glial cell functions can go awry, leading to a neurotoxic effect. An RNAseq study in aged mice uncovered that aged astrocytes had a distinct molecular signature in certain brain regions, when compared to young mice(34, 66). These astrocytes expressed genes related to the inflammatory response and the complement cascade, constituting a reactive phenotype, which could drive synapse loss. Studying glial responses in varying contexts, and to different stimuli, may be key to understanding how glial functions can be harnessed to promote therapies and neuroprotective outcomes in injury, neurodegeneration and aging. *Drosophila* serves as a powerful tool to investigate many of these questions.

Drosophila **as a model organism to study neuronal injury and glial responses**

The experiments in this dissertation have harnessed the genetic tractability of the fruit fly as an *in vivo* model system to explore glial responses to neurodegeneration. *Drosophila* tools allow for the manipulation of distinct populations of cells using binary expression systems and the multitude of transgenic tools that exist in the fly. The upstream activation sequence (UAS)/Gal-4 system, co-opted from yeast and developed as a fruit fly tool by Brand and Perrimon, allows us

to use cell-type specific promoters to express the Gal-4 transcription factor, which in turn binds to a UAS sequence to induce gene expression(67). Other binary systems have been developed, including the LexA/Aop and QF/QS systems, which allow for the manipulation of multiple different cell types within a single fly line(68, 69). In this dissertation, I use the UAS/Gal-4 and LexA/Aop systems to express specific transgenes, RNA interference (RNAi) constructs, as well as fluorescent markers. The fluorescent labeling of cellular and sub-cellular components also lends itself to imaging and the visualization of biological processes. Beyond the genetic and imaging tools that exist in *Drosophila*, various injury paradigms have been developed, which allow me to ask questions about neuronal and glial mechanisms that are engaged following an axotomy.

Injury models in *Drosophila*

Olfactory receptor neuron (ORN) injury

The ORN injury paradigm is a well-described tool to study neuron-glia interactions following axotomy, and is the primary method used in this dissertation(70). Cell bodies of ORNs reside in the odor-sensing structures of the fly, the antennae and the maxillary palps, which send their projections to the AL region of the brain (Fig. 1A). There, they form synapses at distinct glomeruli onto secondary projections. Surgical ablation of the 3rd antennal segment and/or the maxillary palps results in an axotomy of ORN projections, and their subsequent degeneration over time(71). Antennae contain approximately 80% of ORNs, while maxillary palps contain the remaining 20%. As a result, the effects of larger and smaller, more localized injuries can be studied through the removal of either the antennae or the maxillary palps. Ensheathing glial cell bodies reside at the border of the ALs, and they send their projections to subdivide the neuropil and closely associate with ORN projections (Fig. 1B). Ensheathing glia have been shown to expand their membranes, upregulate immune genes, and clear injured projections following axotomy(70, 72-74). This injury can be studied in the fly using the fluorescent labeling of a subset of ORNs, ensheathing glia, and immunolabeling of injury-associated genes.

The adult fly wing

A comparable paradigm exists in the wing of the fruit fly, whereby peripheral projections can be acutely injured and easily imaged by live microscopy methods(75). Cell bodies of mechanosensory projections are distributed along the longitudinal vein 1 (L1) of the fly wing (Fig. 1C). These neurons send their projections into the thorax of the fly and are surrounded by wrapping glia. Depending on the cut site, some projections are injured and degenerate, while others with cell bodies distal to the cut site remain intact. A study has demonstrated that the surrounding wrapping glia remove the debris that results from injury(75). Additionally, because the fly wing is visually clear due to minimal cuticle, it is amenable to live imaging of fluorescently labeled structures and molecules.

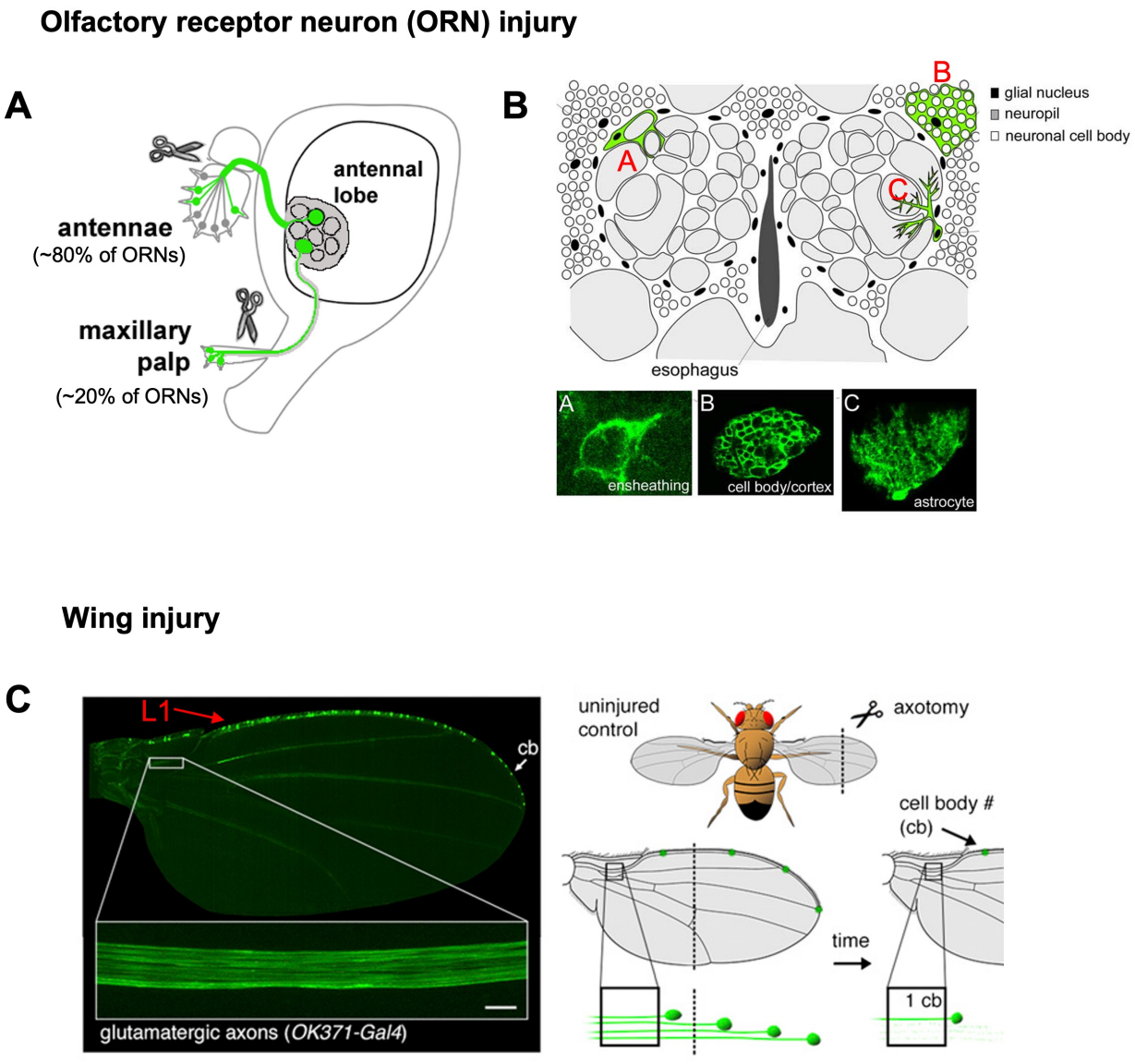

Figure 1: Injury paradigms in the adult *Drosophila* brain and wing
(A) Schematic of the ORN injury from a side view of the fruit fly head. Adapted from MacDonald *et al*., 2006(70). Antennae and/or maxillary palps are surgically removed, transecting ORNs. ORN cell bodies are housed in antennae and maxillary palps, while their axons project into the brain to synapse at the antennal lobes (ALs). **(B)** Schematic of the ALs within the central brain, along with the surrounding glial cell types. A: ensheathing glia. B: cortex glia. C: astrocytes. Adapted from Doherty *et al*., 2009(73). **(C)** Fly wing injury schematic. Adapted from Neukomm *et al*., 2014(75). Glutamatergic neuron cell bodies (cb; green) are distributed along the L1 vein of the wing (red arrow). Transection of the wing will result in injury of some mechanosensory projections, but not others, depending on the cut site.

Ventral nerve cord (VNC) injury

Although *Drosophila* are invertebrates, and therefore do not have spinal cords, the VNC in the thorax of the fly is functionally equivalent. Peripheral neurons project to and from the VNC, such as from the legs and wings of the fly, connecting to specific neuropil regions along the VNC(76). Purice and colleagues (2017) have described an injury paradigm whereby the legs and wings of the fly can be surgically removed, which results in robust activation of glial cells within the VNC (Fig. 2A)(77). Moreover, the fly can be decapitated to exacerbate the injury paradigm and elicit a significant glial response. This novel injury model revealed a large set of differentially expressed genes through transcriptional profiling, including *matrix metalloproteinase 1* (*Mmp-1*), which will be further explored in this dissertation.

The larval system

The previous injury paradigms that I have described are all performed in the adult fly. However, the developing fruit fly system is particularly amenable to genetic and physical manipulation, and a multitude of studies have harnessed the fruit fly larva to study neuron/glia developmental processes, including neuromuscular junction (NMJ) outgrowth and refinement, and even responses to neural injury(78-80). *Drosophila* larvae can be filleted open, exposing the CNS and the segmented musculature that is innervated by motoneurons (Fig. 2B,C)(81, 82). This *in vivo* model can be easily manipulated in a number of ways, including surgical and laser ablation, drug application, live imaging, and electrophysiological manipulation. The animal can be kept alive through this process by bath application of a hemolymph-like solution (HL-3) and allows scientists to study various biological questions *in vivo*.

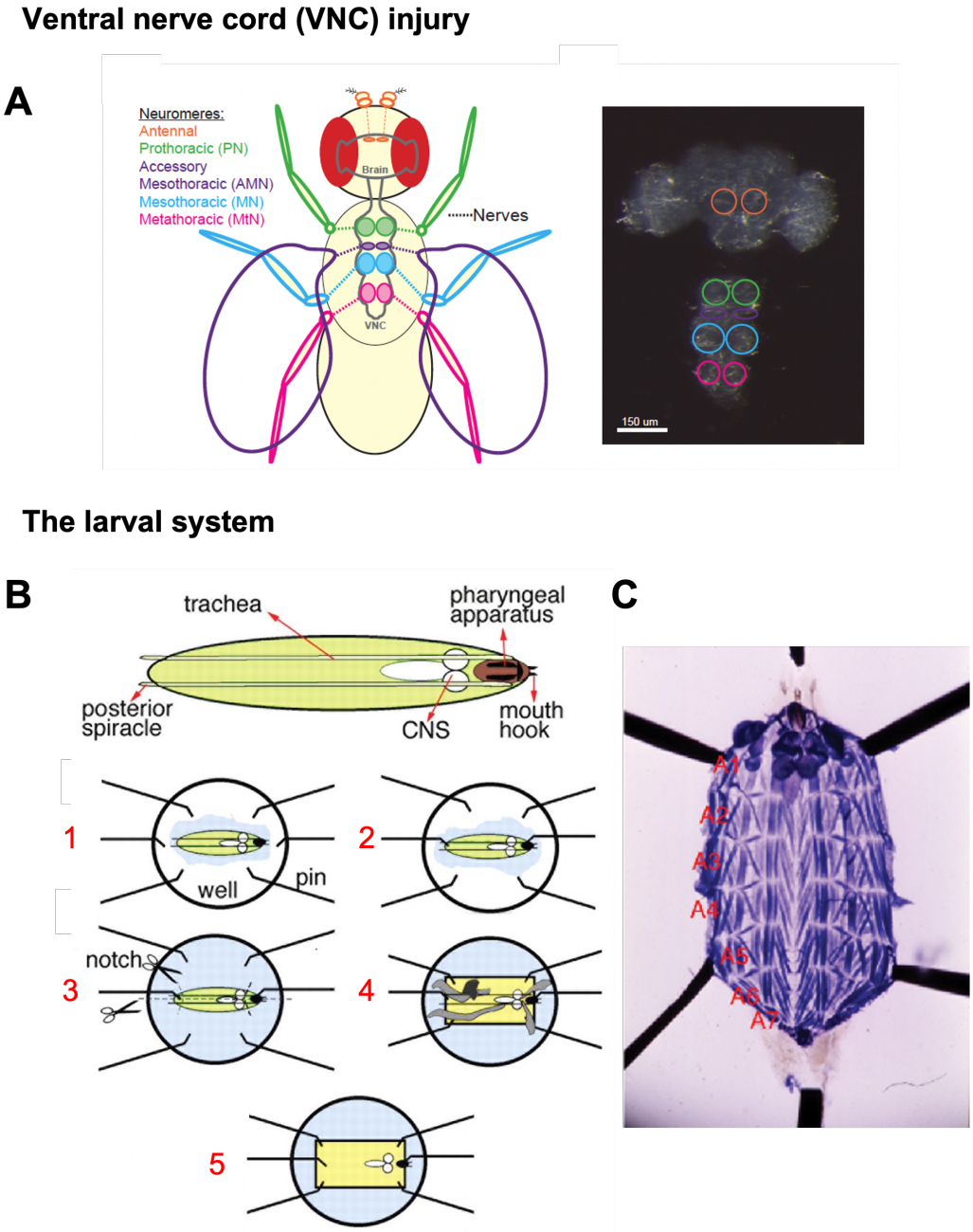

Figure 2: The *Drosophila* ventral nerve cord (VNC) and the larval preparation
(A) Schematic of the adult *Drosophila* body, including the brain and the VNC. Taken from Purice *et al*., 2017(77). Color coding corresponds to specific neuromere regions. Orange: antennal, receive projections from ORNs. Green: prothoracic, receive projections from legs. Purple: accessory mesothoracic, receive projections from wings. Cyan: Mesothoracic, receive projections from legs. Magenta: metathoracic, receive projections from legs. Neuromeres in the brain and VNC are circled with the corresponding colors. **(B)** Schematic of the larval *Drosophila* dissection/fillet. Adapted from Ramachandran & Budnik, 2010(82). 1: larva is placed in a well with hemolymph-like solution. 2: pins are placed in posterior and anterior end of the larva and stretched. 3: larval is cut open between the spiracles. 4: organs are removed, keeping the nervous system intact. 5: remainder of the pins are used to stretch out the larva. **(C)** Representative image of the stretched-out larva indicating the muscle segments (A1-A7). Adapted from Ramachandran & Budnik, 2010(82).

Signaling mechanisms modulating neuron-glia interactions following injury

Neuronal events

Neurons are vulnerable to a variety of insults, including crush, stretch, axotomy, and disease(83). In response to some of these injuries, neurons can undergo a process that is distinct from apoptosis, initiating a neuron-intrinsic program first described by Augustus Waller in 1850, where he observed the degeneration of a frog tongue nerve following transection(84, 85). Studies have demonstrated that Wallerian degeneration (WD) is conserved between species, from *Drosophila* to mammals, and involves rapid breakdown and disintegration of the axon(83, 86, 87). Under physiological conditions, glial cells infiltrate the area of damage and clear cellular debris(20, 36). Some neuron to glia signaling mechanisms following injury have been elucidated; however, questions still remain about the pathways utilized between these cells to initiate glial immune responses.

Wallerian degeneration and Calcium signaling

WD has been described in three distinct phases, which begins with axonal injury(87). Immediately after damage to the neuron, the acute axonal degeneration stage begins, whereby the region of the axon near the injury site fragments. This is followed by a lag phase, where the detached axon remains intact. In the mouse sciatic nerve, this latent phase lasts approximately 40 hours, while in *Drosophila* ORNs it is between 6 and 8 hours(70, 88). Finally, fragmentation occurs, which rapidly degrades the axon into small pieces that are cleared by phagocytic cells(89). Many studies have focused on elucidating the molecular signaling events that mediate this neuron-intrinsic process, and due to their amenability to genetic manipulation, *Drosophila* have contributed greatly to proposing a WD pathway.

Following axotomy, the E3 ubiquitin ligase highwire is activated, which leads to the degradation of nicotinamide mononucleotide adenylyltransferase (Nmnat), an enzyme required

for nicotinamide adenine dinucleotide (NAD+) synthesis(90-92). This step causes the reduction of NAD+ and activates sterile alpha and armadillo motif (Sarm) protein, a signaling molecule that has been shown to act downstream of Toll receptors(93, 94). Along this pathway, axundead is activated in ORNs and the wing to induce degradation(95). The direct mechanism by which the Sarm pathway results in axon degeneration is still unclear; however, microtubule and neurofilament breakdown contribute to the fragmentation of the axon(96).

Much progress in understanding WD has also come from a mutant mouse line(97). The mutation was traced back to a fusion protein, which is produced by the joining of two genes: Nmnat1 and the N-terminus of Ube4b, an E4 ubiquitin ligase(98). Researchers observed that injured axons in these mice survived 10 times longer than WT animals; therefore, the mutant fusion was named Wallerian degeneration slow (Wlds)(97, 99). In the *Drosophila* ORN model, expression of Wlds in olfactory projections results in axon survival for up to 3 weeks after axotomy(70, 71). Furthermore, Wlds has been shown to delay axon degeneration in models of TBI, neuropathy, glaucoma, and PD(100).

Ca^{2+} entry into the neuron plays a substantial role in WD; it is both necessary and sufficient for axon degeneration, while chelating Ca^{2+} can delay axon degeneration(101-104). Ca^{2+} imaging in zebrafish has shown that there appear to be two distinct phases of Ca^{2+} increase within the neuron following axotomy. The first is a local wave of Ca^{2+}, which occurs right after axotomy at the injury site. The second wave is more global and occurs throughout the cell just before fragmentation(105). Vargas and colleagues (2015) found that Wlds blocks the second Ca^{2+} wave, but not the first. In a larval *Drosophila* model, Wlds suppressed the first wave(105, 106). Studies have found a role for Ca^{2+} during WD in the activation of calpain, a calcium-dependent cysteine protease, which is thought to destabilize microtubules(107). Many intrinsic mechanisms have been elucidated in neurons following injury, but after the onset of WD, how do neurons communicate “find me” and “eat me” signals to glia?

Injury signals released from neurons

Cells rely on adenosine triphosphate (ATP) for energy, while cellular damage can result in the release of large amounts of ATP into the extracellular environment. This response has been demonstrated to stimulate microglial proliferation and reactive astrogliosis in the nervous system(108, 109). In an experiment examining the role of ATP as a chemoattractant following neuronal injury, Davalos *et al*., 2005 demonstrated that microglia rapidly change their morphology and migration in response to a laser ablation injury(17). Microglial activation through the P2Y purinergic G protein-coupled receptor (GPCR) allows for detection and extension of microglial processes to the site of neuronal injury.

Finally, recent work has uncovered the role of PtdSer in phagocyte function during development and injury. PtdSer localizes to the inner leaflet of the plasma membrane; however, its exposure results in cell engulfment by professional phagocytes(110, 111). This process is conserved from invertebrates to mammals(112). In the embryonic brains of zebrafish, microglia lacking PtdSer receptors are unable to properly clear apoptotic cells that result from development(113). In *C. elegans*, necrotic cells expose PtdSer in response to elevation of cytoplasmic Ca^{2+}(114). In *Drosophila*, PtdSer is exposed on degenerating dendrites after physical injury and during remodeling(110). In the visual system, damaged photoreceptors cause the upregulation of glial fibrillary acidic protein (GFAP) in Müller glia in response to PtdSer(115). Studies have demonstrated that NAD+ disruption, previously described in the process of WD, controls PtdSer exposure(110). Although some mechanisms have been uncovered, it is unclear whether neurons might utilize other signals and signaling pathways in glia for different stages of the glial immune response.

Glial events

As previously described in this introduction, glial responses to neuronal injury are varied and often context dependent. Importantly, glial activation can result in both neuroprotective and

neurotoxic outcomes for the brain. Therefore, it is vital to uncover which glial responses are engaged following neuronal injury, as this could lead to new therapeutic targets in the field of clinical neuroscience. I have previously discussed the neuronal events that follow an injury, and in this section, I will highlight some of the major glial pathways that are activated. I will pay particular attention to studies that have been conducted in *Drosophila* and that are of interest in relation to the studies presented in this dissertation.

Draper (Drpr) receptor

Drpr is an engulfment receptor expressed in a variety of glial subtypes, including ensheathing glial cells in the *Drosophila* nervous system(70). It is highly conserved across species: as Ced-1 in *C. elegans* and MEGF10 in mammals, and is required for the detection of apoptotic cells, cellular debris, protein aggregates, and PtdSer(116). In the fruit fly, Drpr is an essential component of the innate immune glial response to axotomy, allowing ensheathing glia to undergo transcriptional changes, cytoskeletal remodeling, and the initiation of phagocytosis(117-121). In the ORN injury model described earlier, $drpr^{-/-}$ flies were unable to clear severed projections from the ALs(70). Activation of the Drpr pathway has several downstream effects (Fig. 3). In the presence of an injury signal, Scr42A is activated, and through its kinase activity phosphorylates the intracellular domain of Drpr(122). This allows for SH2 ankyrin repeat kinase (Shark) to bind and initiate cytoskeletal rearrangement of the ensheathing glial cell. Drpr activates the adaptor protein Ced-6, which is required for glial phagocytic activity(123). Drpr also regulates its own expression in response to injury, whereby Rac1, a GTPase, signals through the transcription factor Stat92E to upregulate *drpr*(74, 124). This is required for ensheathing glial engulfment of axonal debris. The robust upregulation of *drpr* mRNA is observable by qPCR at 3 hours post-injury (hpi), while the protein is significantly upregulated at 18-24hpi(119). These initial findings characterizing glial signaling in an event of axotomy, highlight the importance of transcriptional regulation in orchestrating a proper glial immune response.

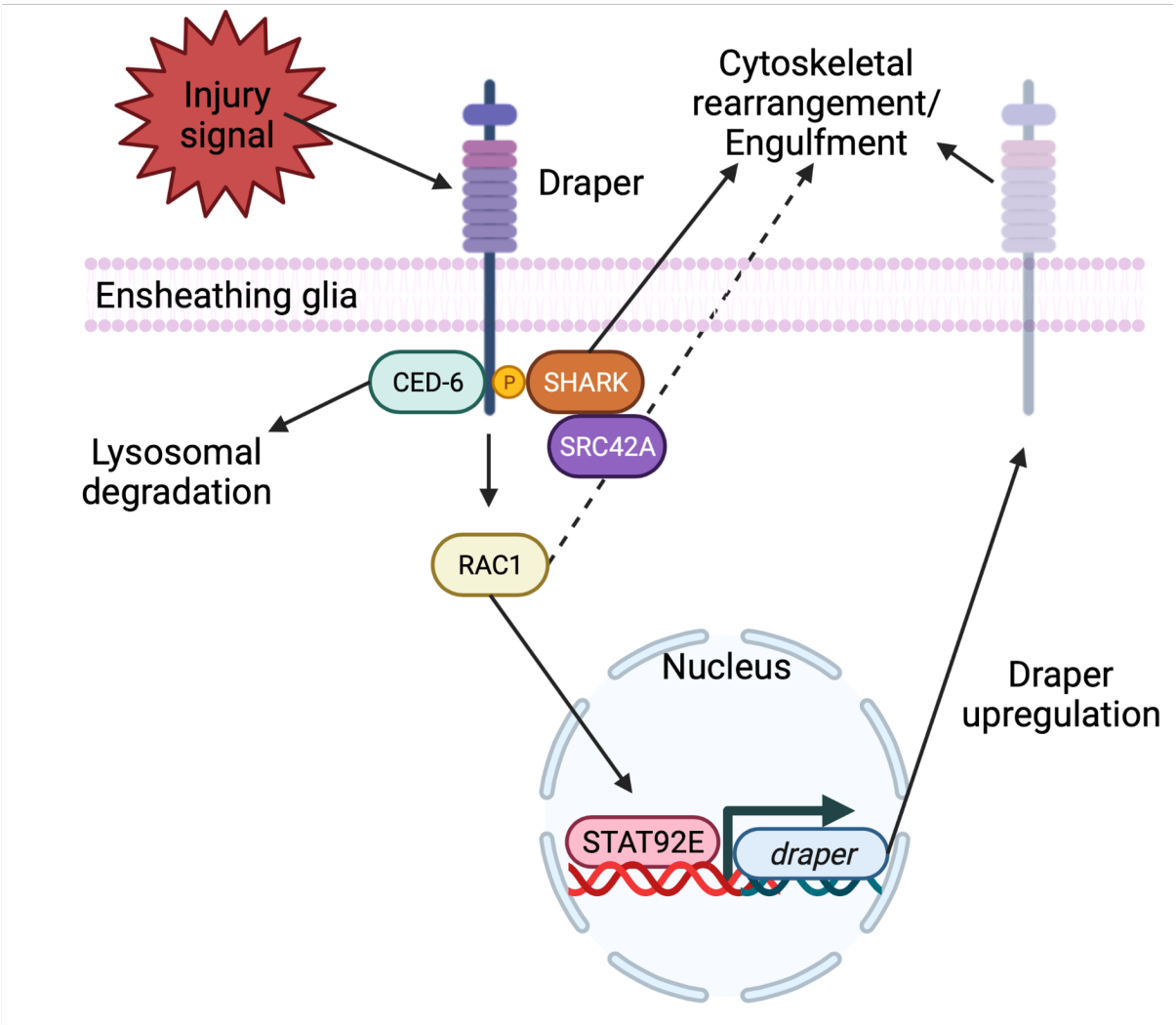

Figure 3: The Draper (Drpr) pathway
The engulfment receptor Drpr is activated ensheathing glial cells in response to an injury signal. Src42a phosphorylation of Drpr leads to Shark binding and results in cytoskeletal remodeling and the engulfment of cellular debris. Ced-6 is activated by Drpr and plays a role in ensheathing glial phagocytosis, while Rac1 initiates the Stat92E-dependent upregulation of *drpr*, which is required for glial engulfment function. Adapted from MacDonald *et al.*, 2013 and Doherty *et al.*, 2014(72, 74).

Matrix metalloproteinase 1 (Mmp-1)

Previous work by a graduate student in the Logan lab uncovered a new transcriptional target of the Drpr pathway (Fig. 4). In an RNAseq screen, Purice and colleagues (2017) demonstrated that Mmp-1 is upregulated in injured VNCs(77). Mmps have been implicated in cancer, cell migration, and ECM remodeling(125, 126). Our group showed that Mmp-1 upregulation in ensheathing glia is necessary for clearance of injured ORN projections(77). Additionally, they determined that Mmp-1 was upregulated through the Drpr pathway, specifically c-Jun N-terminal kinase (JNK) and janus kinase/signal transducer and activator of transcription (JAK/STAT) signaling, which activates the transcription factors activator protein 1 (AP-1; dimer composed of c-Fos and c-Jun) and Stat92E to induce Mmp-1 expression. The study hypothesized that Mmp-1 is secreted from the ensheathing glial cell to remodel the ECM through its protease activity following injury, which would allow ensheathing glial membranes to infiltrate areas of damage and phagocytose injured projections.

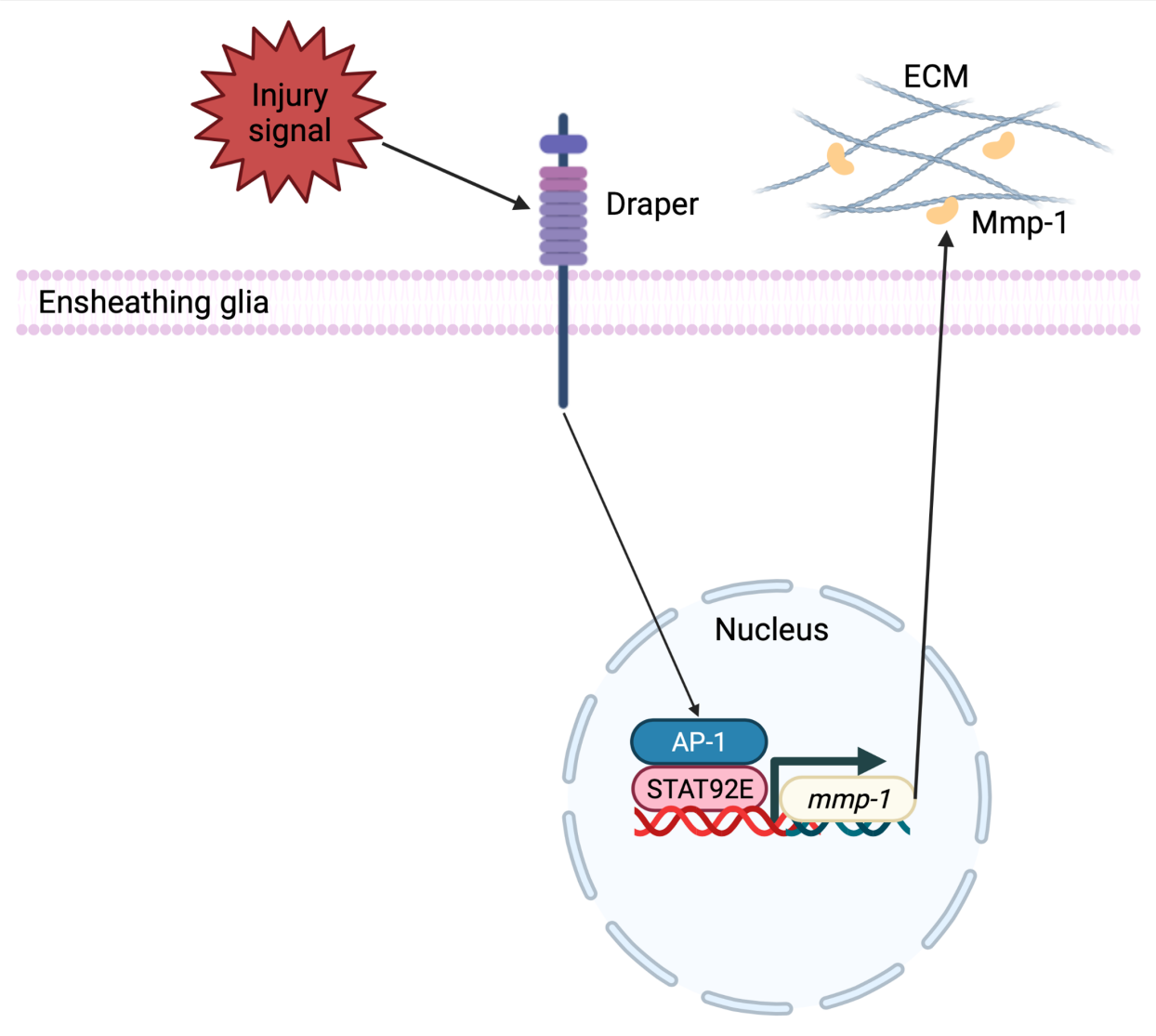

Figure 4: The Matrix metalloproteinase 1 (Mmp-1) pathway
The engulfment receptor Drpr is activated ensheathing glial cells in response to an injury signal. Draper signals through the JNK and JAK/STAT pathways to induce the AP-1 and Stat92E-dependent upregulation of *mmp-1*. Mmp-1 is likely secreted from glial cells to induce extracellular matrix (ECM) remodeling. Adapted from Purice *et al*., 2017(77).

Insulin-like signaling (ILS)

The insulin signaling pathway has been extensively studied in the context of development, growth, and energy homeostasis; however, not much is known about its role in brain injury(127, 128). A handful of studies have presented conflicting results regarding the role of insulin signaling activation in response to neuronal trauma(129-131). It is unclear whether the activation of this pathway promotes or inhibits neuronal survival following injury. To untangle how insulin signaling might play a role in this process, a study from our lab examined the conserved ILS pathway in the fruit fly. The *Drosophila* insulin receptor (InR) is a receptor tyrosine kinase which is homologous to the vertebrate insulin receptors(128). Musashe *et al*., 2016 found that following ORN injury, ensheathing glial InR phosphorylation results in Akt-1/Stat92E activation and subsequent *drpr* upregulation (Fig. 5)(132). This pathway is required for adequate clearance of injured ORN projections. These results summarize the glial findings; however, the researchers also found that perturbing the processing of InR ligands, the insulin-like peptides (Ilps), or their release via dense core vesicles from neurons, significantly attenuated InR phosphorylation and Drpr upregulation. We hypothesize that DCVs could serve as a signal from injured neurons to the surrounding glial cells; however, their role in injury signaling has not been extensively investigated.

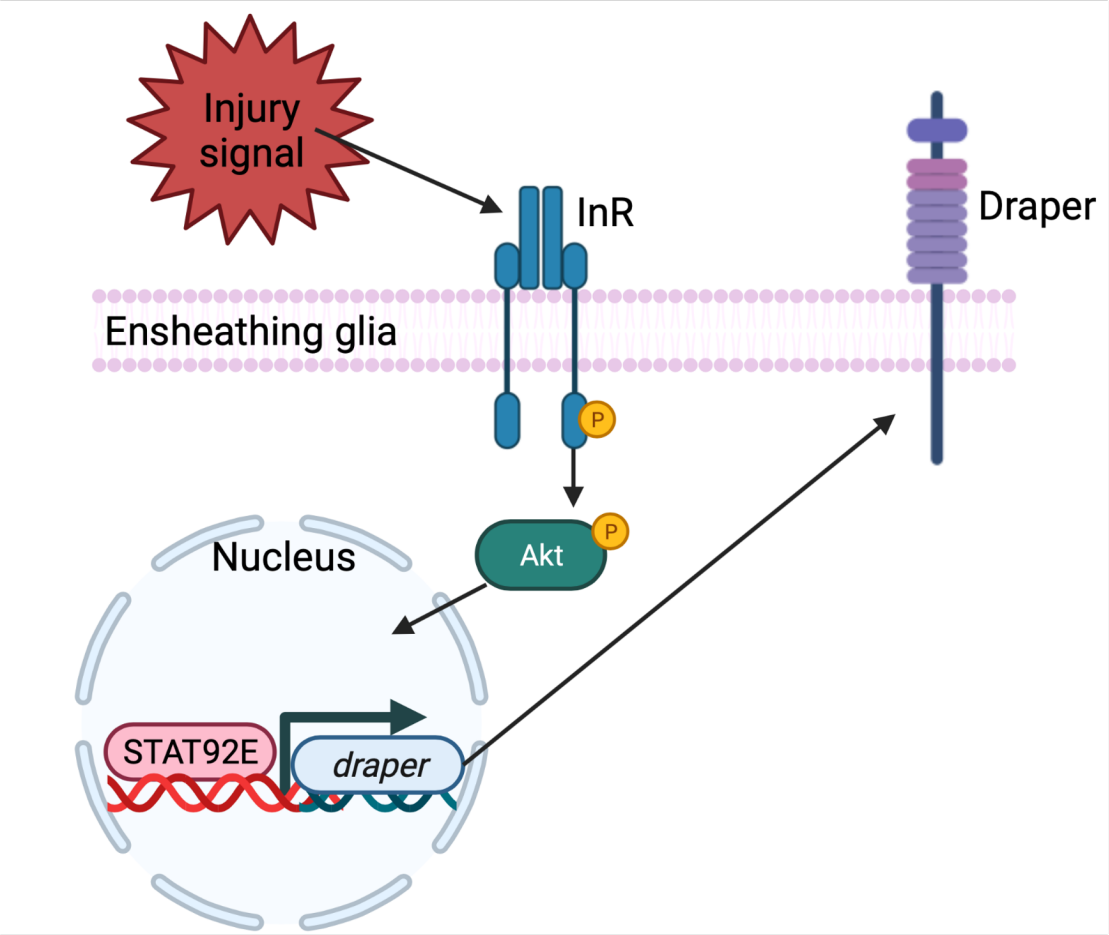

Figure 5: The insulin-like signaling (ILS) pathway
The insulin receptor (InR) is activated by an injury signal, resulting in its phosphorylation. InR activation leads to Akt-1 phosphorylation and the Stat92E-dependent upregulation of the Drpr receptor. Adapted from Musashe *et al*., 2016(132).

Is there a role for dense core vesicles (DCVs) in injury and disease?

DCVs get their name from their appearance by electron microscopy, where they can be observed as a lipid bilayer surrounding a dark core (Fig. 6A)(133). Their role in the body is multi-faceted and DCVs can be found in a number of organs ranging from the brain to the pancreas(134). DCVs release their contents through the regulated secretory pathway, and much like synaptic vesicles (SVs), they have a paramount impact in brain development and signaling between neurons, acting through both GPCRs and ion channels(134). DCVs have also been found in astrocytes; however, their role in glia is less well studied. In *Drosophila* neurons, DCV cargo includes Ilps, the ligands of the InR, which is activated on glial cells to engage the ILS pathway in responses to neuronal injury(135, 136). The ILS pathway is necessary for glia to upregulate a well-described immune gene and clear degenerating projections(132). In this section, I will provide some background on these specialized vesicles and their proposed role as a neuronal injury signal.

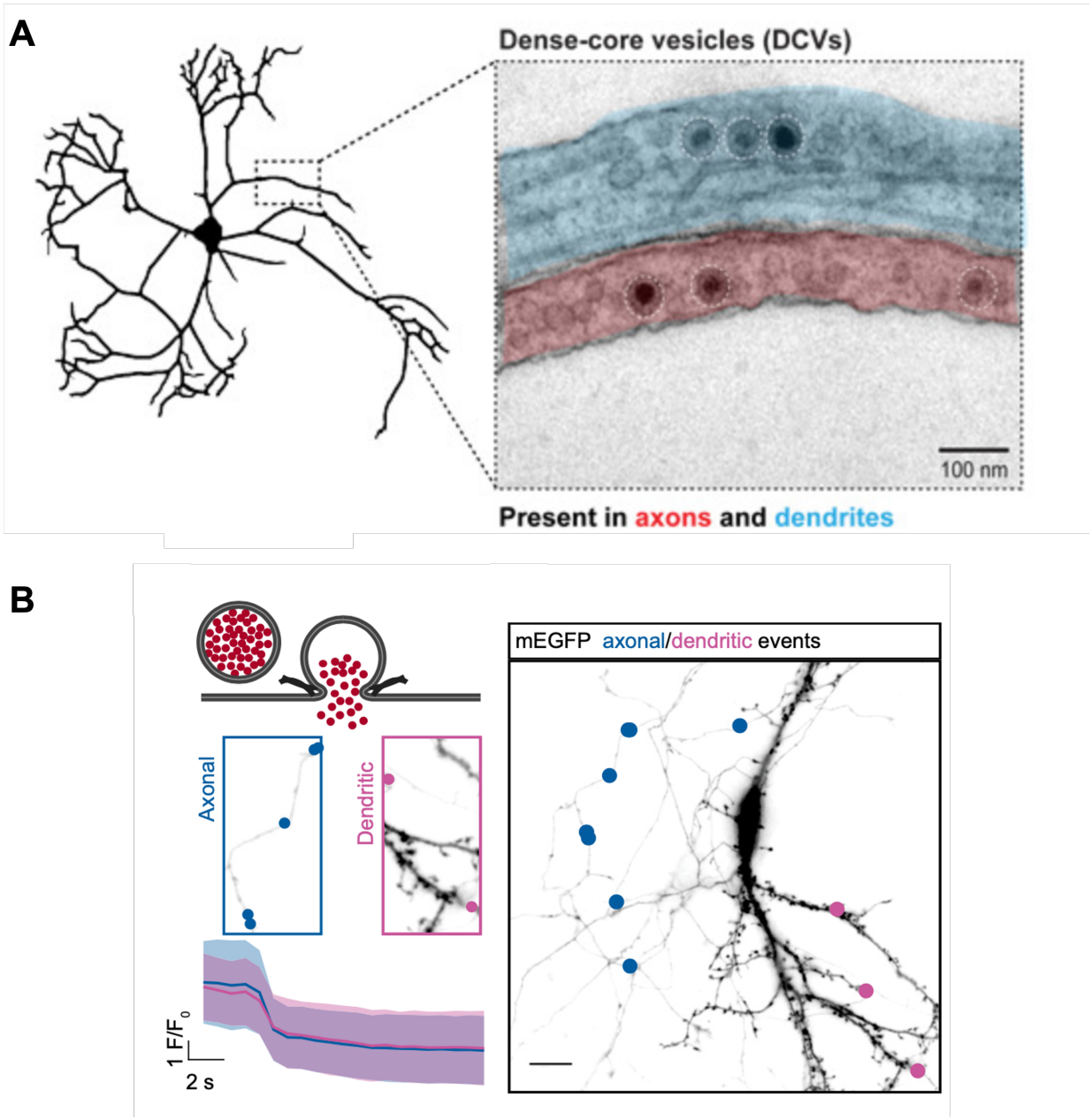

Figure 6: Dense core vesicles (DCVs) in axons and dendrites
(A) Transmission electron micrograph of dense core vesicles (white dotted circle) in axons (red) and dendrites (blue) of cultured neurons. **(B)** DCV fusion events in axons (blue) and dendrites (magenta), measured using neuropeptide Y (NPY)-mCherry as a reporter. NPY-mCherry fluorescence (F/F_0) is decreased following DCV release of cargo, indicating fusion. Modified from Persoon *et al.*, 2018(133).

DCVs

Biogenesis

Following synthesis, proteins that are destined for DCVs move from the endoplasmic reticulum (ER) through the Golgi stacks, where they may undergo post-translational modifications. DCV cargo includes neuropeptides (*e.g.*, neuropeptide Y; NPY) and neurotrophic factors (*e.g.*, BDNF), which are required for neuronal growth and survival, along with synaptic plasticity(134, 137). Cargos that are targeted to DCVs begin to aggregate in the trans-Golgi network (TGN). This process has been demonstrated to require an acidic environment and the presence of Ca^{2+}(138-140). Moreover, sorting receptors and cargo-binding proteins have been proposed as mechanisms to mediate DCV-specific cargo packaging(141, 142). The journey of a DCV begins at the Golgi apparatus, where immature vesicles bud from the TGN in a clathrin-dependent manner(143). The small GTPases Rab2 and Rab6 have also been shown to mediate DCV budding(134). Proton pumps on DCVs mediate their maturation, further acidifying the vesicle lumen(144). Mature DCVs then begin traveling along microtubules to cites of release in axons and dendrites.

Trafficking in neurons

DCV trafficking is a unique process, whereby association with distinct adaptor and motor proteins allows for the movement of DCVs in both an anterograde and retrograde direction. In cultured hippocampal neurons, Dynactin was found to play a role in bidirectional transport of DCVs, allowing for them to associate with the motor protein Dynein for retrograde movement(145). In a *Drosophila* study, anterograde movement was mediated by KIF1A, a kinesin-3 motor protein(146). Further studies at the fruit fly NMJ have also demonstrated that DCVs circulate in motoneurons, much like sushi on a conveyor belt(147, 148). Wong *et al*., 2018 found that DCVs travel to distal boutons first and make their way back toward the soma, with only a small

percentage of them being captured at each bouton(147). Moreover, the switch from anterograde to retrograde is mediated by the switch of the aforementioned motor proteins(149).

Exocytosis

Like SV release, DCV exocytosis is Ca^{2+}-dependent; however, it requires greater and more prolonged rises in Ca^{2+}(150). And while SVs release their contents at the synaptic active zone, DCVs can be released extrasynaptically, along axons and even from dendrites (Fig. 6B)(133, 151). Presumably, this allows DCV cargo to have a more widespread signaling effect, not just at the synapse. Although the locations of DCV and SV release in neurons differ, both types of vesicles require the *N*-ethylmaleimide-sensitive factor attachment protein receptor (SNARE) complex at the plasma membrane(152, 153). But how do neurons differentially regulate DCV and SV release?

In mammalian and invertebrate models, the DCV-associated calcium-activated protein for secretion (Caps) has emerged as a potential mediator of DCV, but not SV, release. Mammals have two Caps isoforms, Caps-1 and Caps-2; they are highly homologous and likely perform similar functions(154, 155). In *C. elegans* and *Drosophila*, Caps is encoded by a single gene(156-158). In rat brain homogenates, Caps was observed to localize to DCVs but not SVs(159). Null Caps mutants in *C. elegans* resulted in perturbed DCV docking and exocytosis, while at the *Drosophila* NMJ, Caps was also demonstrated to regulate DCV release(156, 157). It is thought to function as the Ca^{2+}-sensing component of the DCV release machinery, and also play a role in docking vesicles at sites of release by initiating SNARE complex assembly(152, 160-162). It is also important to note that some studies have also found a role for Caps in mediating SV release; however, this might be a secondary effect of disrupting DCV release by Caps knock out (KO)(156, 163).

Target as an injury or disease signal

DCVs have been implicated in a variety of diseases, including neurodevelopmental, neuropsychiatric, as well as neurodegenerative disorders. Given the important role that DCVs and their cargo play in neuronal development and signaling, they have been studied in the context of schizophrenia, fragile X syndrome, Parkinson's disease, and AD(164-167). DCVs may also play a role in the pathology of Huntington's disease (HD), a progressive neurodegenerative disorder caused by a polyglutamine (polyQ) expansion in the Huntingtin (HTT) gene. A study examining the interaction between the Huntingtin (Htt) protein and DCVs in *Drosophila* larval motoneurons found that KO of Htt resulted in reduced retrograde DCV transport(168). This complements previous work investigating polyQ Htt, which demonstrated that the aberrant form of the protein inhibited BDNF vesicle movement.

Finally, a *C. elegans* model of amyotrophic lateral sclerosis (ALS) demonstrated a direct link between neuronal DCV signaling and innate immunity(169). Veriépé and colleagues (2015) showed that SV and DCV release from motoneurons expressing the mutant ALS genes TAR DNA binding protein 43 (TDP-43) or Fused in Sarcoma (FUS) were necessary for the activation of an innate immune pathway in intestinal and hypodermal cells (Fig. 7). In their model, SV and DCV exocytosis from motoneurons expressing the mutant ALS genes results in the activation of the toll interleukin-1 receptor signaling pathway, an ortholog of the mammalian Sarm1, in motoneurons and distal cells. In motoneurons, this results in degeneration, while in the intestinal and hypodermal cells it engaged an antimicrobial defense pathway, resulting in the upregulation of nlp-29, an antimicrobial peptide. Blocking DCV or SV release significantly diminished the amount of motoneuron degeneration and blocked the innate immune pathway activation in ALS mutant animals. Given the link between DCVs and various disease states, as well as findings in *Drosophila* implicating neuronal DCV release in glial activation, I was interested in further elucidating how these vesicles might function as a neuron-glia injury signal.

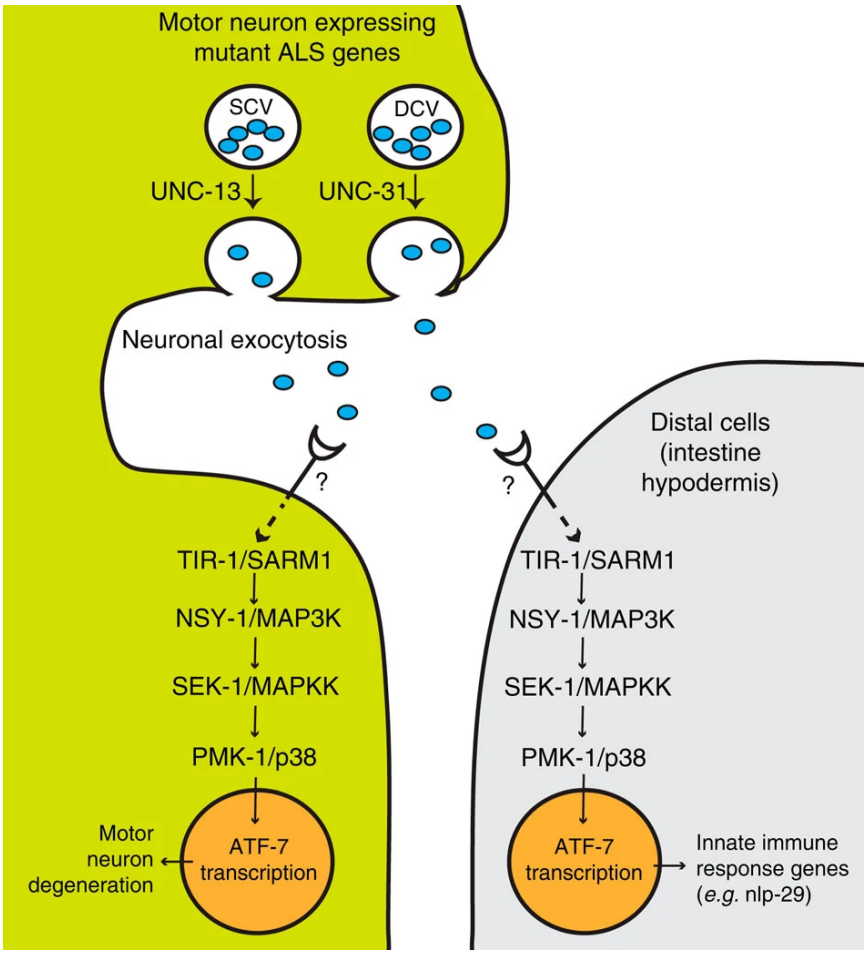

Figure 7: The role of DCVs in a *C. elegans* model of amyotrophic lateral sclerosis (ALS)
DCV and SV release from motoneurons expressing mutant ALS genes activates motoneuron degeneration and the innate immune response in distal cells through the Sarm1 pathway. Taken from Vériépe *et al*., 2015(169).

CHAPTER 2: EXAMINING THE ROLE OF NEURONAL DCV RELEASE IN THE GLIAL INJURY RESPONSE

Abstract

Glial cells play an essential role in maintaining neuronal health. Microglia function as the resident immune cells of the brain, they respond to pathogenic insults and degenerating neurons by becoming reactive and infiltrating areas of damage. Their ability to phagocytose and degrade neuronal debris has been demonstrated to confer neuroprotection at sites of injury. In the event of an axotomy, neurons signal through a variety of mechanisms, and initiate intracellular cascades to induce proliferation, cytoskeletal changes, and phagocytic activity. Studies in *Drosophila melanogaster* have aimed at elucidating the genetic and molecular changes enabling glia to become reactive. The glial engulfment receptor Draper is essential for initiation of cytoskeletal remodeling and phagocytic activity following axotomy, while the recently characterized matrix metalloproteinase-1 (Mmp-1) is required for extracellular matrix remodeling and glial clearance of neuronal debris. Despite these findings, less is known about the intrinsic axonal changes that occur in neurons to elicit glial responses. Questions remain regarding the signaling mechanisms used by neurons when they are injured, how such signals are released from severed projections, what prompts their release, and how these signals are transduced to produce glial responses. *Drosophila* serves as a tractable model to examine the pathways by which neurons signal to glia upon axotomy. We have previously demonstrated that neuropeptide-containing dense core vesicles (DCVs) are released from ORN projections following axotomy. This activates the insulin-like signaling (ILS) pathway, which elicits STAT92E-dependent draper upregulation. However, the role of DCVs in eliciting glial responses to injury are not fully understood.

Introduction

Glia are a vital cell type within the brain, carrying out essential and varied functions(2). While the complexity of neurons has been extensively studied, we are gaining increasing insight into the multitude of roles glial cells play in maintaining neuronal health and homeostasis, influencing action potential propagation and synaptic transmission, as well as responding to pathogens(170). In addition, upon neuronal injury and degeneration, glia are vital in conferring protection against neurotoxic inflammation and sequestering the area of damage to prevent further cell death(17, 171-175). In order to carry out these functions, glia become reactive and induce changes in gene expression, proliferation, cytoskeletal arrangement, motility, and phagocytic activity to clear axons undergoing degeneration(72, 174). Although we are broadening our insight into the role of glia in the nervous system, the signaling between neurons and glia following injury, as well as the transduction of these signals to elicit glial responses, remains elusive.

In our lab, we employ *Drosophila* as a model system to study conserved glial responses to injury(176, 177). This is possible, in part, due to the availability of a number of genetic tools, and our capability to visualize different populations of cells. The Drosophila CNS contains three major glial subtypes, which associate closely with neurons and carry out functions similar to mammalian glia(3). Astrocytes occupy the neuropil regions and play a role in modulating synaptic signaling. Ensheathing glia extend their processes along the neuropil and enwrap axonal projections, while cortex glia reside in the cortical regions of the *Drosophila* brain and surround neuronal cell bodies. The peripheral nerves of the fruit fly are covered by perineurial and subperineurial glia, along with wrapping glia, which extend around sensory and motor projections. In the context of injury, ensheathing glia have been found to be the principal phagocytic cell responsible for clearing cellular debris following axotomy(73).

The response of ensheathing glia to acute axotomy is regulated by a number of signaling cascades, which induce genetic and morphological changes to allow these cells destroy

structures such as damaged neurons or apoptotic cells(118, 122). Draper, an engulfment receptor expressed on ensheathing glia, but not astrocytes, is required for the initiation of cytoskeletal remodeling and phagocytic activity following axotomy(70). Downstream of the Draper receptor, the JNK signaling pathway activates AP-1 and STAT92E-dependent upregulation of transcriptional targets(72, 74, 178). Among these targets is draper, which is positively regulated through this cascade, as well as the recently characterized Mmp-1(77). The upregulation of both in ensheathing glia after injury has been found to be necessary for the clearance of severed axons. Despite our increasing knowledge of injury-activated glial pathways, further work is necessary to elucidate how canonical signaling mechanisms may act in parallel with, or converge on, novel pathways.

Previous work in our lab has implicated the ILS as a novel pathway regulating glial clearance of cellular debris following acute axotomy(132). A well characterized ORN injury paradigm was employed, where the *Drosophila* third antennal segments or maxillary palps are ablated to induce WD in the ORN projections(80). Due to the tractability of the *Drosophila* model system, degeneration of these axons can be visualized, while changes in glial molecular mechanisms can be characterized after injury. Musashe and colleagues (2016) found that, upon axotomy, the InR is activated and signals through Akt-1 to clear degenerating axons. This is achieved through STAT92E-dependent upregulation of Draper(132).

Injured neurons were hypothesized to release DCVs. These vesicles transport neuropeptides, including the activating ligands of the *Drosophila* InR: insulin-like peptides 1-8 (Ilps)(135, 142). Moreover, disruption of neuropeptide processing by proprotein convertase 2 (PC2) RNAi or perturbation of Ca^{2+}-dependent DCV release by knockdown of Ca^{2+}-activated protein for secretion (Caps) attenuates InR activation and reduces Draper levels in injured conditions(132). These results suggest a model in which DCVs play a role in neuron-glia signaling after ORN axotomy; however, the mechanisms and dynamics of this process have not yet been fully elucidated.

DCVs have been characterized in a number of cell types, ranging from neurons to neuroendocrine, endocrine, and hemopoietic cells(179). Their physiological functions are distinct and varied across these cell types. In neurons they play a role in the regulation of processes such as brain development and synaptic plasticity(180, 181). A study has also found that disruption of DCV release is associated with cognitive and mood disorders(182). DCVs are packaged at the TGN, where neuropeptides, neurotrophic factors, and monoamines are loaded into vesicles(137, 183). DCVs are then transported along the microtubule network by motor proteins to sites of release along axons and dendrites(147, 184-186). As with SVs, release of DCVs has been demonstrated to be mediated by Ca^{2+} influx; however, their release is not limited to the synapse(185, 187). Several studies have explored the mechanisms involved in DCV release, and specifically the Ca^{2+} sensing components of its release machinery(149, 160, 188). Among these proteins is Caps, which regulates Ca^{2+}-triggered exocytosis(157, 162). Upon Ca^{2+} entry, Caps is thought to dock DCVs at the plasma membrane and prime them for secretion by initiating SNARE complex assembly(156, 161). Although the mechanisms behind DCV exocytosis are well studied across species, their role in injury-mediated release remains elusive. In this chapter, we explore the role of DCVs in neuron-to-glia signaling following axotomy.

Results

DCVs are significantly reduced in injured ORNs along a time course

In order to assess DCV dynamics following ORN injury, we performed a unilateral antennal ablation and observed DCVs within ONR projections using two well-described markers of DCV cargo, atrial natriuretic peptide (ANF)-GFP and Ilp2-GFP(147, 189). Using the Gal-4/UAS system, DCV markers were expressed in a subset of ORNs, which were also labeled with tdTomato. This method allows for the detection of DCVs as GFP+ puncta in uninjured and injured ORNs within the same brain along a time course after antennal ablation. We find that ANF-GFP-labeled DCVs are reduced within injured projections starting at 30 minutes post-injury (mpi) although this is not

a significant reduction (Fig. 1A, B). However, at later timepoints after axotomy (75 and 120 mpi), DCVs are significantly decreased when compared to uninjured projections (Fig. 1A, B). These results are recapitulated using a separate DCV marker, Ilp2-GFP. Here, significant DCV reduction is already detected at the 30 mpi timepoint and DCV puncta within the injured projections are further reduced at 75 and 120 mpi (Fig. 2C, D). In the case of both markers, the number of DCVs per axon volume (μm^3) begins to plateau by 120 mpi. This could be explained by the use of non-endogenous DCV markers and the resulting high levels of ANF-GFP and Ilp2-GFP expression. Moreover, examination of later timepoints (4, 6, 8 hpi) after axotomy reveals that this plateau persists (data not shown).

To determine whether DCV reduction is axotomy-specific, we wanted to compare the quantity of another organelle in uninjured and injured ORNs. For this experiment, GFP-tagged mitochondria were expressed in a subset of projections and a unilateral antennal ablation was performed (Fig. 2C). We found that mitochondria are not reduced as a result of injury at a timepoint where we detect significant DCV reduction, 2 hours post-injury (hpi) (Fig. 2D). Taken together, these results indicate that DCVs are reduced from ORNs in an injury-dependent manner, suggesting that DCV contents may be released from neurons after axotomy. Although the injury model in the brain allows us to assay snapshots of DCV behavior, it is not particularly amenable to live imaging and observation of post-axotomy DCV dynamics. For this reason, we turn to the *Drosophila* wing.

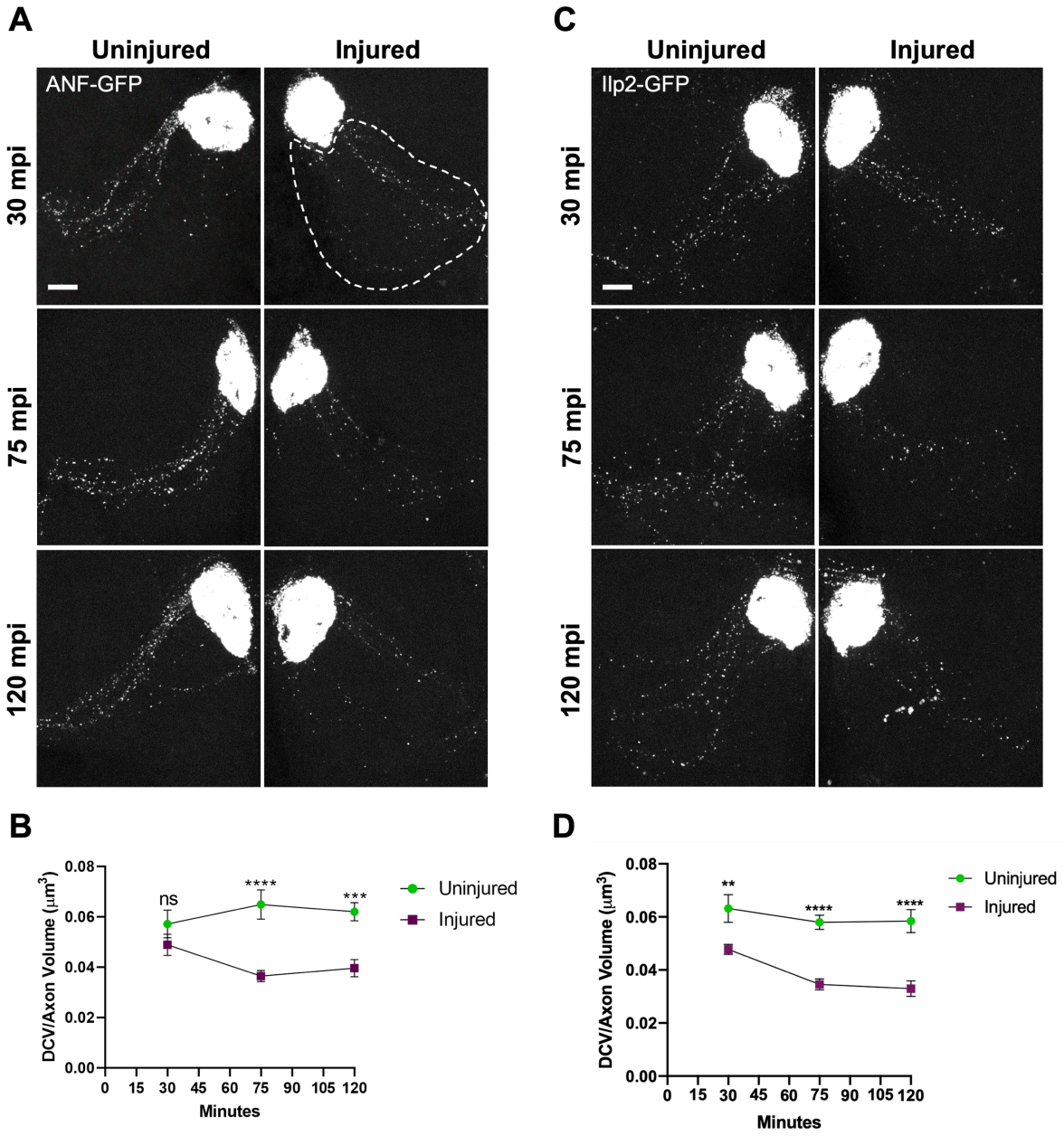

Figure 1: DCVs are reduced in injured ORN projections

(A) Representative images of ANF-GFP labeled DCVs in a subset of uninjured and injured (unilateral antennal; 30, 75, 120 mpi) ORN projections from the same brain. Images are maximum intensity projections (MIPs): 25 µm. Scale bar: 10 µm. Genotype: UAS-ANF-GFP/+ or Y;+/+;Or22a-Gal4, 10X-UAS-myr-tdTomato/+ **(B)** Quantification of ANF-GFP puncta within ORN projection volumes (μm^3; dotted area in Fig. 3A). 30 min uninjured (n=9), 30 min injured (n=10), 75 min uninjured (n=11), 75 min injured (n=12), 120 min uninjured (n=12), 120 min injured (n=12). Mean ± SEM. Two-way ANOVA (Sidak's *post hoc* test). Ns: non-significant, ***p<0.001, ****p<0.0001. **(C)** Representative images of Ilp2-GFP labeled DCVs in a subset of uninjured and injured (unilateral antennal; 30, 75, 120 mpi) ORN projections from the same brain. Images MIPs: 25 µm. Scale bar: 10 µm. Genotype: ;UAS-Ilp2-GFP/+;Or22a-Gal4, 10X-UAS-myr-tdTomato/+ **(D)** Quantification of Ilp2-GFP puncta within ORN projections volumes. 30 min uninjured (n=12), 30 min injured (n=12), 75 min uninjured (n=13), 75 min injured (n=13), 120 min uninjured (n=11), 120 min injured (n=10). Mean ± SEM. Two-way ANOVA (Sidak's *post hoc* test). **p<0.01, ****p<0.0001.

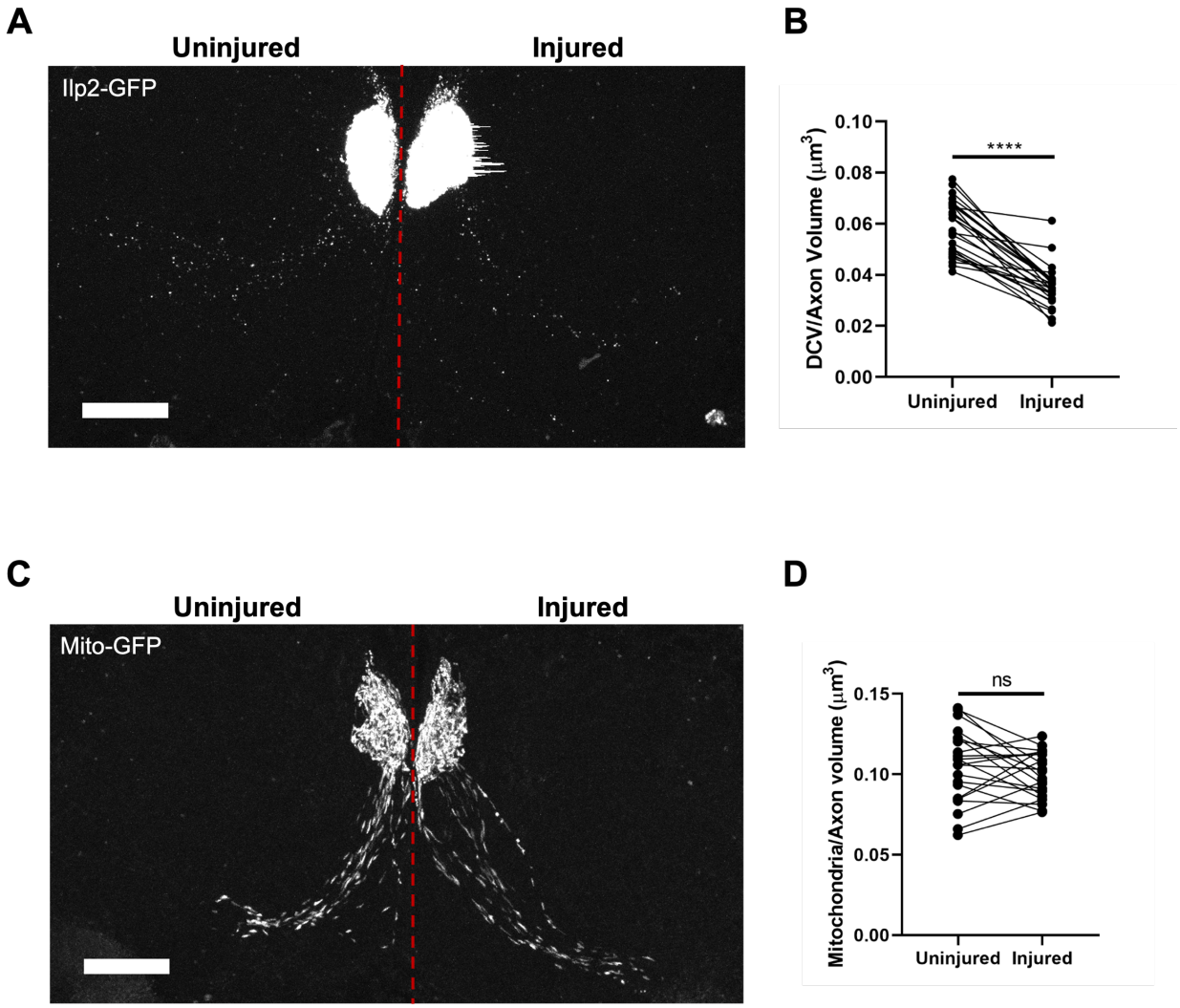

Figure 2: DCV reduction in ORNs is axotomy-specific
(A) Representative image of Ilp2-GFP labeled DCVs in a subset of uninjured and injured (unilateral antennal; 2 hpi) ORN projections from the same brain. Images are MIPs: 25 µm. Scale bar: 20 µm. Genotype: ;UAS-Ilp2-GFP/+;Or22a-Gal4, 10X-UAS-myr-tdTomato/+. **(B)** Quantification of Ilp2-GFP puncta within ORN projection volumes (μm^3). Uninjured (n=26), injured (n=26). Individual data points. Paired *t*-test. ****p<0.0001. **(C)** Representative images of mito-GFP labeled mitochondria in a subset of uninjured and injured (unilateral antennal; 2 hpi) ORN projections from the same brain. Images are MIPs: 25 µm. Scale bar: 20 µm. Genotype: ;UAS-mito-HA-GFP/+;Or22a-Gal4, 10X-UAS-myr-tdTomato/+. **(D)** Quantification of mito-GFP within ORN projection volumes (μm^3). Uninjured (n=22), injured (n=22). Individual data points. Paired *t*-test. Ns: non-significant.

Live imaging reveals that neuronal DCV movement is halted following axotomy in the fly wing

A well-described injury model exists in the fruit fly wing, whereby mechanosensory neurons can be severed and undergo the conserved process of WD(75, 190, 191). The cell bodies of these neurons are present along the L1 vein of the wing, and they send their projections into the thorax of the fly (Fig. 3A). As a result, cuts made to the wing will injure some projections, but not others, depending on the site of the cut and the site of imaging. By using a motoneuron-specific driver, OK371-Gal4, we are able to express tdTomato to visualize the neurons, along with the DCV marker, Ilp2-GFP, and observe DCV dynamics in uninjured and injured wings. Live imaging can be performed through the cuticle of the wing by sticking the body of the fly to a coverslip with UV polymerizable glue and spreading the wing in halocarbon oil against the coverslip.

In an uninjured wing, we find that DCV movement is dynamic within neuronal projections and is observable in the anterograde and retrograde direction, as previously reported in the literature (Fig. 3C). However, when the wing is cut, DCV movement is almost immediately halted at 5 mpi (approximately the time it takes to cut the wing and take the preparation to the microscope for imaging) (Fig. 3D). Moreover, when examining a later timepoint after injury (60 mpi), movement remains halted (Fig. 3E). When assessing these videos, it is also interesting to note that DCV movement is halted in both in injured and uninjured projections. Near the site of the cut at 5 mpi, we observe that DCVs in intact projections have stopped trafficking (Fig. 3D; yellow arrowhead). This result is recapitulated at a later timepoint, 60 mpi, more distal to the cut site (Fig. 3E; yellow arrowhead). Previous work by Hsu and colleagues (2020) has demonstrated that the movement of other vesicles and organelles is halted in response to injury of the fly wing, in both uninjured and injured mechanosensory neurons, and this is mediated by the wrapping glia surrounding the glutamatergic projections(192). These results, coupled with the reduction of DCVs in our static imaging experiments, lead us to hypothesize that DCVs may be released from projections following axotomy as an injury signal to the surrounding glia.

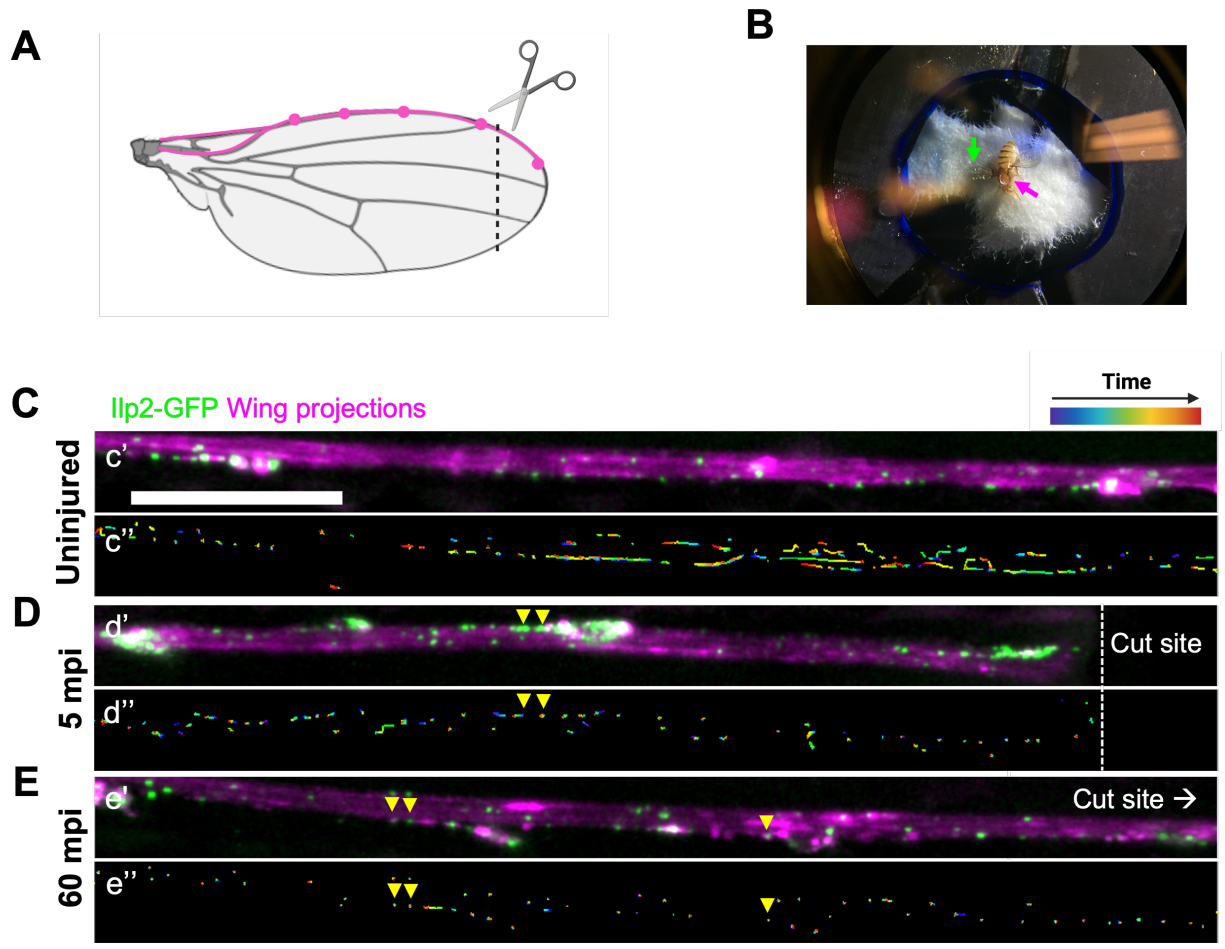

Figure 3: DCV movement is halted in neuronal projections following axotomy
(A) Schematic of wing injury. Glutamatergic projections in the L1 vein of the wing are labeled using tdTomato. Cell bodies of neurons are distributed along the length of the L1 vein. Created using Biorender.com **(B)** Example of wing live imaging set-up. Fly affixed to coverslip using UV polymerizable glue (magenta arrow) with wing spread against coverslip in halocarbon oil (green arrow). **(C-E)** Ilp2-GFP labeled DCVs in tdTomato-labeled glutamatergic projections of the wing. Still frames from live imaging videos. C: 1 min, 52sec. D: 2 min, 18sec. E: 2 min, 18sec. Yellow arrowheads indicate halted DCVs in uninjured projections. MIPs: 3.04µm. Scale bar: 20µm. Genotype: ;OK371-Gal4, UAS-Ilp2-GFP, 10X-UAS-myr-tdTomato/+; **(c-e'')** Time lapse tracking of DCVs within neuronal projections. Heat map corresponds to movement of DCVs through time. **(c')** Uninjured wing. **(d')** Injured wing, 5 mpi. White dotted line indicates cut site. **(e')** Injured wing, 60 mpi. Image taken distal to cut site.

The role of Ca^{2+} in DCV release and WD

Ca^{2+} entry into an injured neuron is required to initiate the process of WD, while it is also necessary for DCV release under physiological conditions(106, 156). The expression of Wlds blocks axonal fragmentation following axotomy by increasing the Ca^{2+} buffering capacity of mitochondria(193). As a result, we were interested in examining the result of Wlds expression in ORNs on DCV number after an injury event. The expression of Wlds in a subset of ORNs results in axon fragmentation being blocked 24 hpi (Fig. 4A). We hypothesized that by buffering Ca^{2+}, Wlds would block the DCV reduction we observe following axotomy. Previous work in zebrafish has demonstrated that there are two waves of Ca^{2+} entry into injured neurons: immediately after axotomy, and just preceding fragmentation(105). Therefore, we selected timepoints with significant DCV reduction following antennal injury and before fragmentation, which occurs at 6-8-hpi in flies.

Surprisingly, Wlds expression in ORNs did not block DCV reduction after injury at any of the timepoints assayed. DCVs were reduced to similar levels in both controls and Wlds-expressing neurons (Fig. 4B). There is evidence to suggest that the effects of Wlds are dose-dependent, and it would be interesting to examine how DCV number would be affected with the expression of an additional copy of Wlds(194, 195). Moreover, it would be important to assess the time course of Ca^{2+} entry into injured projections, as well as the effects of Wlds on Ca^{2+} spikes after injury. There is conflicting evidence as to whether the initial Ca^{2+} increase after axotomy, or the one immediately preceding fragmentation, is blocked by Wlds expression, depending on the model organism(105, 193). Another approach would be to express a selective blocker of DCV release in ORNs to observe the effect on DCV reduction after injury. A tool that could be used is Caps RNAi, which is thought to perturb the Ca^{2+}-sensing component of the DCV release machinery(147, 156).

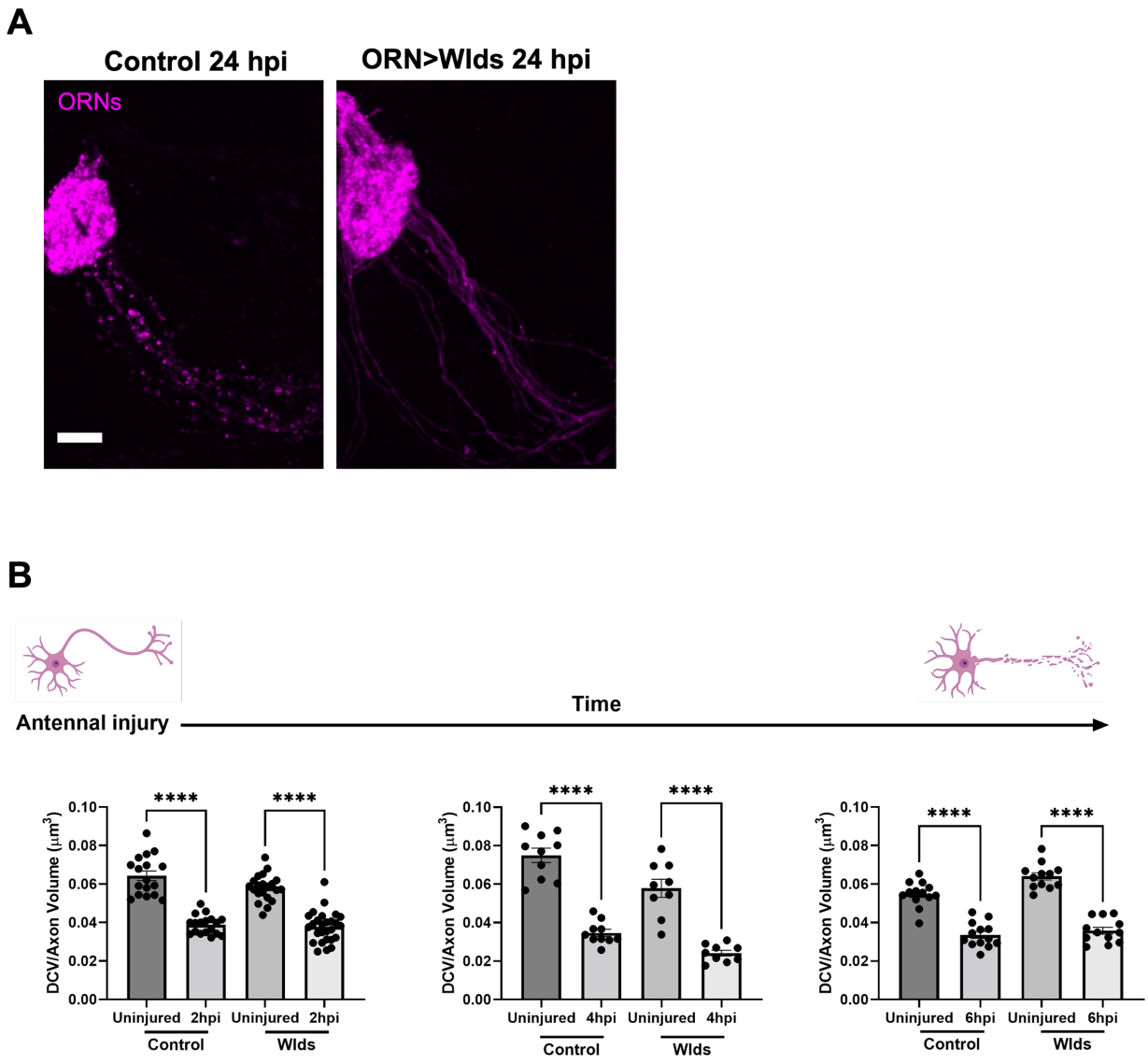

Figure 4: Wlds expression in ORNs does not block DCV reduction following injury
(A) Expression of Wlds in ORNs blocks fragmentation of axonal projections 24 hpi (antennal). Images are MIPs: 31 µm. Scale bar: 10 µm. Control genotype: ;UAS-Ilp2-GFP/elav-LexA;Or22a-Gal4, 10X-UAS-myr-tdTomato/+. Wlds genotype: ;UAS-Ilp2-GFP/elav-LexA;Or22a-Gal4, 10X-UAS-myr-tdTomato/Aop-Wlds. **(B)** Quantification of Ilp2-GFP puncta within ORN projection volumes (μm^3). 2 hpi: control uninjured (n=17), control injured (n=18), Wlds uninjured (n=21), Wlds injured (n=27). 4 hpi: control uninjured (n=10), control injured (n=10), Wlds uninjured (n=9), Wlds injured (n=9). 6 hpi: control uninjured (n=13), control injured (n=13), Wlds uninjured (n=12), Wlds injured (n=12). Mean ± SEM. One-way ANOVA (Sidak's *post hoc* test). ****p<0.0001. Created using Biorender.com

The ILS pathway in glia regulates responses to neuronal injury

Work by a previous graduate student in the lab uncovered that the ILS pathway is engaged in glia in response to neuronal injury(132). In this model, the InR on ensheathing glia is activated by its ligands, Ilps, which results in phosphorylation and the downstream activation of Akt and Stat92E (Fig. 5). This causes the upregulation of the well-described immune receptor, Draper, and the clearance of degenerating projections. As Ilps are the ligands of the InR and are packaged into DCVs as cargo, we posit that DCV release from injured neurons activates downstream immune signaling in the surrounding ensheathing glia. The involvement of DCV release in the context of brain development has been well-described; however, it has not yet been investigated as an injury signal from neurons to glial cells(180, 181). Musashe *et al*., 2016 began to uncover the role of DCV release in glial immune regulation, finding that perturbation of DCV release results in a significant attenuation of InR phosphorylation and Draper upregulation, pointing to DCV release as an injury signal from neurons.

Moreover, our lab has recently shown that Mmp-1 upregulation is also required by glial cells to infiltrate areas of damage and clear axonal debris(77). Mmp-1 is a secreted protein, which has been demonstrated to clear ECM and is robustly upregulated in ensheathing glia by 3 hpi at the mRNA and 24 hpi at the protein level(77, 196, 197). As a result, we wanted to examine whether the Mmp-1 response was regulated by the ILS pathway, downstream of the InR. To do this, we expressed the dominant negative form of the InR (dnInR) in all glial cells in a temporally restricted manner (using Gal80ts) and induced a maxillary palp injury. In injured control brains, Mmp-1 is robustly upregulated in the location of maxillary palp glomeruli of the ALs (Fig. 6A). However, in brains with glia expressing the dnInR, the Mmp-1 response was noticeably diminished (Fig. 6A). When the Mmp-1 fluorescence was quantified withing a region of interest (ROI) of the ALs and normalized to uninjured controls, we found that the Mmp-1 response is significantly attenuated (Fig. 6B). This data suggests that the ILS is involved in Mmp-1 regulation in ensheathing glia following ORN injury.

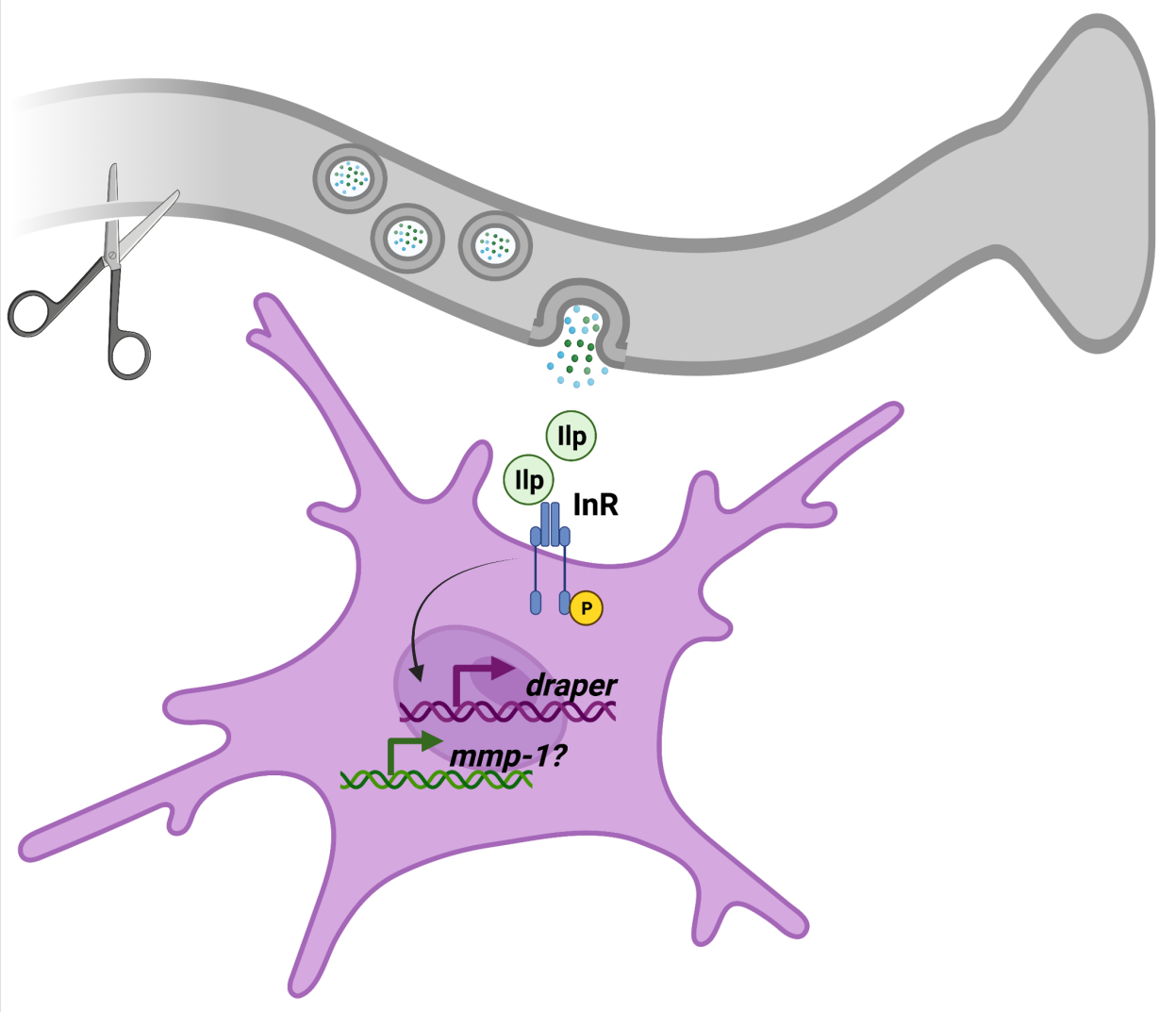

Figure 5: The ILS pathway is engaged in glia following neuronal injury
InR pathway schematic adapted from Musashe *et* al., 2016(132). Previous research has demonstrated that ensheathing glial InR activation after neuronal injury results in the upregulation of the well-described immune gene *draper*. The ligands of the InR, insulin-like peptides (Ilps), result in InR phosphorylation and activation of downstream signaling. Created using Biorender.com

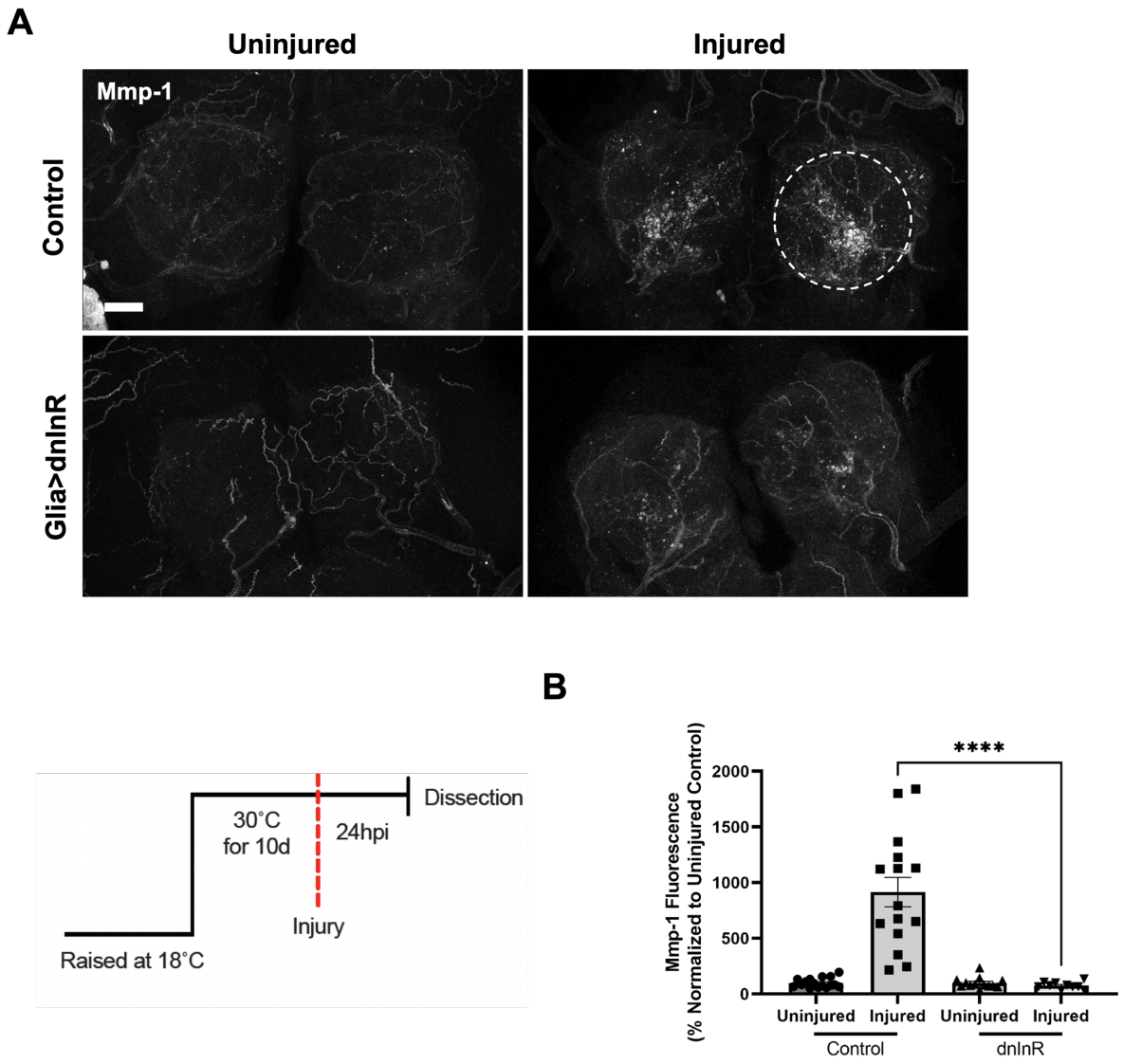

Figure 6: The ILS pathway is involved in Mmp-1 regulation in ensheathing glia following axotomy. **(A)** Representative images of Mmp-1 immunostaining in uninjured and injured (maxillary palp; 24 hpi) antennal lobes (ALs). Dotted circle represents ROI used for quantification. Images are maximum intensity projections (MIPs): 25 µm. Scale bar: 20 µm. Control genotype: ;Or85e-mCD8-GFP, tub-Gal80ts/+;repo-Gal4/+. dnInR genotype: ;Or85e-mCD8-GFP, tub-Gal80ts/+;repo-Gal4, InR^{ex15}/UAS-dnInR. Flies were raised at 18˚C and moved to 30˚C for 10 days before injury. They were maintained at 30˚C for 24 hpi until dissection. **(B)** Quantification of Mmp-1 fluorescence normalized to uninjured controls and represented as a percentage. Control uninjured (n=16), control injured (n=15), dnInR uninjured (n=13), dnInR injured (n=10). Mean ± SEM. One-way ANOVA (Sidak's *post hoc* test) ****p<0.0001.

DCV release is required for upregulation of the glial immune gene Mmp-1

Next, we wanted to determine whether DCV release from injured neurons was required for Mmp-1 regulation in glia. Few tools exist for the specific perturbation of DCV release, and among the best characterized is the disruption of the Ca^{2+}-sensing component of the DCV release machinery: Caps. Caps localizes to DCVs and initiates SNARE complex assembly, and thus the release of DCV cargo (e.g., Ilps) by full-fusion or kiss-and-run fusion events (Fig. 7A)(156, 159, 198). To test whether DCV release is functioning as a signal from injured ORNs to glia, we expressed a previously described Caps RNAi transgene using a pan-ORN driver in a temporally restricted manner. 24 hours post maxillary palp injury, we find that there is very little Mmp-1 expression within injured ALs of Caps RNAi expressing brains, as compared to controls (Fig. 7B). The significant attenuation of the glial Mmp-1 response is evident when the fluorescence is quantified within ROIs, highlighting that DCV release from ORNs is required to elicit a robust Mmp-1 response after injury (Fig. 7C).

We wanted to use a separate tool to validate our Caps RNAi results, but due to the limited number of methods to block DCV release, we turned to a more widespread approach: the expression of tetanus toxin light chain (TeTXLC) in ORNs. This method blocks all SNARE-dependent exocytosis, including SV and DCV release(199). Due to the detrimental effects of blocking vesicle release on a large scale, we induced the expression of TeTXLC for only 24hrs. Then, we evaluated the glial expression of both Drpr and Mmp-1 following ORN axotomy and found that the expression of TeTXLC in projections results in significantly attenuated responses for both proteins (Fig. 8C). Taken together, these results suggest that DCV-mediated signaling from injured projections is required for the adequate upregulation of immune genes in ensheathing glia.

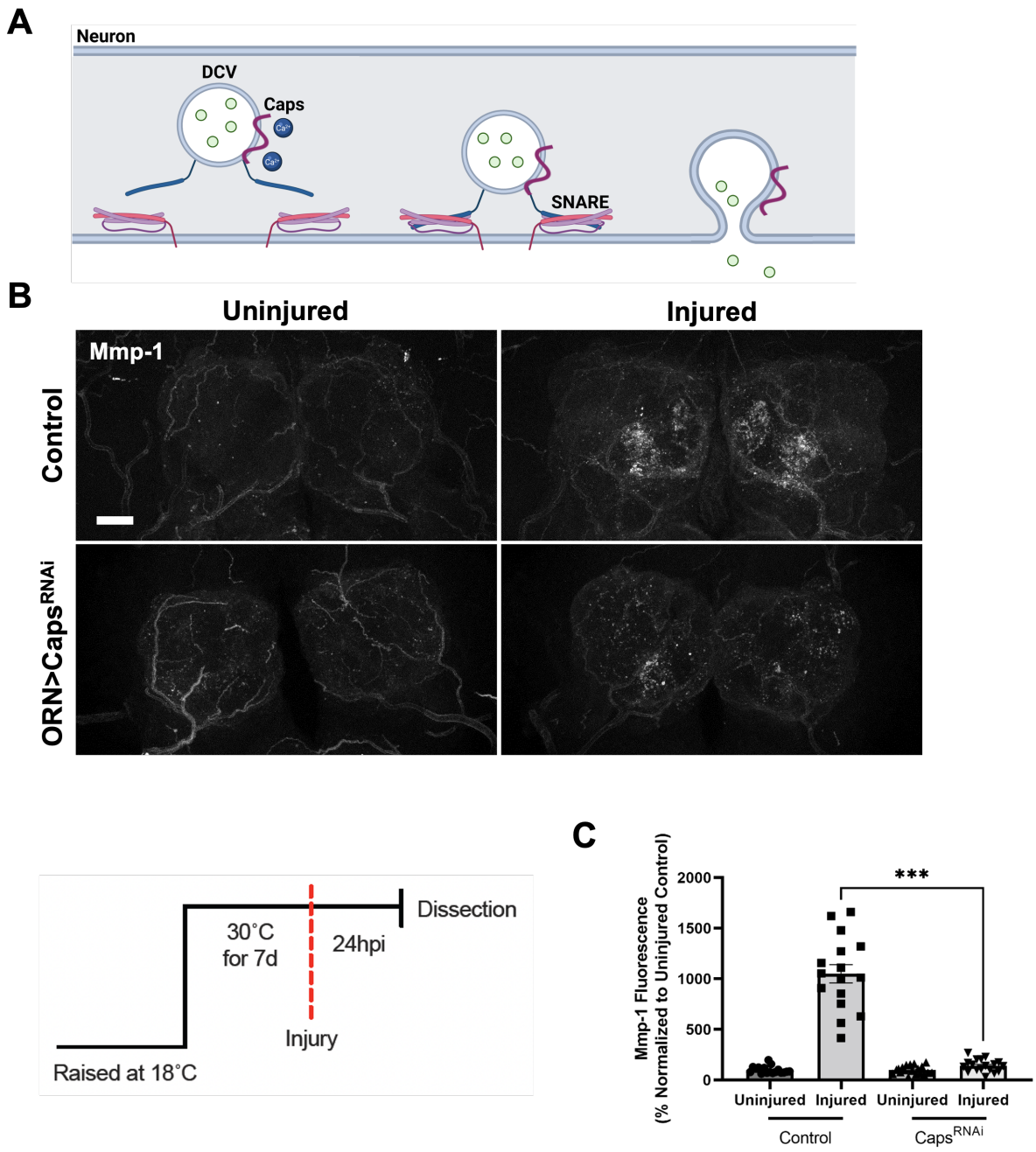

Figure 7: Perturbation of DCV release results an in attenuated glial response following injury.
(A) Schematic representation of DCV release from neurons in response to calcium (Ca^{2+}). Caps: Calcium-activated protein for secretion. Created using Biorender.com **(B)** Representative images of Mmp-1 immunostaining in uninjured and injured (maxillary palp; 24hpi) ALs. Images are MIPs: 25 µm. Scale bar: 20 µm. Control genotype: pebbled-Gal4/+ or Y;+/+;tub-Gal80ts, UAS-Dicer2/+. ORN>$Caps^{RNAi}$ genotype: pebbled-Gal4/+ or Y;UAS-$Caps^{RNAi}$/+;tub-Gal80ts, UAS-Dicer2/+. Flies were raised at 18˚C and moved to 30˚C for 7 days before injury. They were maintained at 30˚C for 24 hpi until dissection. **(C)** Quantification of Mmp-1 fluorescence normalized to uninjured controls and represented as a percentage. Control uninjured (n=12), control injured (n=17), $Caps^{RNAi}$ uninjured (n=17), $Caps^{RNAi}$ injured (n=19). Mean ± SEM. One-way ANOVA (Sidak's *post hoc* test) ****p<0.0001.

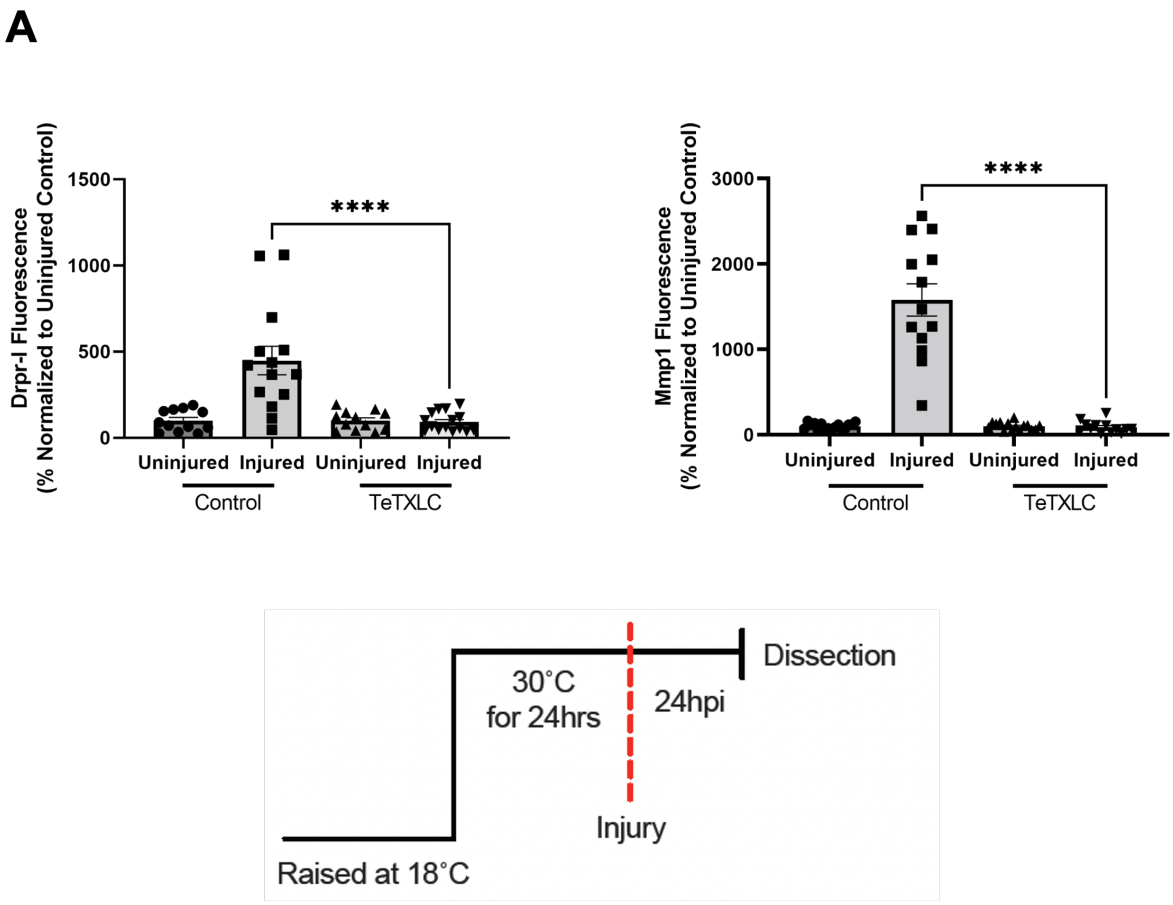

Figure 8: Perturbation of DCV and SV release results in attenuated glial response after injury. **(A)** Quantification of Draper-I (Drpr-I) and Mmp-1 fluorescence in uninjured and injured (maxillary palp; 24hpi) brains following tetanus toxin light chain (TeTXLC) expression in ORNs. Normalized to uninjured controls and represented as a percentage. Control genotype: pebbled/+ or Y;+/+;tub-Gal80ts/+. Flies were raised at 18˚C and moved to 30˚C for 24hrs before injury. They were maintained at 30˚C for 24hpi until dissection. TeTXLC genotype: pebbled/+ or Y;UAS-TeTXLC/+;tub-Gal80ts/+. Drpr-I: Control uninjured (n=12), control injured (n=14), TeTXLC uninjured (n=12), TeTXLC injured (n=15). Mean ± SEM. One-way ANOVA (Sidak's *post hoc* test) ****p<0.0001. Mmp-1: Control uninjured (n=16), control injured (n=13), TeTXLC uninjured (n=15), TeTXLC injured (n=13). Mean ± SEM. Kruskal-Wallis test (Dunn's *post hoc* test) ****p<0.0001.

Perturbation of DCV release disrupts ORN clearance by glia

The ultimate result of immune gene upregulation by glia is the phagocytosis and destruction of degenerating neuronal projections that result from an ORN injury. Given our findings that DCVs mediate neuron-glia communication following axotomy, we hypothesized that perturbation of DCV release would disrupt the process of ORN clearance by glia. To evaluate our hypothesis, we performed a clearance assay of the ALs, whereby we can use a presynaptic active zone antibody (Brp/nc82) to quantify ORNs that are present before and after an injury. In this experiment, we induced a maxillary palp and antennal injury, effectively severing all ORNs, and observed the presence of presynaptic sites in the ALs 6 dpi. In controls, ORNs were largely cleared by glia at the 6-day timepoint; however, when DCV release was perturbed by Caps RNAi, glia failed to clear projections to the same levels as controls (Fig. 9A). This was evident when the Brp staining was quantified across multiple brains, demonstrating that disruption of DCV release from injured neurons causes a deficit in the clearance capacity of glial cells (Fig. 9B). In conclusion, we find that DCV release appears to contribute to glial immune gene upregulation after axotomy, and their removal of projections undergoing degeneration.

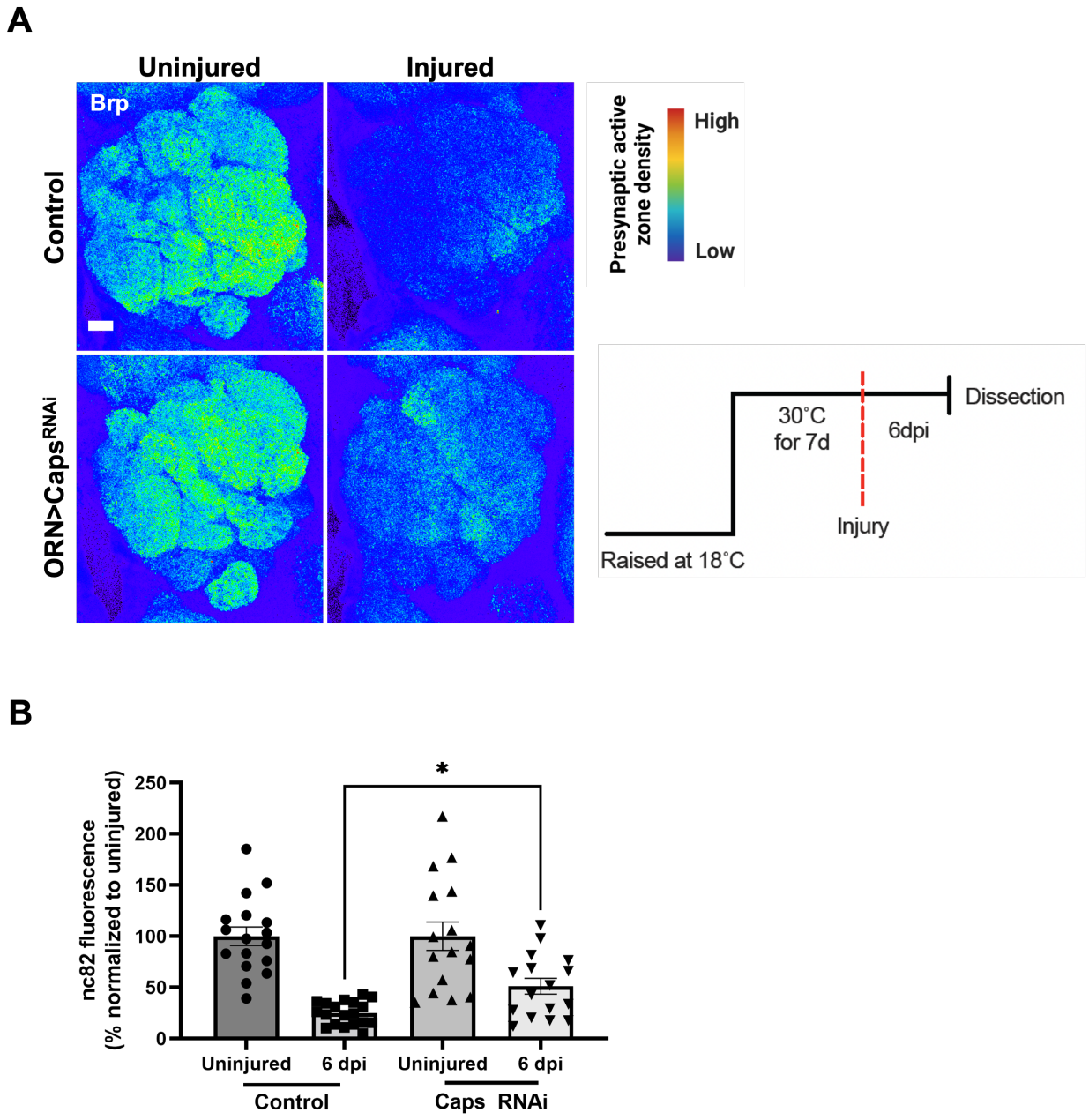

Figure 9: Perturbation of DCV release disrupts glial clearance of injured ORNs.
(A) Representative images of Bruchpilot (Brp) immunostaining in single ALs of uninjured and injured (antennal and maxillary palp; 6 dpi) brains. Brp staining indicates presynaptic active zones. Images are MIPs: 25 µm. Scale bar: 10 µm. Control genotype: pebbled-Gal4/+ or Y;+/+;tub-Gal80ts/+. ORN>Caps^{RNAi} genotype: pebbled-Gal4/+ or Y;UAS-Caps^{RNAi}/+;tub-Gal80ts, UAS-Dicer2/+. Flies were raised at 18˚C and moved to 30˚C for 7 days before injury. They were maintained at 30˚C for 6 dpi until dissection. **(B)** Quantification of Brp fluorescence within ALs. Normalized to uninjured controls and represented as a percentage. Control uninjured (n=17), control injured (n=19), Caps^{RNAi} uninjured (n=16), Caps^{RNAi} injured (n=16). Mean ± SEM. One-way ANOVA (Sidak's *post-hoc* test) *p<0.05.

Supplemental Results

Due to the lack of tools available to block DCV release, we have also generated fly lines with various point mutations in the C2 domain of Caps, aiming to make dominant negative constructs that could be used along with Caps RNAi. The C2 domain of Caps is vital for its dimerization at the vesicle membrane(155). These constructs were based on previous work by Petrie *et al*., 2016, where the researchers showed that a C2 domain deletion and point mutations in the C2 domain resulted in a loss of DCV exocytosis function in PC12 cells(200). Based on these findings, we made L → E and G → E point mutation constructs at positions 468 and 476, respectively, with the help of Amy Sheehan from the Freeman lab. Both point mutations constructs were expressed in ORNs and evaluated for effects on the Mmp-1 response following maxillary palp injury. The LE point mutation did not influence the Mmp-1 response, while the GE point mutation resulted in a very modest attenuation compared to a WT Caps control in pilot experiments; however, these results will need to be substantiated. These fly lines have also been shared with our collaborator, Edwin Levitan at the University of Pittsburgh, who will evaluate the effect of the point mutations on DCV release at the larval NMJ, where fluorescent tools can be used to measure levels of DCV release. Finally, we aim to generate a C2 deletion construct in the future to evaluate its ability to phenocopy our Caps RNAi results presented in this chapter.

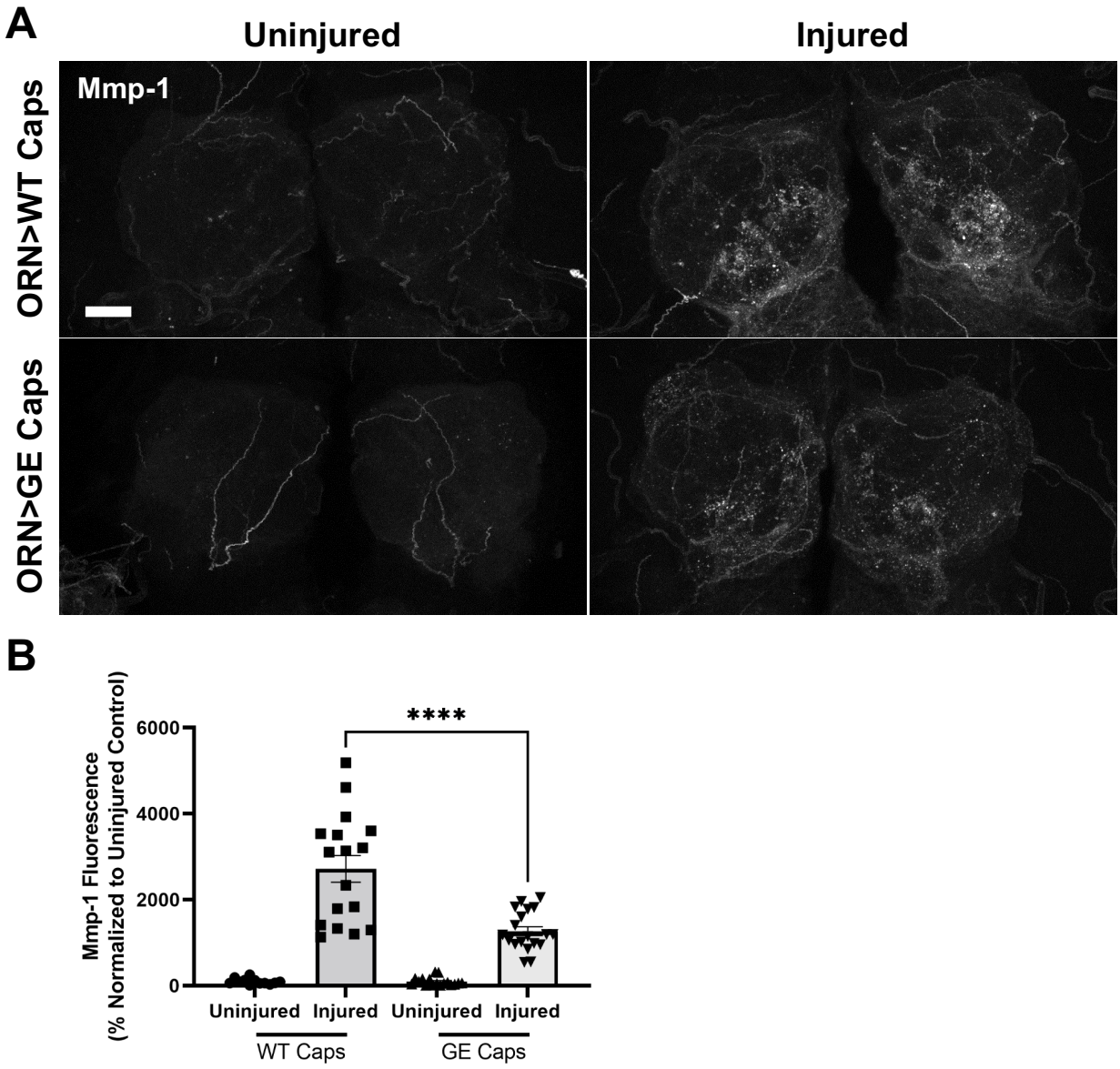

Supplementary Figure 1: Perturbation of DCV release from neurons attenuates Mmp-1 response in glia following axotomy.
(A) Representative images of Mmp-1 immunostaining in uninjured and injured (maxillary palp; 24 hpi) ALs. Images are MIPs: 31 µm. Scale bar: 20 µm. WT Caps genotype: pebbled-Gal4/+ or Y;UAS-WT Caps/+;tub-Gal80ts/+. GE Caps genotype: pebbled-Gal4/+ or Y;UAS-GE Caps/+;tub-Gal80ts/+. **(B)** Quantification of Mmp-1 fluorescence normalized to uninjured controls and represented as a percentage. WT Caps uninjured (n=17), WT Caps injured (n=16), GE Caps uninjured (n=19), GE Caps injured (n=18). Mean ± SEM. Kruskal-Wallis test (Dunn's *post hoc* test) ****p<0.0001.

Discussion

Much of the work in this chapter has focused on elucidating the signaling mechanisms that connect neurons and glia following an axonal injury, specifically how neurons signal to glia, and how glia transduce those signals to elicit the appropriate immune responses. In this chapter, we have added to the growing evidence that DCV exocytosis serves as an injury signal from injured neurons to glial cells. We find through our static imaging experiments that DCVs are reduced in injured olfactory projections within the ALs of the central brain over a time course after injury. Moreover, we posit that this reduction corresponds to DCV release, as opposed to trafficking away in the axon, due to halting of DCV movement observed by live imaging in wing axons following injury. We hypothesize that DCVs are halted and primed for release from injured projections after an axotomy. Ascertaining DCV exocytosis in the context of injury is an ongoing effort within the lab, as only few tools exist to accurately assess DCV release *in vivo*. In the appendix of this thesis, I detail the work that has been completed to build a new tool to examine DCV release within the intact fly brain and allow for a better investigation of our hypothesis.

Future experiments examining DCV release from injured neurons should test whether the reduction of DCVs from ORNs following axotomy can be blocked using the tools available to perturb DCV release (e.g., Caps RNAi, dnCaps, TeTXLC). We initially tested whether Wlds could potentially block the reduction of DCVs in our unilateral ORN ablation assay. However, we found that using only the Gal-4/UAS system results in titration, and a reduction in DCV numbers even in uninjured projections, compared to controls without the Wlds transgene. In the experiment presented in this chapter, we turned to adding the LexA/Aop system for the expression of Wlds; although, one copy of the gene did not affect DCV reduction following injury. It would be interesting to test the addition of multiple copies of Wlds, as mentioned earlier, or the use of different tools, such as Caps RNAi, the dnCaps constructs, or TeTXLC, for their ability to block DCV reduction after injury in the LexA system. Such experiments could further bolster our argument that DCV reduction from ORNs can be tied to vesicular release following neuronal injury.

Furthermore, new evidence suggests that DCV-associated small GTPases, namely Rab2 and Arl8, regulate DCV transport within axons. Using *Drosophila* larvae, Lund *et al*., 2021 found that Rab2 localizes to DCVs to interact with the motor protein complex(201). The researchers found that Rab2 was required for bidirectional axonal transport of DCVs, while Arl8 was also required for transport, it was also necessary for the entry of DCVs into the axonal compartment. These findings, along with our novel dnCaps constructs that are currently being tested, could add to the genetic toolkit available to perturb DCV trafficking and release.

Examining the downstream effects of DCV release from injured neurons, our results indicate that, through the ILS pathway, DCVs regulate the ability of glia to upregulate Mmp-1 and properly infiltrate areas of damage to clear degenerating projections. Although the role of DCVs in modulating Draper upregulation has been previously established, we provide novel evidence for their role in regulating a secreted immune molecule following ORN axotomy(132). We found that perturbing DCV release from neurons had a significant impact on Draper and Mmp-1 upregulation in glia at the protein level. However, our lab is also interested in teasing apart how glial responses to injury are regulated at the transcriptional and translation level. It is known that mRNA and protein expression are not always correlated, and there are multiple levels of regulation within cells in response to various stimuli. Is DCV release required for certain steps of immune gene upregulation in glia, but not others? Are different injury signals responsible for changes in transcription, translation, and localization of glial immune genes? How may these processes be altered in disease states or aging?

To address some of the aforementioned questions, we have adapted a novel fluorescence *in situ* hybridization (FISH) method for the *Drosophila* brain, with which we can detect immune transcripts and their associated ribosomes. In the next chapter (Chapter 3) of this dissertation, I will detail this new method, named FLARIM v2.0, and how it can provide us with interesting observations about glial biology and answers about these cells' response to neuronal injury. Moreover, in the conclusion of this dissertation (Chapter 4), I will explain how we have used this

novel method in preliminary experiments to further tease apart the role of DCV release in glial transcription and translation of immune genes.

Materials and Methods

ORN Axotomy Assay & Brain Dissection

For unilateral antennal ablation experiments, flies were anesthetized on a CO_2 pad and the right 3rd antennal segment of the fly was plucked using forceps as previously described(120). For all other ablation experiments, both antennae and/or maxillary palps were ablated (see figure legends for details). For dissections, fly heads were pulled and fixed in 4% PFA+0.1% TX for 20 min at RT on a rocker. Heads were then washed using 1X PBS-TX (0.01%) on a rocker at RT (3x2 min). Brains were dissected in 1X PBS-TX (0.1%). Brains were fixed in 4% PFA+0.1% TX for 20min at RT on a rocker. Then, brains were washed in 1X PBS-TX (0.1%) at RT on a rocker at RT (3x2 min). Brains were mounted in Vectashield (Vector Labs) under #1.5 coverslips and imaged.

Fly husbandry and temperature shift

Crosses were set up and flies were raised in 25˚C humidity-controlled incubators. Experiments requiring temporally restricted expression of transgenes contained tubulin-Gal80ts in their genetic background. These crosses were set up and raised at 18˚C. See figures and figure legends for details about specific experimental paradigms. Flies from 4-14 days post-eclosion (dpe) were used for experiments, except in the case of wing experiments, where 1dpe flies were used to avoid injury to wings during the life of the fly.

Wing Injury Assay & Live Imaging

To induce a wing injury, flies were anesthetized, and the wing was cut using Fine Science Tools scissors. For live imaging experiments, the abdomen of the fly was affixed to a #1.5 24x60 mm

coverslip using UV polymerizable glue. The wing was then spread out against the coverslip using a paintbrush dipped in halocarbon oil 27. The coverslip was placed in a magnetic imaging chamber and imaged.

Microscopy & Analysis

Samples were imaged on a Zeiss LSM 700 with a Zeiss 40X 1.4NA oil immersion plan-apochromatic lens. Brains within the same experiment were imaged on the same day, using the same microscope settings. Volocity 3D Image Analysis Software (Quorum Technologies) was used for DCV and mitochondria quantification within ORN volumes, as well as Mmp-1, Drpr, and Brp total fluorescence quantification within AL ROIs. Imaris Cell Imaging Software (Andor Technology) at the OHSU Advanced Light Microscopy Core (ALMC) was used for live image and motion tracking analysis in the wing. GraphPad Prism 8 (Graphpad Software) was used for statistical analysis: Student's t-test, One-way ANOVA (Sidak's *post hoc* test), Kruskal-Wallis test (Dunn's *post hoc* test), Two-way ANOVA (Sidak's *post hoc* test); see figure legends for details. Outliers were identified using the ROUT method (Q=1%). Normality of datasets was determined using the D'Agostino-Pearson normality test.

dnCaps Constructs

Point mutation and WT Caps constructs were synthesized with the help of S. Speese and A. Sheehan (Freeman Lab). Transgenic flies were generated by BestGene.

Antibodies

The following primary antibodies were used: mouse anti-Mmp-1 (3A6B4, 3B8D12, 5H7B11, 14A3D2; Developmental Studies Hybridoma Bank [DSHB]) at 1:50 each at a 1:1:1:1 ratio, mouse anti-Drpr (8A1 or 5D14; DSHB) at 1:400, mouse anti-nc82 (Bruchpilot; DSHB) at 1:50. All

secondary antibodies (Jackson ImmunoResearch: 715-545-151, 715-295-150) were used at a 1:400 dilution.

Drosophila stocks

UAS-ANF-GFP (X; BDSC 7001), UAS-Ilp2-GFP (II; gift from E. Levitan and D. Deitcher), Or22a-Gal4 (III; BDSC 9951), 10X-UAS-myr-tdTomato (III; BDSC 32221), UAS-mito-HA-GFP (II; BDSC 8442), OK371-Gal4 (II; BDSC 26160), 10X-UAS-myr-tdTomato (II; BDSC 32222), elav-LexA (II; BDSC 52676), Aop-Wlds (III; gift from M. Freeman), Or85e-mCD8-GFP (II; (202)), tubulin-Gal80ts (II; BDSC 7108), repo-Gal4 (III; BDSC 7415), InR^{ex15} (III; (203)), UAS-dnInR (III; BDSC 8253), pebbled-Gal4 (X; BDSC 80570), tubulin-Gal80ts (III; BDSC 7018), UAS-Dicer2 (III; gift from T. Lee), UAS-Caps RNAi (II; VDRC 110055), UAS-TeTXLC (II; BDSC 28838).

CHAPTER 3: FLARIM v2.0, AN ADAPTED METHOD TO QUANTIFY TRANSCRIPT-RIBOSOME INTERACTIONS *IN VIVO* IN THE *DROSOPHILA* BRAIN

Modified from: Richer, P., Speese, S.D., Logan, M.A. (2021) FLARIM v2.0, an improved method to quantify transcript-ribosome interactions *in vivo* in the *Drosophila* brain. bioRxiv. doi: https://doi.org/10.1101/2021.08.13.456301(204)

Abstract

Neural injury triggers striking immune reactions from glial cells, including significant transcriptional and morphological changes, but it is unclear how these events are coordinated to mount an effective immune response. Here, we present a new variant of the Fluorescence assay to detect ribosome interactions with mRNA (FLARIM), which we term FLARIM v2.0, to visualize single immune gene transcripts and association with ribosomes in glia responding to neurodegeneration. Specifically, using an *in vivo* axotomy assay in *Drosophila,* we show that matrix metalloproteinase-1 (Mmp-1) mRNAs and associated ribosomes are detected in distal processes of reactive glia where they are actively engulfing degenerating axonal material, suggesting that local translation is an important component of the glial immune response to axotomy. This work also validates our enhanced FLARIM assay as a promising tool to investigate mechanisms of mRNA transport and translation in a wide range of *in vitro* and *in vivo* paradigms.

Introduction

Glial cells respond swiftly to neuronal trauma, pathogenic insult, and degeneration(2, 170, 205). Following neuronal damage, activated glia undergo distinct transcriptional, morphological, and functional changes(173-175). In many cases, reactive glia are neuroprotective, releasing pro-survival factors and clearing damaged neurons through phagocytic engulfment(206, 207). Thus, understanding how glial immune responses are activated and carried out will offer new insight into approaches that could delay the onset or progression of a range of neurodegenerative disorders and injury conditions.

The fruit fly, *Drosophila melanogaster*, offers a powerful genetic *in vivo* model to explore evolutionarily conserved glia-neuron signaling events after neural injury(12, 117, 118). For example, after axotomy, adult *Drosophila* axons undergo a classic Wallerian degeneration (WD) program, and local glial cells display striking immune responses to invade injury sites and rapidly clear degenerating axonal material(70, 83, 103). Notably, nerve injury triggers robust transcriptional changes, including upregulation of the conserved glial engulfment receptor Draper and the secreted protease matrix metalloproteinase-1 (Mmp-1)(70, 72, 74, 77, 119, 122, 123, 178, 208).

Our lab has recently shown that upregulation of Mmp-1 is necessary for timely glial clearance of degenerating axonal projections in the olfactory system of adult flies(77). Mmp-1 is secreted from local ensheathing glial cells, likely to facilitate extracellular matrix remodeling, allowing glia to extend membrane processes into neuropil regions and clear degenerating olfactory receptor neuron axons(77, 197). Notably, the cell bodies of ensheathing glial cells responding to degenerating axons in the olfactory system do not enter neuropil regions, which raises interesting questions about how key immune molecules are released within the neuropil at injury sites(70, 73). Previous work in other model systems has indeed demonstrated that directed mRNA transport and local translation are important for glia to carry out normal functions. For example, in oligodendrocytes, myelin basic protein transcripts are localized to oligodendrocyte

processes to adequately myelinate axons in an activity-dependent manner, while astrocytes have been shown to influence interactions at tripartite synapses and the gliovascular interface through a subset of discrete localized and locally translated transcripts(209-213).

In order to further explore the transcriptional and translational changes that are essential for proper glial responses to damaged axons, our lab has utilized various single molecule fluorescence *in situ* hybridization (smFISH) techniques for the detection of individual transcripts and a new variation of Fluorescence assay to detect ribosome interactions with mRNA (FLARIM), referred to as FLARIM v2.0, to detect ribosome association with *mmp-1* transcripts in glial cells following nerve injury(214). smFISH has been employed in glial cells and various *Drosophila* tissues to detect individual mRNAs; however, previous studies have not yet employed mRNA and ribosome detection together in the context of neuronal injury *in vivo*(215-222). Here, we have utilized single molecule inexpensive FISH (smiFISH), hybridization chain reaction (HCR), and FLARIM, in order to visualize *mmp-1* transcript localization and translation in reactive glia following axotomy(214, 223-225). Our findings reveal that *mmp-1* transcripts are localized to and associate with ribosomes at distal glial processes at injury sites, suggesting that local translation of Mmp-1 may be an important mechanism by which glia access and phagocytically clear neuronal debris.

Results

Ensheathing glia respond to olfactory receptor neuron injury in *Drosophila*

Axotomy in the adult *Drosophila* antennal system is a well-characterized model to investigate the molecular and cellular underpinnings of axon degeneration and glial immune responses (Fig. 1A)(70, 226). The olfactory receptor neuron (ORN) cell bodies reside in the external olfactory organs of the fly, the antennae and maxillary palps, and project to the antennal lobes of the central brain, where they synapse onto second order neurons(20, 227). Surgical removal of the antennae and maxillary palps results in axotomy of the ORNs, which undergo

typical WD over the course of days, after which they are cleared by the surrounding glial cells(70, 120). In the antennal lobes, glial cell bodies (ensheathing glia and astrocytes) are located at the very edges of the antennal lobes and extend projections to closely associate with neuropil regions (axons, dendrites, and synapses) and demarcate olfactory glomeruli (Fig. 1B)(3, 12). In context of ORN injury, ensheathing glia have been demonstrated to phagocytose and clear degenerating projections(73).

Individual ensheathing glial cells have highly complex morphologies, with extensive fine processes that interact with multiple glomeruli within the antennal lobe (Fig. 1B, Supp. Fig. 1)(3, 228, 229). In the event of an injury, the cell bodies of ensheathing glia remain positioned at the outskirts of the antennal lobes, while the processes further invade glomeruli to clear degenerating ORNs(70, 73, 77). This raises the question of how intracellular signaling is mediated within ensheathing glial cells from the cell body to the distal processes after an injury event. In order to explore this question, we utilized multiple smiFISH methods to study how a well characterized immune gene, *mmp-1*, is localized and regulated at the transcriptional and translational level following ORN axotomy.

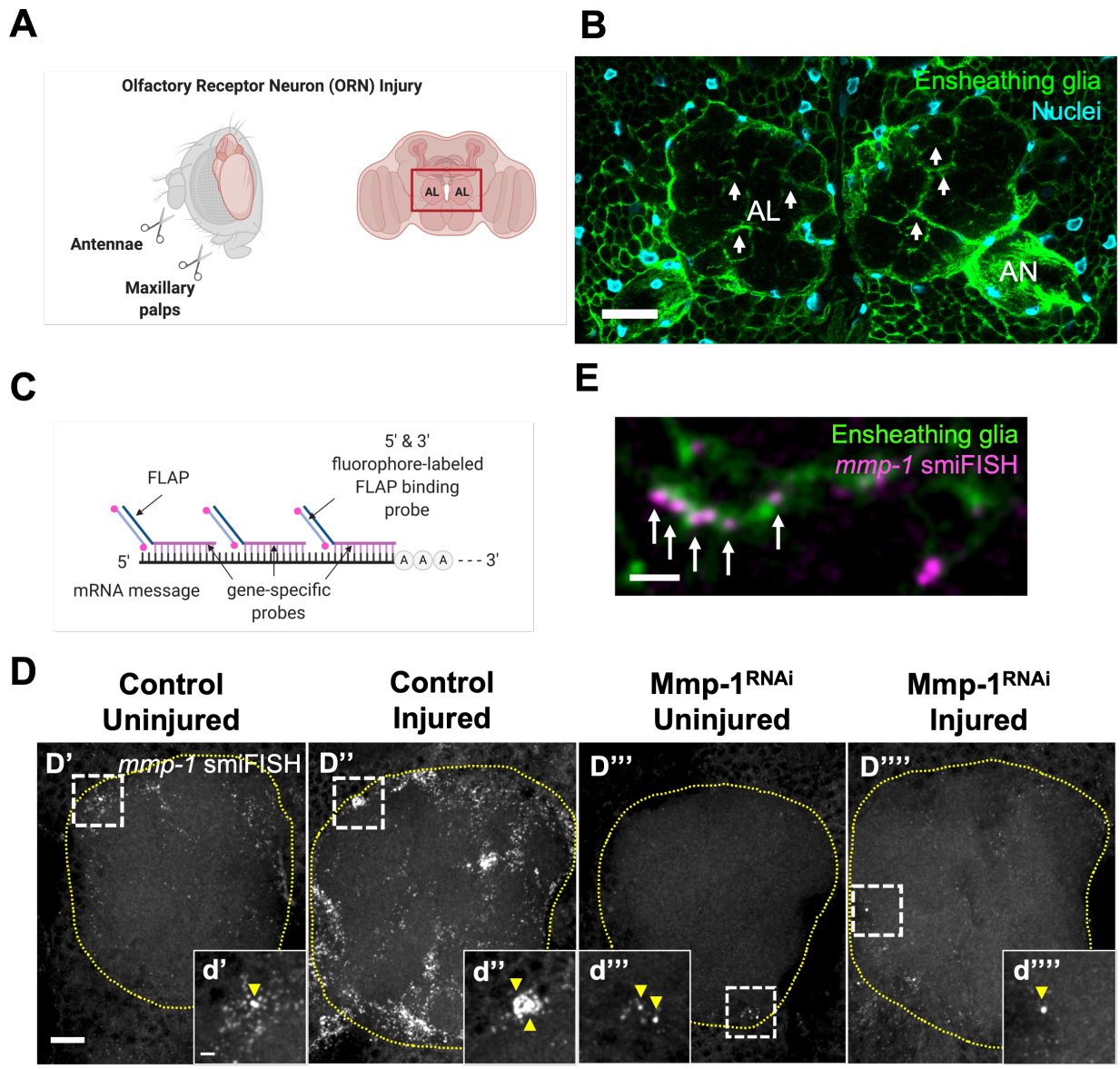

Figure 1: *mmp-1* transcripts are upregulated in ensheathing glia following neuronal injury
(A) Schematic representation of the olfactory receptor neuron (ORN) injury, demonstrating the removal of the 3rd antennal segments and maxillary palps. ORN cell bodies in the aforementioned structures extend their projections to the antennal lobes (ALs) of the central fly brain (red box). Created with BioRender.com **(B)** Representative image of ensheathing glia surrounding the ALs in an uninjured brain. White arrows indicate ensheathing glial fine processes within ALs. AL: antennal lobe, AN: antennal nerve. Single slice (1 µm). Scale bar: 20 µm. Genotype: *;UAS-mCD8::GFP/UAS-mCD8::GFP;TIFR-Gal4/UAS-LacZ::NLS*. **(C)** smiFISH schematic. Created with BioRender.com (D'-D'''') Representative images of *mmp-1* smiFISH in uninjured and injured (4.5hpi) single ALs (yellow dotted line). Images are MIPs: 3.75 µm. Scale bar: 10 µm. Control genotype: *;tub-Gal80^{ts}/+;repo-Gal4/+*. Mmp-1^{RNAi} genotype: *;tub-Gal80^{ts}/UAS-Mmp-1^{RNAi};repo-Gal4/+*. **(d'-d'''')** High magnification images of *mmp-1* smFISH (white box), representing single transcripts and transcription start sites (yellow arrows). MIP: 3.75 µm. Scale bar: 2 µm. (E) High magnification image of *mmp-1* transcripts in ensheathing glial processes (white arrows) 4 hpi. Single slice: 0.43 µm. Scale bar: 2 µm. Genotype: *;UAS-mCD8::GFP/UAS-mCD8::GFP;TIFR-Gal4/UAS-LacZ::NLS.*

smiFISH reveals upregulation and localization of *mmp-1* transcripts following neuronal injury

Our previous RNAseq and qPCR studies have demonstrated that the *mmp-1* transcript is acutely upregulated in the central nervous system (CNS) and ventral nerve cord (VNC) of the fly following neuronal injury. As prior research has shown that *mmp* transcripts can be localized to subcellular compartments and locally translated in an activity-dependent manner, we wanted to determine the localization of *mmp-1* mRNA in ensheathing glia following ORN axotomy(230, 231). In order to accomplish this, we utilized smiFISH to detect the *mmp-1* transcript following injury (Fig. 1C)(224). The Mmp-1 smiFISH probeset included 41 probes and was designed utilizing Oligostan (Supp. Table 1)(224). Our previous RNAseq and qPCR data suggested that there is a strong transcriptional response in the ensheathing glia 3 hours post ORN axotomy(77). As a result, we used this as a starting point for our smiFISH studies.

In accordance with our qPCR and RNAseq data, we found that smiFISH reveals a low level of *mmp-1* transcript present in the uninjured brain, with the highest amount of transcript being expressed in cells surrounding the antennal lobe, likely ensheathing glia (Fig. 1D). In response to injury, we observe a significant increase in the amount of *mmp-1* transcript detected at 4.5 hpi (Fig. 1D''). Interestingly, when labeling ensheathing glial membranes with GFP, we also observed the localization of the *mmp-1* smiFISH signal to fine processes following injury (Fig. 1E).

To determine if the Mmp-1 probeset is specific to the *mmp-1* transcript, we performed an injury experiment where Mmp-1 was knocked down in all glia using RNAi. As expected, the RNAi knockdown eliminated most of the smiFISH signal (Fig. 1D'''-D''''). We did however detect large spots of Mmp-1 transcript right outside the antennal lobe, where the nuclei of ensheathing glia are located (Fig. 1d'-d''''). We posit that these large intense puncta represent the site of Mmp-1 transcription in the nucleus, as the transcript would not be subject to RNAi mediated degradation until it was transported to the cytoplasm (Supp. Fig. 2)(224, 232).

The FLARIM v2.0 method can be used to detect mRNAs and associated ribosomes

While the smiFISH approach allowed us to localize the *mmp-1* transcript to distal glial processes following neuronal injury, it does not give us insight into whether there may be local translation of the transcript at distal sites. Currently, the most accepted method for investigating local translation is the use of photoconvertible fluorescent timer proteins, however this approach requires tagging the protein of interest in the context of native mRNA with all its regulatory 5' and 3' elements(233, 234). More recently, a non-transgenic approach was developed to assess the ribosome load on a transcript of interest while maintaining spatial localization within the cell. This method, Fluorescence assay to detect ribosome interactions with mRNA (FLARIM), utilizes pairs of oligonucleotide probes that bind separately to ribosomes and to the mRNA of interest (Fig. 2A)(214). When these probes are in close proximity, they form a full sequence for a linker probe carrying a complete Hybridization Chain Reaction (HCR) initiator (Fig. 2A)(223, 225).

While the original method was able to robustly assess the ribosome load on transcripts of interest, it has never been used *in vivo* on whole mount tissue. Moreover, the use of the linker probe requires a 2nd round of hybridization before initiating the HCR reaction. Lastly, the original method made use of separate pools of gene specific probes for transcript localization and ribosome association, which can be problematic on short transcripts where probe binding sites may be limiting (Fig. 2A). To address these drawbacks, we have utilized split initiator technology to include half an HCR initiator, split B3 initiator, for reporting ribosome association on the 3' end of the gene specific probe and the other half of the B3 initiator on the 3' end of a set of 25 probes that will hybridize to the 18S rRNA (Supp. Fig. 3 and 4, Supp. Tables 2 and 3)(223, 225). Finally, we tagged the gene specific probes with a different full HCR initiator (B2) on the 5' end to allow for transcript localization (Supp. Table 3)(223, 225). By taking advantage of new developments in oligonucleotide synthesis, Integrated DNA Technologies' oPools Oligo Pools service, we are able to synthesize a probeset for a gene of interest for ~$100 USD. We are calling this modified version FLARIM v2.0, and we herein demonstrate that this relatively inexpensive method is able to

achieve transcript localization and ribosome association at depth in whole mount tissue (Fig. 2B, Supp. Fig. 5).

In FLARIM v2.0, probes are first hybridized to the transcript of interest and to 18S ribosomes. Then, during the detection stage, fluorescent metastable hairpins are used to generate signals via HCR (Supp. Fig. 5). On the gene-specific probe, the full initiator sequence opens up a set of hairpins to create a fluorescent signal indicating the presence and localization of the mRNA transcript. Moreover, when the split initiators of the 18S ribosome probes and the gene-specific probes are reconstituted, a second set of hairpins are opened, creating a distinct fluorescent signal to allow for mRNA-ribosome association detection (Fig. 2B).

The dual detection method produces diffraction limited spots, if amplification is carried out for shorter periods of time and allows for transcript and ribosome detection within cells by fluorescent co-labeling, providing spatiotemporal resolution. The fluorescent tags on hairpins can also be varied to accommodate multiplexing within the same sample. Additionally, FLARIM v2.0 can be used to investigate mRNA localization and local translation in response to various stimuli, such as neuronal injury. We decided to assess the regulation of *mmp-1* following axotomy using the FLARIM v2.0 method.

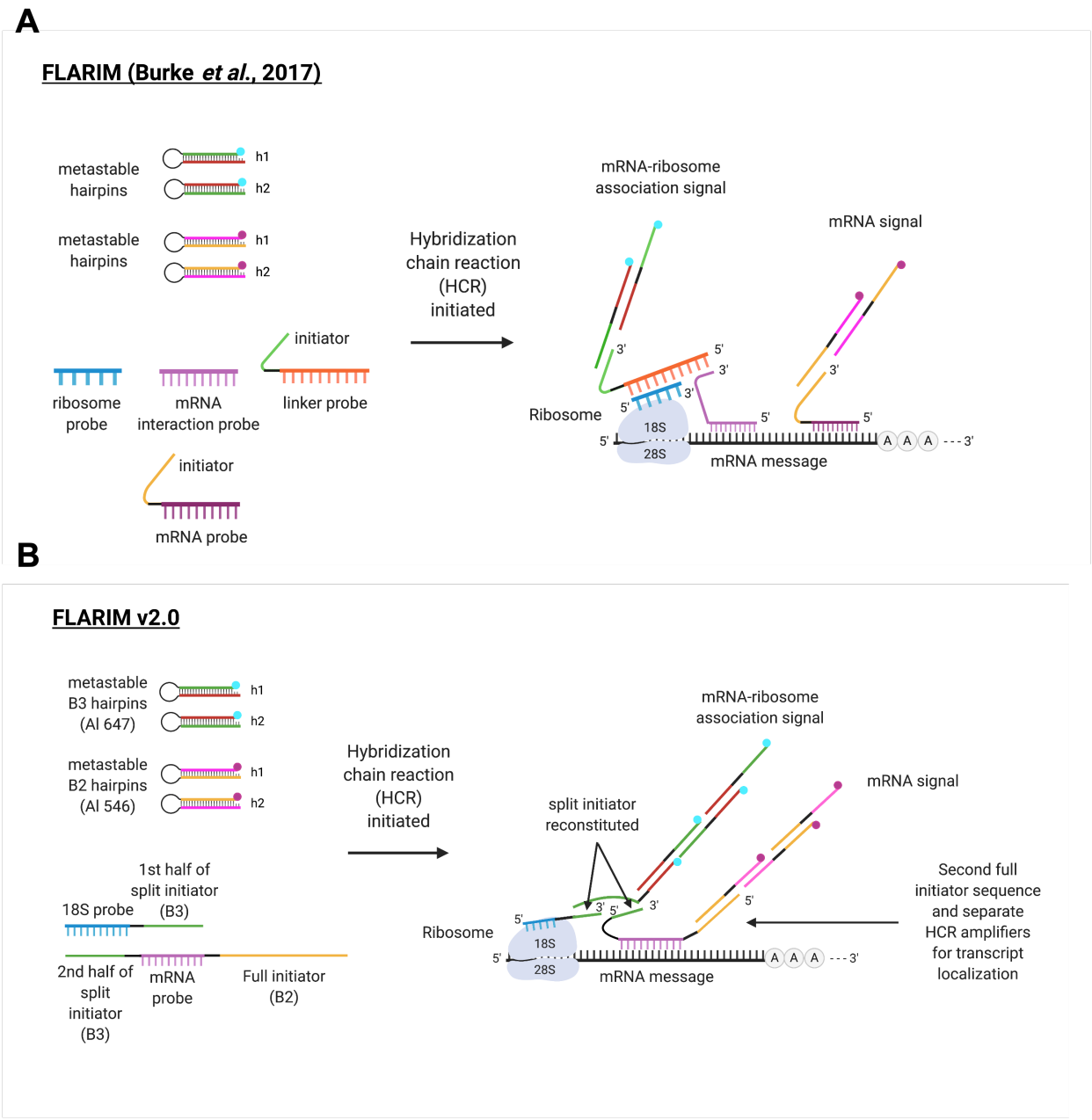

Figure 2: Novel FLARIM v2.0 probeset
(A) FLARIM (Burke *et al*., 2017)(214): Utilizes 4 probes to achieve distinct mRNA and ribosome-specific signals by HCR amplification and allows for assessment of ribosome load on transcripts of interest. **(B)** FLARIM v2.0: Utilizes 2 probesets: 1) an 18S ribosome-specific probe with the first half of a split B3 initiator and an mRNA-specific probe with the second half of the split B3 initiator and 2) a full B2 initiator on the 5' end of the gene specific probe. This B2 initiator allows for transcript localization and aids in quantification by creating a normalization channel for the FLARIM signal Hybridization with these probesets and amplification using metastable hairpins generates a separate fluorescent signal for mRNA and mRNA-ribosome association detection *in vivo.* Created using Biorender.com.

Application of the FLARIM v2.0 method in the *Drosophila* ORN injury model

In order to validate our Mmp-1 probeset and explore how an immune gene is regulated following axotomy, the FLARIM v2.0 method was tested in the context of the ORN injury model (Fig. 3A). In uninjured brains, transcripts are sparse and localized to the edges of the antennal lobes, where ensheathing glial cell bodies are located. Some transcripts are also associated with ribosomes, generating a FLARIM signal and indicating that some translation may be occurring under basal conditions. In brains that have undergone an ORN injury, there is a robust upregulation of the *mmp-1* transcript (magenta) and ribosome-association (cyan) signal both around the antennal lobes and within them (Fig. 3A). These results mirror the time course of Mmp-1 protein upregulation following antennal and maxillary palp injury, which is robust 1-day post-injury (dpi)(77). Transcription start sites are also observable in ensheathing glial nuclei as intense puncta (magenta), lacking a ribosome-association signal (cyan) (Supp. Fig. 6). Moreover, labeling of ensheathing glial cell membranes with GFP allows for the localization of *mmp-1* mRNAs and associated ribosomes within the antennal lobes 20 hpi. To quantify these results, a total fluorescence intensity analysis of each signal was completed within the antennal lobes. The total intensity of both *mmp-1* transcript and ribosome-association signals significantly increased within antennal lobes 20 hpi (Fig. 3B). High-resolution imaging and quantification of *mmp-1* mRNA and ribosome-association puncta in a smaller ROI of the ALs reveals a similar trend (Supp. Fig. 7).

A series of control experiments were also conducted to ascertain the specificity of the probesets and our signal. In the absence of hybridized probes, the hairpins amplified alone do not generate a fluorescent signal (Fig. 3A, B). Additionally, hybridization of only the 18S FLARIM probes does not result in a signal, as only half of the initiator sequence is present, and hairpins are unable to open and generate a fluorescent signal (Fig. 3A, B). Moreover, the unbound sB3 18S FLARIM probe does not result in background when brains are incubated with the Mmp-1 probeset (Supp. Fig. 8). We also determined that the *mmp-1* probeset was specific to our

transcript of interest. Upon Mmp-1 RNAi knockdown in glial cells, *mmp-1* mRNA and ribosome-association signals were significantly diminished in the injured condition (Fig. 4A, B, C).

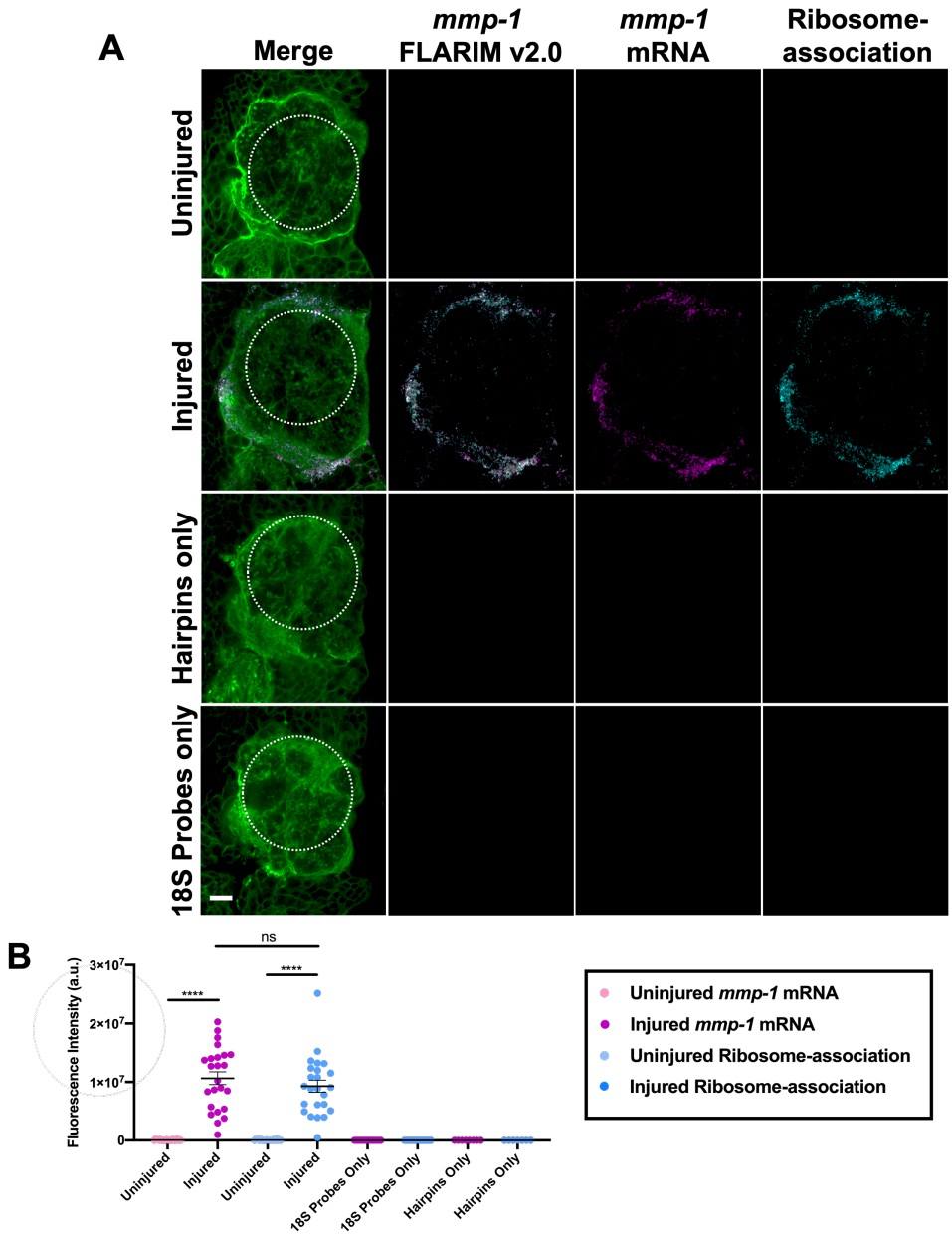

Figure 3: FLARIM v2.0 to detect *mmp-1* in the *Drosophila* ORN injury model
(A) Representative images of *mmp-1* FLARIM v2.0 probeset in uninjured and injured ALs with ROIs quantified (dotted circle). *Mmp-1* FLARIM v2.0: merge of *mmp-1* mRNA and ribosome-association signal. Injured: 20 hpi. Hairpins only: 20 hpi (no probes, only amplification with fluorescent hairpins). 18S Probes only: 20 hpi (18S FLARIM probes with one half of the split initiator sequence and amplification with fluorescent hairpins). Single slice: 0.5 µm. Scale bar: 20 µm. Genotype: *;UAS-mCD8::GFP;TIFR-Gal4*. **(B)** Quantification of *mmp-1* FLARIM v2.0 total intensity (a.u.) in ALs. *mmp-1* mRNA Uninjured (n=22), *mmp-1* mRNA Injured (n=24), Ribosome-association Uninjured (n=22), Ribosome-association Injured (n=24), *mmp-1* mRNA 18S Probes Only (n=16), Ribosome-association 18S Probes Only (n=14), *mmp-1* mRNA Hairpins Only (n=8), Ribosome-association Hairpins Only (n=7). Mean ± SEM; Uninjured *mmp-1* mRNA and Injured *mmp-1* mRNA: t-test ****(p<0.0001); Uninjured Ribosome-association and Injured Ribosome-association: Mann-Whitney test ****(p<0.0001); non-significant (ns).
(Continued on next page)

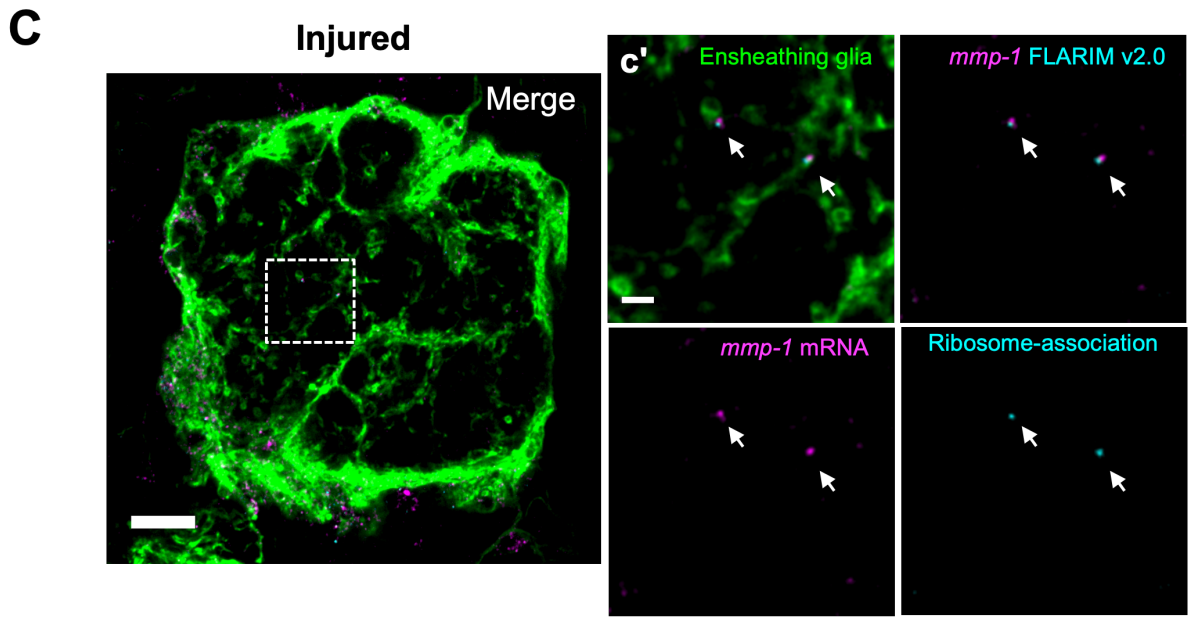

Figure 3 continued: FLARIM v2.0 to detect *mmp-1* in the *Drosophila* ORN injury model
(C) Representative image of *mmp-1* FLARIM v2.0 probeset in an injured AL (20 hpi). Single slice: 0.5 µm. Scale bar: 10 µm. Genotype: *;UAS-mCD8::GFP/UAS-mCD8::GFP;TIFR-Gal4/TIFR-Gal4*. (c') *mmp-1* transcripts are associated with ribosomes in ensheathing glial processes (white arrows). Single slice: 0.5 µm. Scale bar: 2 µm.

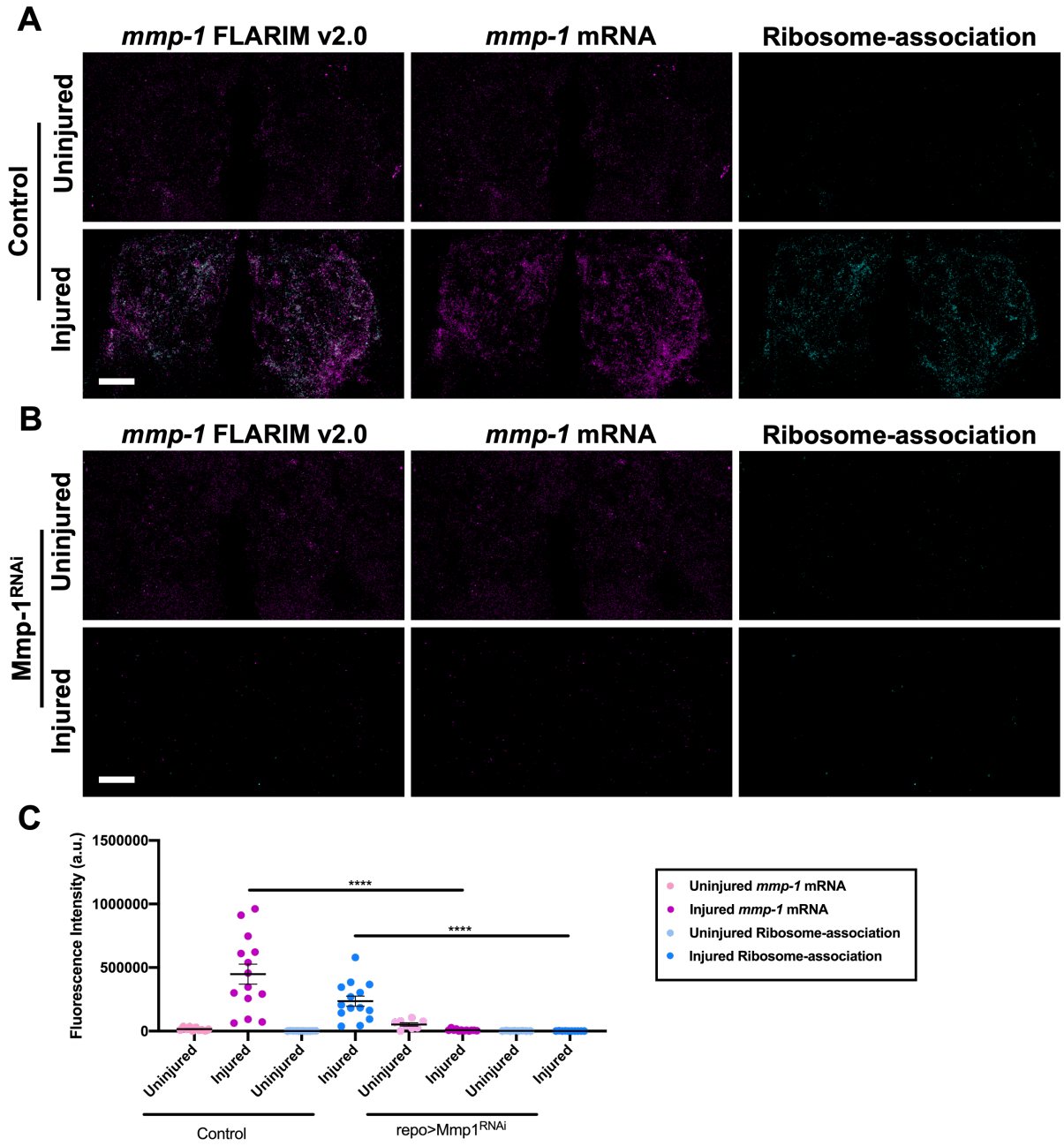

Figure 4: FLARIM v2.0 is specific to the *mmp-1* transcript and its associated ribosomes
(A) Representative images of *mmp-1* FLARIM v2.0 in control uninjured and injured (20 hpi) brains. *Mmp-1* FLARIM v2.0: merge of *mmp-1* mRNA and ribosome-association signal. MIP: 15.5 µm. Scale bar: 20 µm. Genotype: *;tub-Gal80^{ts}/+;repo-Gal4/+*. **(B)** Representative images of *mmp-1* FLARIM v2.0 in brains expressing Mmp-1 RNAi in all glial cells (repo>Mmp-1^{RNAi}). *Mmp-1* FLARIM v2.0: merge of *mmp-1* mRNA and ribosome-association signal. MIP: 15.5 µm. Scale bar: 20 µm. Genotype: *;tub-Gal80^{ts}/UAS-Mmp-1^{RNAi};repo-Gal4/+*. (C) Quantification of *mmp-1* FLARIM v2.0 total intensity (a.u.) in ALs. Control: Uninjured *mmp-1* mRNA (n=10), Injured *mmp-1* mRNA (n=14), Uninjured Ribosome-association (n=11), Injured Ribosome-association (n=14). repo>Mmp-1^{RNAi}: Uninjured *mmp-1* mRNA (n=8), Injured *mmp-1* mRNA (n=12), Uninjured Ribosome-association (n=8), Injured Ribosome-association (n=10). Mean ± SEM; Mann-Whitney test ****(p<0.0001).

mmp-1 mRNA and associated ribosomes are localized to injured ORN glomeruli

In addition to inducing an acute ORN injury by ablating both *Drosophila* odor-sensing structures (antennae and maxillary palps), a more localized injury can be performed by ablating only the maxillary palps. These structures contain approximately 20% of ORNs that project back to the ALs(72). To assess *mmp-1* mRNA distribution and ribosome-association in a localized injury model, maxillary palps were surgically ablated and the FLARIM v2.0 signal was imaged 20 hpi. Moreover, a subset of maxillary palp ORNs were labeled with GFP using an odorant receptor-specific driver (Or85e-Gal4) to localize the uninjured or injured ORNs. The GFP+ glomeruli of these ORNs reside at a ~10 μm depth within the ALs, suggesting that they are at a distance from ensheathing glial cell bodies.

As in previous experiments, uninjured brains did not have high levels of *mmp-1* mRNA or associated ribosomes. However, 20 hours after maxillary palp injury, *mmp-1* FLARIM v2.0 signal can be detected within distinct regions of the ALs (Fig. 5A). Additionally, when examining the GFP+ Or85e glomeruli, *mmp-1* mRNA and ribosome-association puncta can be localized to the injured glomeruli throughout the z-plane of the AL (Fig. 5B, white arrows). Quantification of the FLARIM v2.0 signal by segmentation to GFP+ glomeruli also demonstrates the significant increase of *mmp-1* transcripts and ribosomes in the injured condition. It is also interesting to note that *mmp-1* FLARIM v2.0 signal can be detected along ORN projections (Fig. 5B, yellow arrows), as well as near the midline of the ALs, which are presumably a distinct subset of maxillary palp glomeruli that are not GFP labeled (Fig. 5A, white arrowheads). Taken together, these results suggest that the immune gene *mmp-1* may be directly transported to the site of the injured ORNs within ensheathing glial cells.

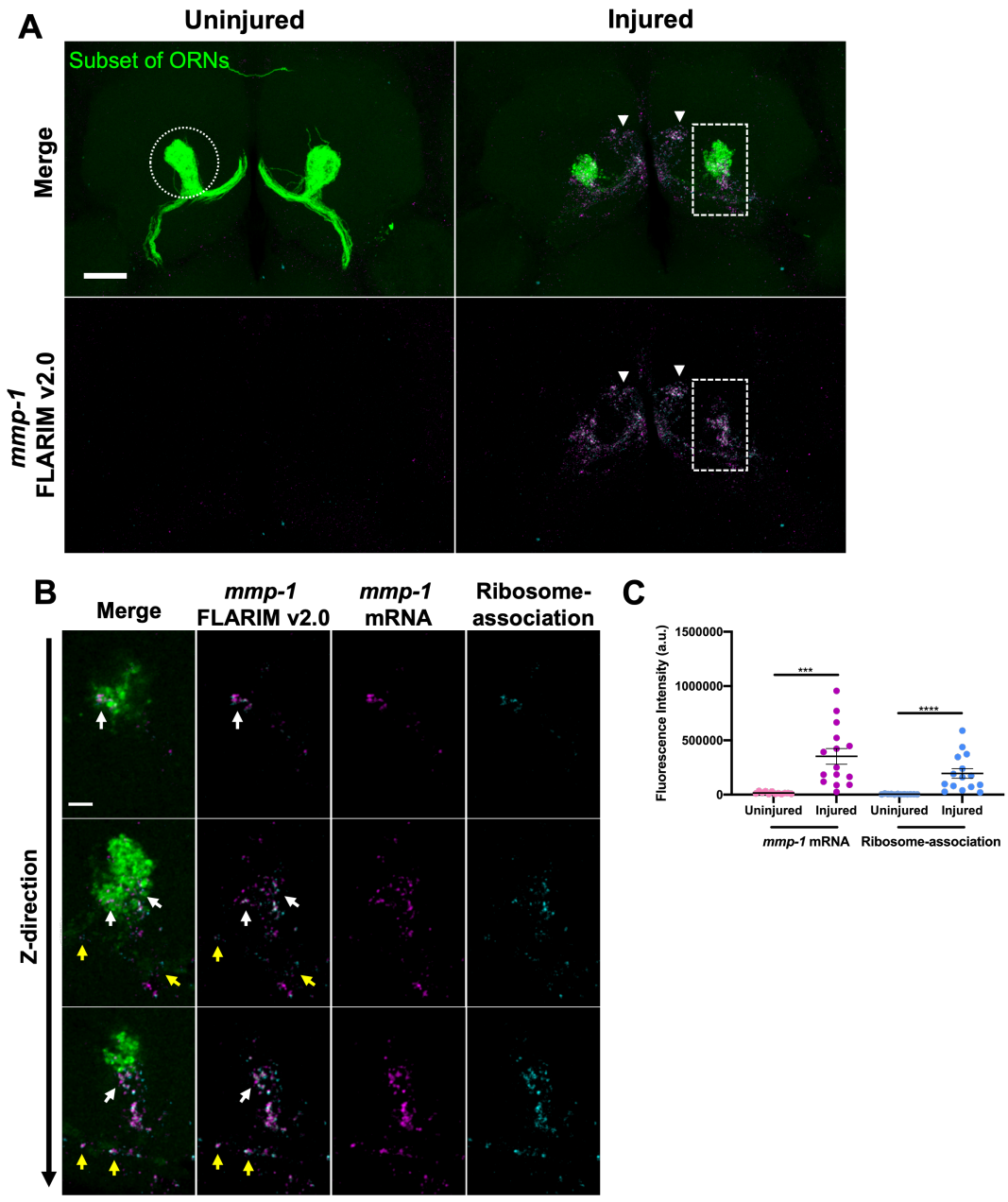

Figure 5: *mmp-1* mRNA and associated ribosomes are localized to injured ORN glomeruli
(A) Representative images of *mmp-1* FLARIM v2.0 probeset in uninjured and injured ALs. Injured: 20 hpi (only maxillary palps ablated). *Mmp-1* FLARIM v2.0: merge of *mmp-1* mRNA and ribosome-association signal. MIP: 20.5 µm. Scale bar: 20 µm. Genotype: *;UAS-mCD8:GFP/+;Or85e-Gal4/+* **(B)** High magnification inset of an ORN glomerulus (Fig. 5A: dotted rectangle) and *mmp-1* FLARIM v2.0 (white arrows) at three positions along the z-axis. Yellow arrows: FLARIM v2.0 along ORN projections. *Mmp-1* FLARIM v2.0: merge of *mmp-1* mRNA and ribosome-association signal. Single slice: 0.5 µm. Scale bar: 5 µm. **(C)** Quantification of *mmp-1* FLARIM v2.0 total intensity (a.u.) in ORN glomeruli (ROI: white dotted circle in Fig. 5A). *mmp-1* mRNA Uninjured (n=12), *mmp-1* mRNA Injured (n=15), Ribosome-association Uninjured (n=12), Ribosome-association Injured (n=15). Mean ± SEM; *mmp-1* mRNA: t-test ***(p<0.001); Ribosome-association: Mann-Whitney test ****(p<0.0001).

Translation machinery is present in ensheathing glial processes

We observe that *mmp-1* transcripts and associated ribosomes are localized to ensheathing glial processes following ORN injury. As a result, we hypothesize that transcript localization and local translation of immune genes may be mechanisms employed by glial cells to mediate responses after a neuronal injury event. This is of particularly interest in relation to Mmp-1, as it is a secreted molecule employed by ensheathing glia to remodel the surrounding extracellular matrix and provide access to sites of damage(77, 197). However, in order for this to occur, translation and secretory machinery must also be present in ensheathing glial processes to properly modify and secrete Mmp-1(211). Evidence for translation machinery in glial processes has been demonstrated by previous groups. For example, a study in mouse astrocytes has shown that along with a local pool of transcripts, endoplasmic reticulum (ER) and Golgi apparatus (GA) are also present in perivascular processes and endfeet(211). Therefore, we performed immunohistochemistry in uninjured and injured brains to assess whether the aforementioned organelles are present in glial projections of the ALs. Super-resolution microscopy allowed for the visualization of ER and GA within ensheathing glial fine processes (Fig. 6A-D). We were able to observe that ER and GA are present under both basal conditions and following ORN injury (Fig. 6A-D). These results further suggest that transcript localization and local translation of immune genes could be supported in glial processes, and could play a functional role in mediating rapid glial responses following neuronal injury

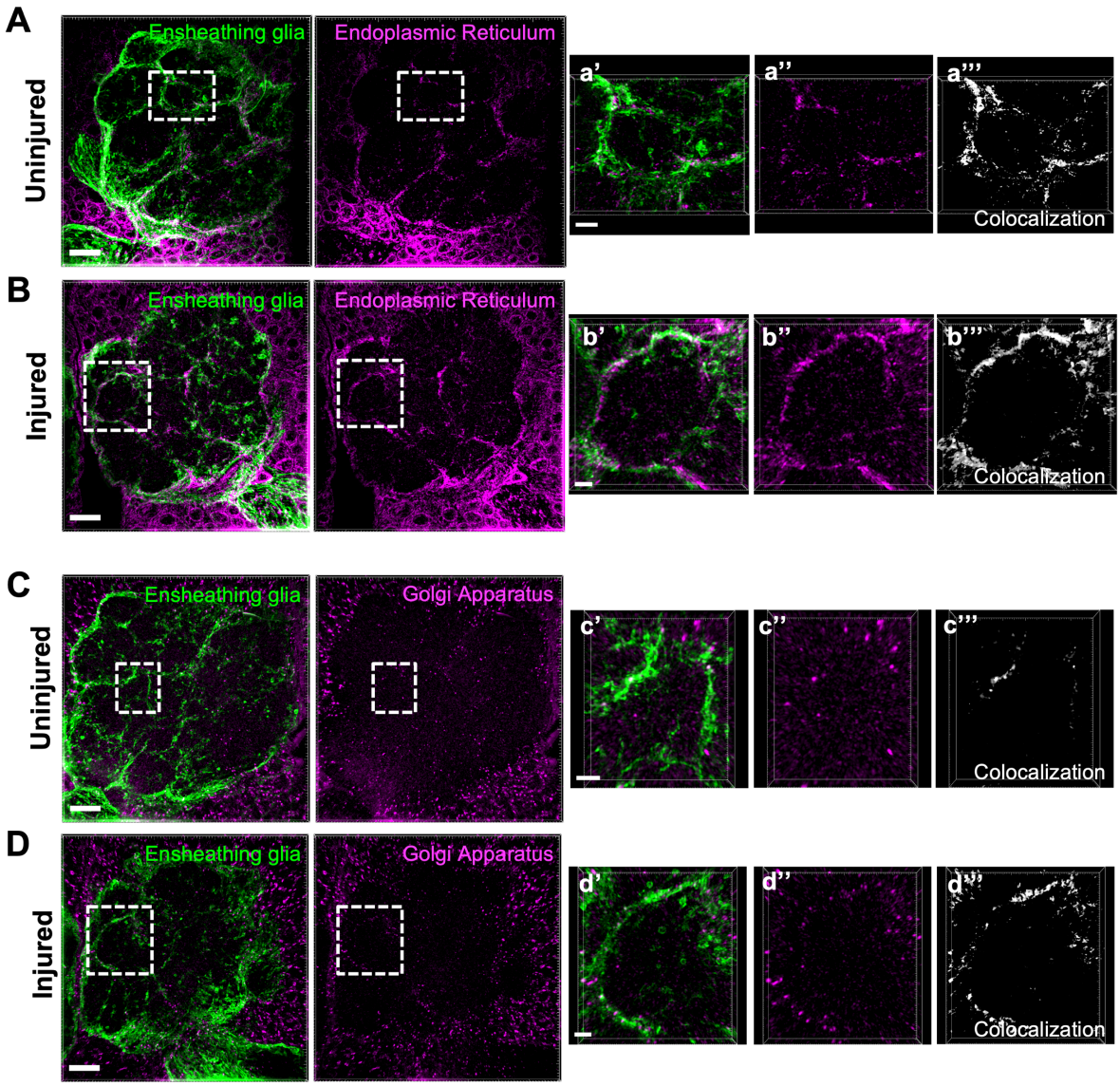

Figure 6: Endoplasmic reticulum and Golgi apparatus are present in ensheathing glial fine processes

(A) Representative super-resolution images of ER immunostaining in an uninjured AL. MIP (1.75 µm). Scale bar: 10 µm. Genotype: *;UAS-mCD8::GFP/UAS-mCD8::GFP;TIFR-Gal4/TIFR-Gal4*. **(a', a'')** ER is present within ensheathing glial fine processes of an uninjured AL. MIP (1.75 µm). Scale bar: 3 µm. **(a''')** Colocalization of ensheathing glia and ER signal**. (B)** Representative super-resolution images of ER immunostaining in an injured (20 hpi) AL. MIP (1.75 µm). Scale bar: 10 µm. Genotype: *;UAS-mCD8::GFP/UAS-mCD8::GFP;TIFR-Gal4/TIFR-Gal4*. **(b', b'')** ER is present within ensheathing glial fine processes of an injured AL. MIP (1.75 µm). Scale bar: 2 µm. **(b''')** Colocalization of ensheathing glia and ER signal. **(C)** Representative super-resolution images of GA immunostaining in an uninjured AL. MIP (1.75 µm). Scale bar: 10 µm. Genotype: *;UAS-mCD8::GFP/UAS-mCD8::GFP;TIFR-Gal4/TIFR-Gal4*. **(c', c'')** GA is present within ensheathing glial fine processes of an uninjured AL. MIP (1.75 µm). Scale bar: 2 µm**. (c''')** Colocalization of ensheathing glia and GA signal. **(D)** Representative super-resolution images of GA immunostaining in an injured (20 hpi) AL. MIP (1.75 µm). Scale bar: 10 µm. Genotype: *;UAS-mCD8::GFP/UAS-mCD8::GFP;TIFR-Gal4/TIFR-Gal4***. (d', d'')** GA is present within ensheathing glial fine processes of an injured AL. MIP (1.75 µm). Scale bar: 2 µm. (d''') Colocalization of ensheathing glia and GA signal.

Supplemental Results

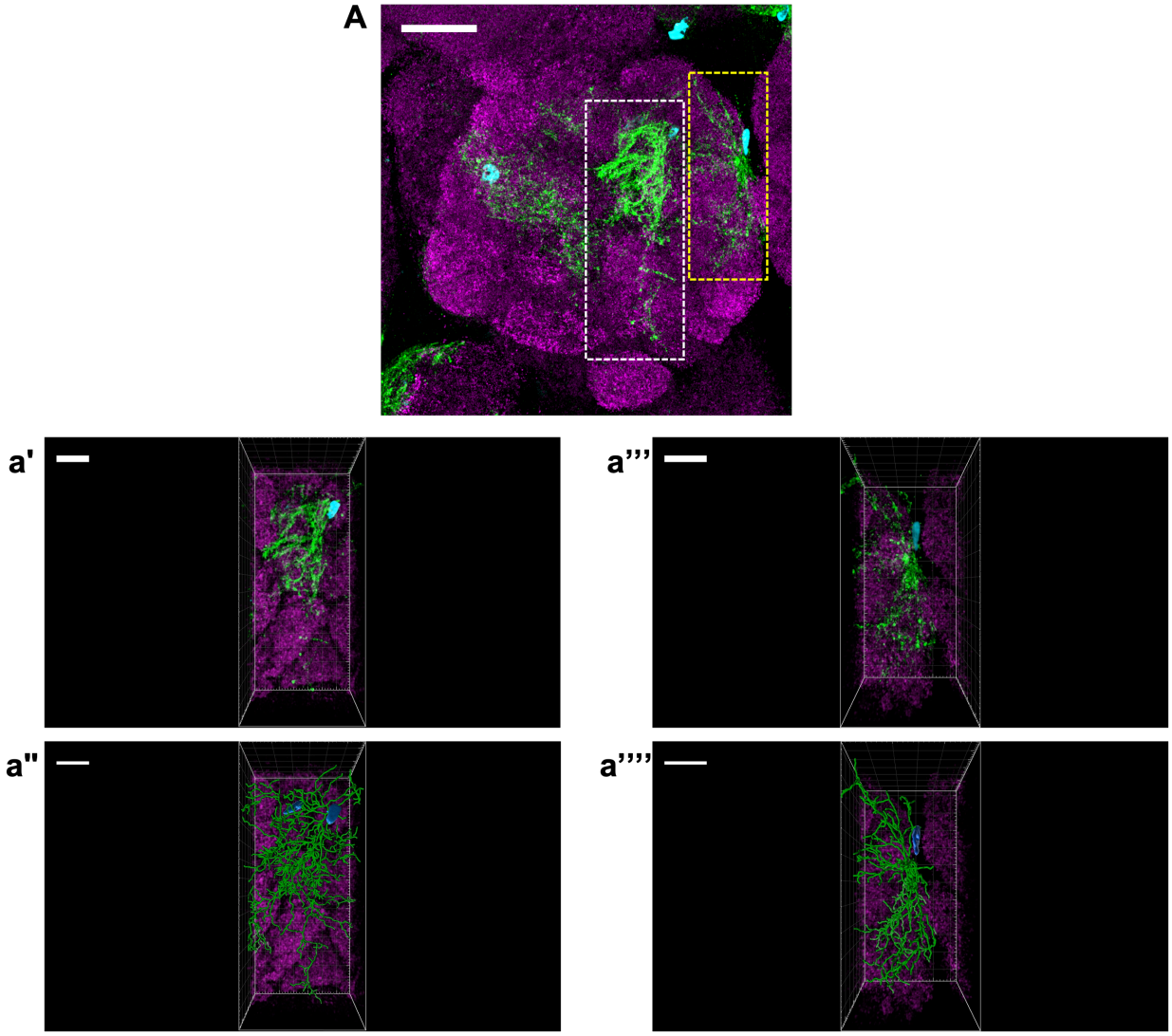

Supplementary Figure 1: Ensheathing glial MARCM clones at the ALs
(A) MIP of 3 or 4 ensheathing glial MARCM clones interdigitating neuronal glomeruli in the AL. MIP: 34.7µm. Genotype: hsFLP/X or Y; FRTG13, UAS-mCD8::GFP/FRTG13, UAS-mCD8::GFP; TIFR-Gal4/+. Scale bar: 20 µm. **(a')** High magnification inset of white dotted rectangle. MIP: 31.2 µm. Scale bar: 10 µm. **(a'')** 3D rendered filaments and nuclei of ensheathing glial processes (white dotted rectangle). MIP: 31.2 µm. Scale bar: 10 µm. **(a''')** High magnification inset of yellow dotted rectangle. MIP: 34.7 µm. Scale bar: 10 µm**. (a'''')** 3D rendered filaments and nuclei of ensheathing glial processes (yellow dotted rectangle). MIP: 34.7 µm. Scale bar: 10 µm.

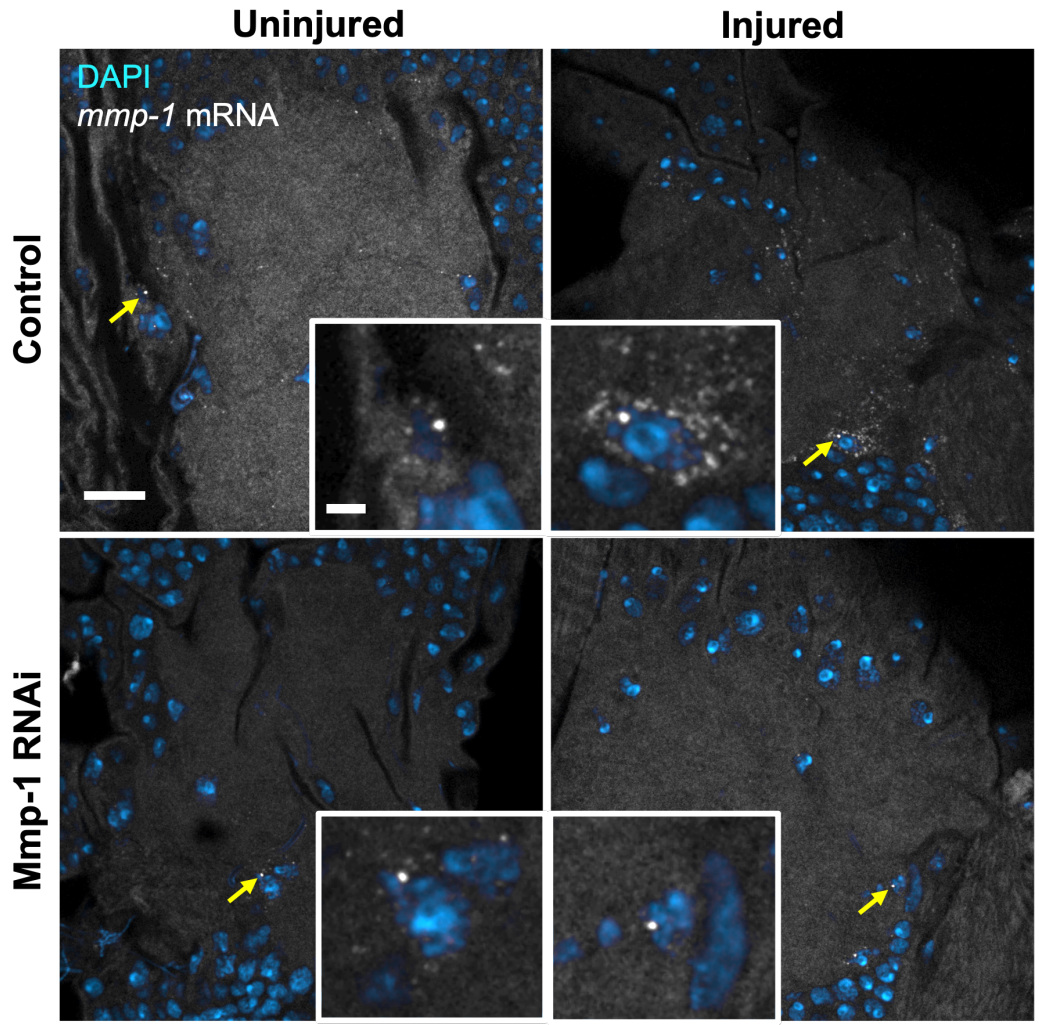

Supplementary Figure 2: mmp-1 transcription start sites in nuclei surrounding ALs
mmp-1 mRNA detected in ALs using smiFISH probes in control and Mmp-1 RNAi brains. Transcription start sites are visible in nuclei (yellow arrows, inset). Control genotype: ;tub-Gal80^{ts}/+;repo-Gal4/+. Mmp-1 RNAi genotype: ;tub-Gal80^{ts}/UAS-Mmp-1^{RNAi};repo-Gal4/+. Single slice: 0.2 µm. Scale bar: 10 µm. Inset scale bar: 2 µm

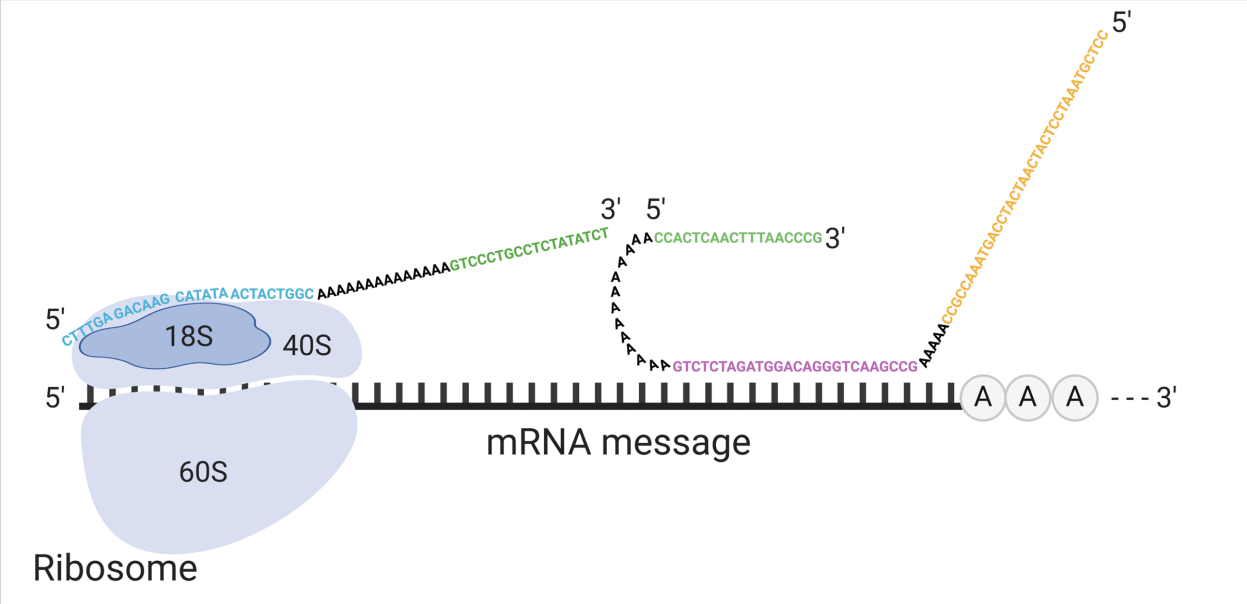

Supplementary Figure 3: Detailed probe schematic
Detailed schematic of *mmp-1* and 18S FLARIM probes in relation to target mRNA and associated ribosomes. Only single sample probes are depicted here for clarity. Adapted from Burke *et al*., 2017(214). Created with BioRender.com.

Legend: single 18S ribosome-specific probe sequence (blue), *mmp-1* probe (magenta), linkers (black), B2 initiator (orange), B3 initiator (green)

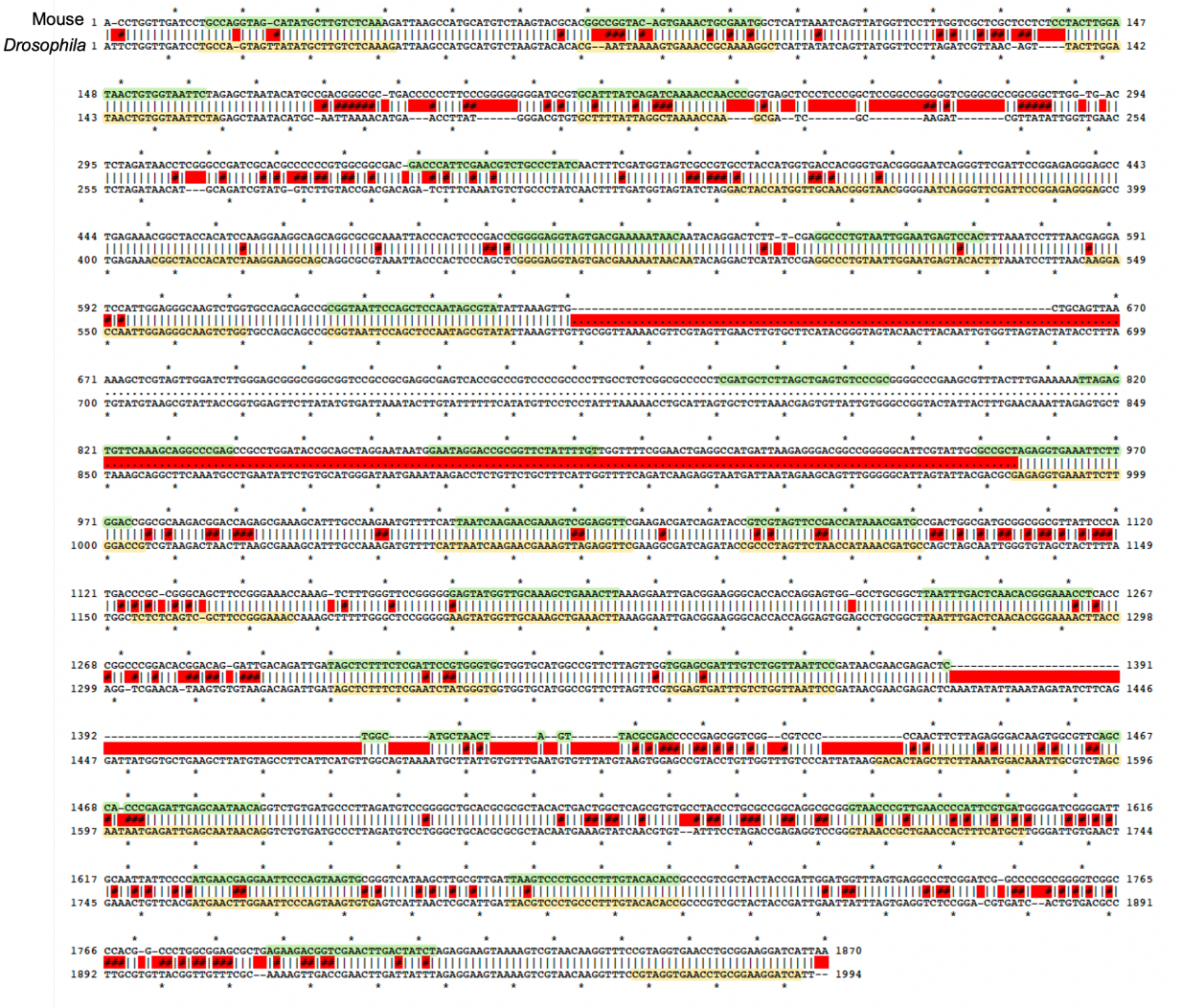

Supplementary Figure 4: Comparison of 18S FLARIM probes
Alignment of mouse (top) and *Drosophila* (bottom) 18S rRNA sequences using A plasmid Editor (ApE) software, with Burke *et al*., 2017(214) 18S FLARIM probes (green) and the probes from this study (yellow) highlighted.

Probeset Design

Probesets

Probeset	Concentration	Probe Volume in Hybridization Buffer	Hybridization Buffer Volume
Mmp-1 smiFISH	0.867 µM	2 µL	100 µL
Mmp-1 HCR B2 FLARIM split B3	2.0 µM	2 µL	100 µL
18S FLARIM split B3	1.6 µM	2 µL	100 µL

FLARIM v2.0 Protocol

1 **Dissection and Hybridization**

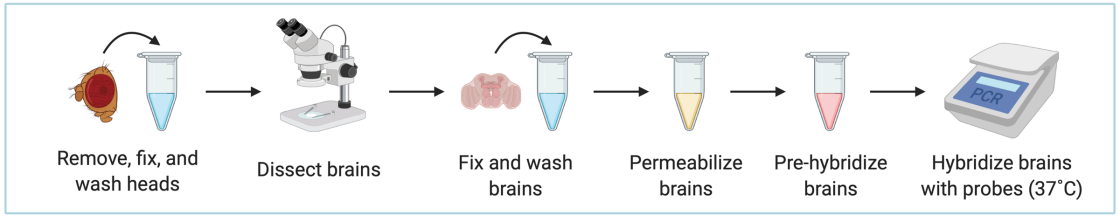

2 **Washes and Amplification**

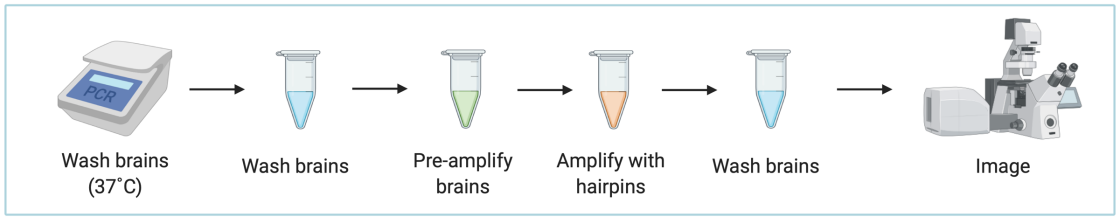

Supplementary Figure 5: Probe design and protocol workflow
Probeset design: Probesets to the transcript of interest were designed using Oligostan (Tsanov *et al.*, 2016(224)) and sequence similarity was compared to noncoding RNAs.
Probesets: Probeset sequences are listed in in Supplementary tables 1, 2, and 3. The smiFISH probeset assembly, protocol, and reagents are described in Tsanov *et al.*, 2016(224). For the Mmp-1 HCR B2 FLARIM split B3 and 18S FLARIM split B3 probesets, the FLARIM v2.0 protocol was used (*see Methods for details*)
FLARIM v2.0 Protocol: Dissection and hybridization: fly brains are dissected and hybridized overnight with gene-specific and 18S ribosome probes in a thermal cycler. Washes and amplification: the following day, brains are washed and amplified with fluorescent hairpins to generate mRNA-specific and ribosome-association signals (*see Methods for details*).
(Continued on next page)

FLARIM v2.0 Protocol Continued

Dissection

1. Pull fly heads and fix in 400 µl of 4% PFA + 0.1% TX at RT on a rocker (20 min)
2. Wash heads in 400 µl of PBS-TX (0.01%) at RT on a rocker (3 x 2 min)
3. Dissect brains in PBS-TX (0.01%)
4. Fix brains in 400 µl of 4% PFA + 0.1% TX at RT on a rocker (20 min)
5. Wash brains in 400 µl of PBS-TX (0.1%) at RT on a rocker (3 x 2 min)
6. Permeabilize brains in 400 µl of PBS-TX (0.5%) at RT on a rocker (20 min)

Probe hybridization & signal amplification

The HCR v3.0 hybridization and amplification protocol has been described previously for whole-mount fruit fly embryos: https://www.molecularinstruments.com/hcr-rnafish-protocols. The protocol was utilized in adult fruit fly brains as follows:

1. Remove PBS-TX (0.5%) and pre-hybridize brains by incubating in 100 µl probe hybridization buffer for 20 min at 37˚C (pre-heat buffer to 37˚C before use)
2. Hybridize brains overnight (16-18 hrs) with probes in a thermal cycler at 37˚C
    - 2 µl probe/100 µl hybridization buffer (probe concentration should be empirically determined for each probeset)
3. Remove hybridization buffer and wash brains using 100 µl probe wash buffer (4 x 15 min) at 37˚C in thermal cycler (pre-heat buffer to 37˚C before use)
4. During washes, snap-cool HCR metastable hairpin h1 and h2 in separate tubes and move amplification buffer to RT
    - 2 µl hairpin/100 µl amplification buffer
    - Snap-cooling: heat hairpins to 95˚C for 90 sec and allow to cool to RT (protected from light)
    - Once cooled, add hairpins to amplification buffer
5. Once washes are complete, remove wash buffer and wash brains again in 100 µl 5X SSC + 0.1% Tween-20 (SSCT) at RT (2 x 5 min)
6. Remove SSCT and pre-amplify brains in 100 µl of amplification buffer at RT (10 min)
7. Remove amplification buffer and add hairpin + amplification buffer mixture to brains
8. Amplify with hairpins (amplification time should be empirically determined for each probeset)
9. Remove amplification buffer and wash brains with 100 µl 5X SSCT at RT (5 min, 2 x 30 min, 5 min)
10. Mount in Vectashield and image

Caution: Probe hybridization and wash buffers contain formamide

Supplementary Figure 5 continued: Probe design and protocol workflow
FLARIM v2.0 Protocol: Dissection and hybridization: fly brains are dissected and hybridized overnight with gene-specific and 18S ribosome probes in a thermal cycler. Washes and amplification: the following day, brains are washed and amplified with fluorescent hairpins to generate mRNA-specific and ribosome-association signals (*see Methods for details*).
Created with BioRender.com (Adapted from “Growing Norovirus in Human Intestinal Enteroids (HIEs)”, by BioRender.com (2020). Retrieved from https://app.biorender.com/biorender-templates)

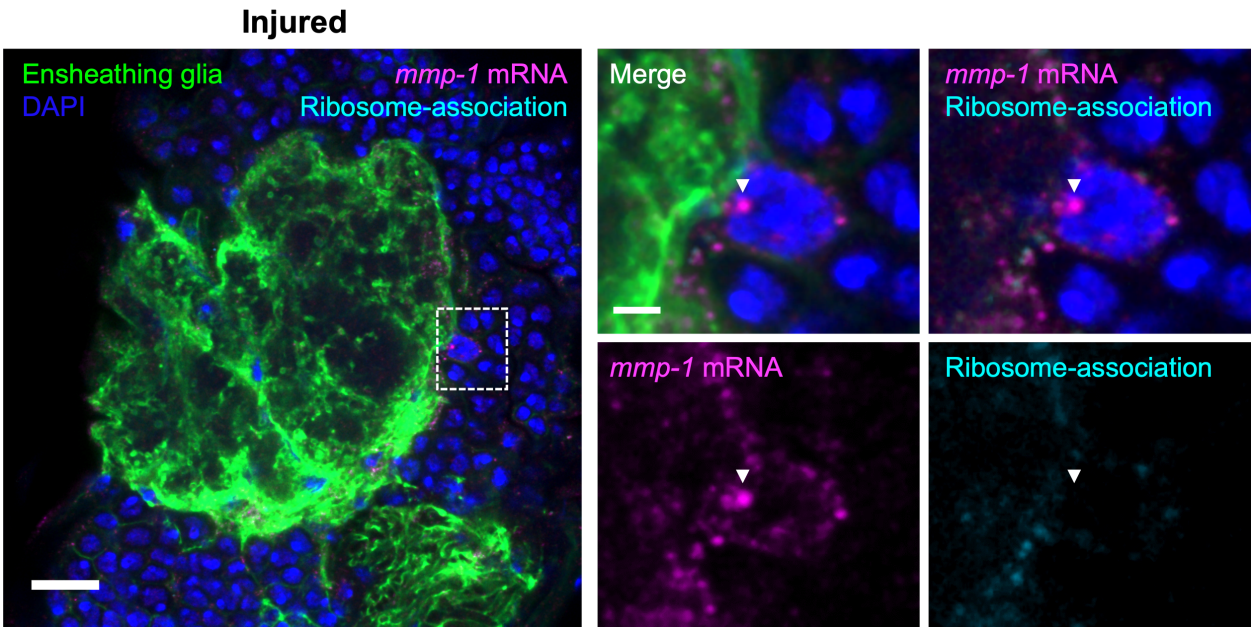

Supplementary Figure 6: Transcription start sites in ensheathing glial nuclei
mmp-1 mRNA and associated ribosomes detected using FLARIM 2.0. High magnification image (dotted rectangle) of transcription start site in ensheathing glial nucleus (DAPI) without ribosome association (white arrowhead). Genotype: *;UAS-mCD8::GFP/UAS-mCD8::GFP;TIFR-Gal4/TIFR-Gal4.* Single slice: 0.21 µm. Scale bar: 10 µm. Inset scale bar: 2 µm.

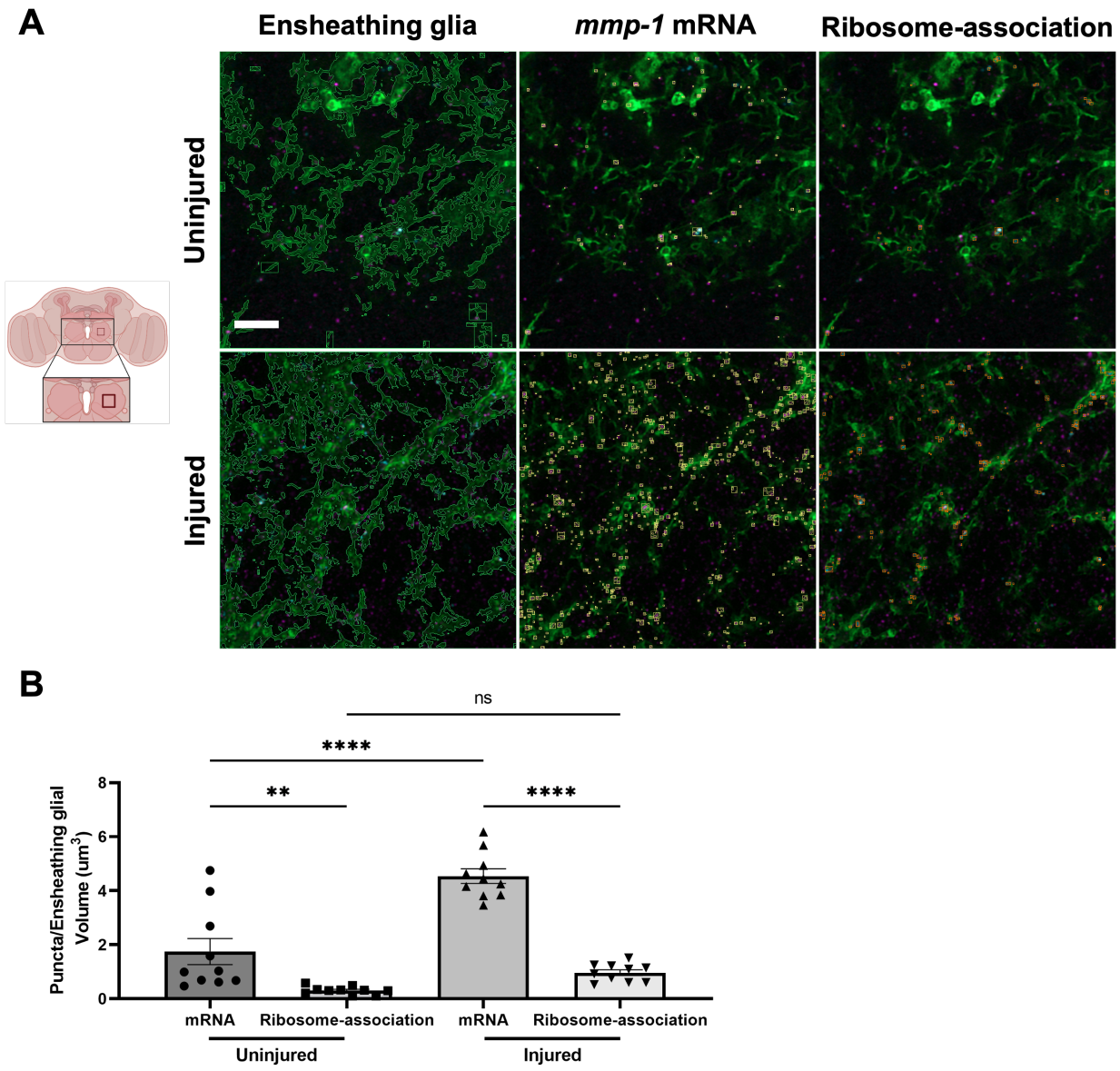

Supplementary Figure 7: High resolution imaging of ensheathing glia within ALs following ORN injury

(A) Representative super-resolution Airyscan images of uninjured and injured AL ROIs (red square). Green outline represents segmentation of ensheathing glial membranes for analysis. Yellow boxes represent *mmp-1* mRNA puncta within ensheathing glial processes for quantification. Orange boxes represent ribosome-association puncta within ensheathing glial processes for quantification. Single slice: 0.15 µm. Scale bar: 5 µm. Genotype: *;UAS-mCD8::GFP/UAS-mCD8::GFP;TIFR-Gal4/TIFR-Gal4*. **(B)** Quantification of *mmp-1* mRNA and ribosome-association puncta in uninjured and injured brains, normalized to ensheathing glial volume. Uninjured mRNA (n=10), uninjured ribosome-association (n=10), injured mRNA (n=10), injured ribosome-association (n=10). Mean ± SEM; One-way ANOVA (Sidak's *post hoc* test); non-significant (ns), **(p=0.0039), ****(p<0.0001).

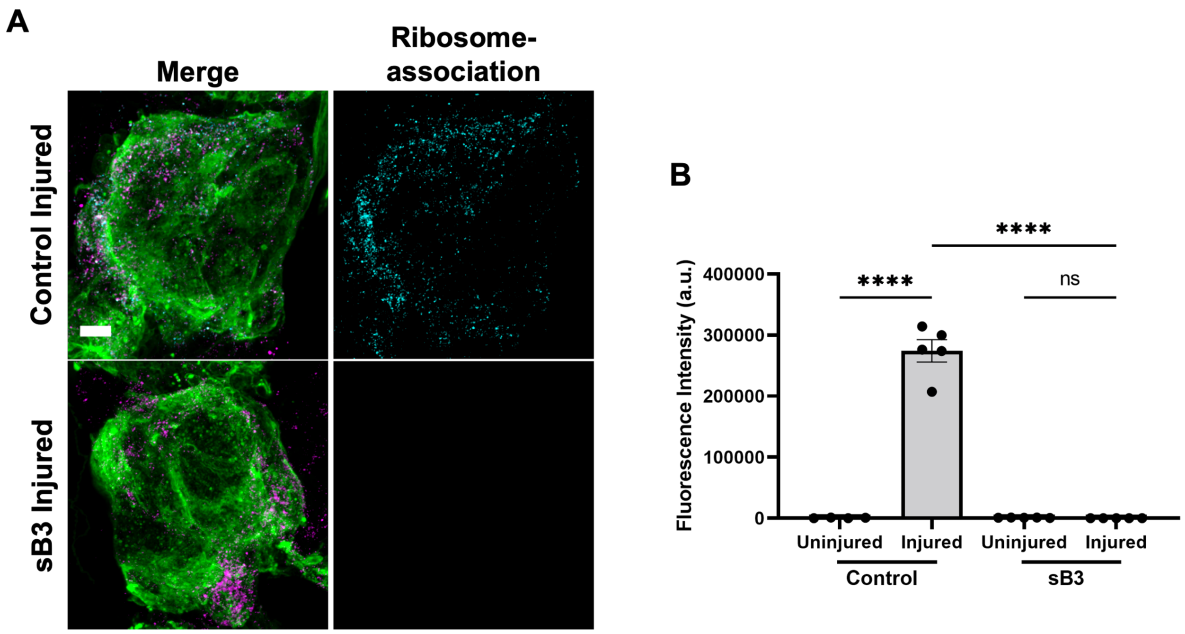

Supplementary Figure 8: Hybridization with sB3 initiator to assess FLARIM background signal
(A) Representative image of injured ALs (20 hpi), hybridized with control probes (Mmp-1 HCR B2/FLARIM sB3 and 18S FLARIM sB3) or with the sB3 initiator (GTCCCTGCCTCTATATCT) [1.6 µM] and Mmp-1 HCR B2/FLARIM sB3 [2.0 µM]. (Supp. Table S4). Single slice: 0.5 µm. Scale bar: 10 µm. Genotype: *;UAS-mCD8::GFP/UAS-mCD8::GFP;TIFR-Gal4/TIFR-Gal4*. **(B)** Quantification of FLARIM fluorescence intensity (a.u.) within ALs. Control uninjured (n=4), Control injured (n=5), sB3 uninjured (n=5), sB3 injured (n=5). Mean ± SEM; One-way ANOVA (Sidak's *post hoc* test); non-significant (ns), ****(p<0.0001).

Probe	Sequence (5′ → 3′)
Mmp-1 smiFISH-1	CTAAGGTTCACAAATGCACTGCCCGTAGGTTACACTCGGACCTCGTCGACATGCATT
Mmp-1 smiFISH-2	AATCGGGCGTCATGGAATCTGTAGTACTTGTTTACACTCGGACCTCGTCGACATGCATT
Mmp-1 smiFISH-3	AGCCGAACTGGGACAGGTAGATCTCTGTTACACTCGGACCTCGTCGACATGCATT
Mmp-1 smiFISH-4	CGACTATGAACACTGAACTTTGGCAGTTTGTCTTACACTCGGACCTCGTCGACATGCATT
Mmp-1 smiFISH-5	GATCTTGGTGGTTAGATAAGGCGGGCAAAGTCTTACACTCGGACCTCGTCGACATGCATT
Mmp-1 smiFISH-6	TATATAGTCACTATCACTTGGGCGAATTTGGCTTACACTCGGACCTCGTCGACATGCATT
Mmp-1 smiFISH-7	CAGGGCACTATCCACACTCTACACTCTTACACTCGGACCTCGTCGACATGCATT
Mmp-1 smiFISH-8	GGCTAGCACAGCTCCCAGTTTCCAAGTTACACTCGGACCTCGTCGACATGCATT
Mmp-1 smiFISH-9	GAGCTCCTTTCCCATGTGCCGACATTTTACACTCGGACCTCGTCGACATGCATT
Mmp-1 smiFISH-10	TTTGGAAACTTTACTCGAGTGGCTAGCGTTGATTACACTCGGACCTCGTCGACATGCATT
Mmp-1 smiFISH-11	GCTGGTATCTCTTAGCTCTTTTAGCTAACGTTACACTCGGACCTCGTCGACATGCATT
Mmp-1 smiFISH-12	GGCTGCGTCAAAGTCATCACCGTTGCTTACACTCGGACCTCGTCGACATGCATT
Mmp-1 smiFISH-13	GTTCGAACTCGTTGTCCGAGCCTTCGACTTACACTCGGACCTCGTCGACATGCATT
Mmp-1 smiFISH-14	TATTACCTGTGGACGAGGGCGTGTTCTTGTTACACTCGGACCTCGTCGACATGCATT
Mmp-1 smiFISH-15	GAATGCCCGTGAAGCCCTCGCTGATTTTACACTCGGACCTCGTCGACATGCATT
Mmp-1 smiFISH-16	CTTAGGGTAGACGCCGTCCATCTGACGTTACACTCGGACCTCGTCGACATGCATT
Mmp-1 smiFISH-17	GAAGAAGTACGTCTTGCCGTTCTTGTAGGTGATTACACTCGGACCTCGTCGACATGCATT
Mmp-1 smiFISH-18	CTTGGAGTCCTTGCAGATGGAGTCGTCTATTACACTCGGACCTCGTCGACATGCATT
Mmp-1 smiFISH-19	TCAGCTGGTTTGTTTTGCGCCCATACAGTTACACTCGGACCTCGTCGACATGCATT
Mmp-1 smiFISH-20	CGCCTTGTCGTCCTCGTCCAACTTGAATTACACTCGGACCTCGTCGACATGCATT
Mmp-1 smiFISH-21	TCAGAGCGGAGCTCTGATCTGAGTGGGTTACACTCGGACCTCGTCGACATGCATT
Mmp-1 smiFISH-22	CCACCTGGAACAGATTGGTGCCTCGAGTTACACTCGGACCTCGTCGACATGCATT
Mmp-1 smiFISH-23	CCATGCTCGCTCTCCACGAACTTGATTTACACTCGGACCTCGTCGACATGCATT
Mmp-1 smiFISH-24	GATCTTGTAGGTGAGGTTCTTCACACGCCTTACACTCGGACCTCGTCGACATGCATT
Mmp-1 smiFISH-25	CGCGAAGCTTTGGAACTCCTCGATGGCTTACACTCGGACCTCGTCGACATGCATT
Mmp-1 smiFISH-26	TGTGTGGTGGTGGAAACGGGTGCCGATTGATTACACTCGGACCTCGTCGACATGCATT
Mmp-1 smiFISH-27	AGGCTCGTCTATTTGTCATGTGGTTCCACTTACACTCGGACCTCGTCGACATGCATT
Mmp-1 smiFISH-28	GCCGCTGGCACTTTGAACTTTATATCACTTACACTCGGACCTCGTCGACATGCATT
Mmp-1 smiFISH-29	TCTTTAGTTTCTTCACAGGGCTGTTTCGAACTTTACACTCGGACCTCGTCGACATGCATT
Mmp-1 smiFISH-30	TGCTGCCCTTGAAGAAGTATATCTTGCCTTACACTCGGACCTCGTCGACATGCATT
Mmp-1 smiFISH-31	CCCTGCGCCGAGTTGAAGAGTGTGTCTTTACACTCGGACCTCGTCGACATGCATT
Mmp-1 smiFISH-32	GAAGGGGGGCGTGGCCGAGTCAACAGTTACACTCGGACCTCGTCGACATGCATT
Mmp-1 smiFISH-33	CCCTTGAAGAAGTACGTGTAGCCATTGGTGTTTACACTCGGACCTCGTCGACATGCATT
Mmp-1 smiFISH-34	CTCTTGGCCGGATCGAAGCGCCAGAATTACACTCGGACCTCGTCGACATGCATT
Mmp-1 smiFISH-35	CCCAAACCATTGCGGCGTCCAGATGGTTACACTCGGACCTCGTCGACATGCATT
Mmp-1 smiFISH-36	CGGGTTCAAAGCCGCGATAGAAGGGCGCTTACACTCGGACCTCGTCGACATGCATT
Mmp-1 smiFISH-37	AAATGCGCGACCGATCTCCGCGTCGATTACACTCGGACCTCGTCGACATGCATT
Mmp-1 smiFISH-38	CAGCGGGGCAGGGACATCAGCTTCATTTACACTCGGACCTCGTCGACATGCATT
Mmp-1 smiFISH-39	TATTTTTGTTTGGTTCTCTCCAATTCCTTGCATTACACTCGGACCTCGTCGACATGCATT
Mmp-1 smiFISH-40	TTTGGATTTCCTCTCATCGTATTCGATATGATTTACACTCGGACCTCGTCGACATGCATT
Mmp-1 smiFISH-41	GCTGGTATCTCTTAGCTCTTTTAGCTAACGTTACACTCGGACCTCGTCGACATGCATT

Gene-specific probe sequence (Mmp-1)
FLAP sequence

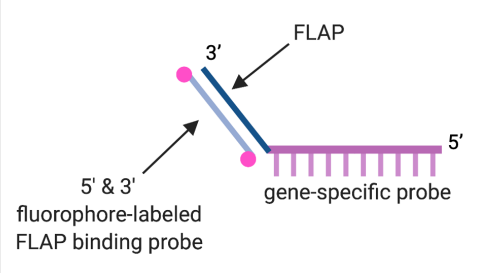

Supplementary Table 1: mmp-1 smiFISH probeset
mmp-1 gene-specific sequences (magenta), FLAP sequence (blue; Tsanov, *et al.,* 2016(224))

Probe	Sequence (5′ → 3′)
18S FLARIM-sB3-1	CTTTGAGACAAGCATATAACTACTGGCAAAAAAAAAAAAAAGTCCCTGCCTCTATATCT
18S FLARIM-sB3-2	GCCTTTTGCGGTTTCACTTTTAATTCGAAAAAAAAAAAAAAGTCCCTGCCTCTATATCT
18S FLARIM-sB3-3	TAGAATTACCACAGTTATCCAAGTAAAAAAAAAAAAAAGTCCCTGCCTCTATATCT
18S FLARIM-sB3-4	CGCTTGGTTTTAGCCTAATAAAAGCAAAAAAAAAAAAAAGTCCCTGCCTCTATATCT
18S FLARIM-sB3-5	TTGTTATTTTTCGTCACTACCTCCCCCAAAAAAAAAAAAAAGTCCCTGCCTCTATATCT
18S FLARIM-sB3-6	AAGTGTACTCATTCCAATTACAGGGCCAAAAAAAAAAAAAAGTCCCTGCCTCTATATCT
18S FLARIM-sB3-7	TATACGCTATTGGAGCTGGAATTACCGAAAAAAAAAAAAAAGTCCCTGCCTCTATATCT
18S FLARIM-sB3-8	CGGTCCAAGAATTTCACCTCTCAAAAAAAAAAAAAAGTCCCTGCCTCTATATCT
18S FLARIM-sB3-9	GAACCTCTAACTTTCGTTCTTGATTAATGAAAAAAAAAAAAAAGTCCCTGCCTCTATATCT
18S FLARIM-sB3-10	GCATCGTTTATGGTTAGAACTAGGGCGAAAAAAAAAAAAAAGTCCCTGCCTCTATATCT
18S FLARIM-sB3-11	AAGTTTCAGCTTTGCAACCATACTTAAAAAAAAAAAAAAGTCCCTGCCTCTATATCT
18S FLARIM-sB3-12	GGTAAGTTTTCCCGTGTTGAGTCAAATTAAAAAAAAAAAAAAGTCCCTGCCTCTATATCT
18S FLARIM-sB3-13	CACCCATAGATTCGAGAAAGAGCTAAAAAAAAAAAAAAGTCCCTGCCTCTATATCT
18S FLARIM-sB3-14	GGAATTAACCAGACAAATCACTCCAAAAAAAAAAAAAAGTCCCTGCCTCTATATCT
18S FLARIM-sB3-15	CTGTTATTGCTCAATCTCATTATTGCTAAAAAAAAAAAAAAGTCCCTGCCTCTATATCT
18S FLARIM-sB3-16	AGCATGAAAGTGGTTCAGCGGTTTACAAAAAAAAAAAAAAGTCCCTGCCTCTATATCT
18S FLARIM-sB3-17	CACACTTACTGGGAATTCCAAGTTCATAAAAAAAAAAAAAAGTCCCTGCCTCTATATCT
18S FLARIM-sB3-18	GGTGTGTACAAAGGGCAGGGACGTAAAAAAAAAAAAAAGTCCCTGCCTCTATATCT
18S FLARIM-sB3-19	TGATCCTTCCGCAGGTTCACCTACGAAAAAAAAAAAAAAGTCCCTGCCTCTATATCT
18S FLARIM-sB3-20	CAATTTGTCCATTTAAGAAGCTAGTGTCAAAAAAAAAAAAAAGTCCCTGCCTCTATATCT
18S FLARIM-sB3-21	GTTTCCCGGGAAGCGACTGAGAGAAAAAAAAAAAAAAGTCCCTGCCTCTATATCT
18S FLARIM-sB3-22	CCAGACTTGCCCTCCAATTGGTCCTTAAAAAAAAAAAAAAGTCCCTGCCTCTATATCT
18S FLARIM-sB3-23	GTTACCCGTTGCAACCATGGTAGTCAAAAAAAAAAAAAAGTCCCTGCCTCTATATCT
18S FLARIM-sB3-24	CTGCCTTCCTTAGATGTGGTAGCCGAAAAAAAAAAAAAAGTCCCTGCCTCTATATCT
18S FLARIM-sB3-25	TCCCTCTCCGGAATCGAACCCTGATAAAAAAAAAAAAAAGTCCCTGCCTCTATATCT

18S ribosome-specific probe sequence
Split initiator sequence (B3)
Spacer

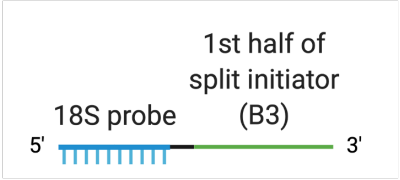

Supplementary Table 2: 18S FLARIM split B3 probe sequences
18S ribosome-specific probe sequences (blue) and B3 split initiator sequence (green; Choi *et al.,* 2014(223)).

Probe	Sequence (5′ → 3′)
Mmp1 HCR-B2/FLARIM-sB3-1	CCTCGTAAATCCTCATCAATCATCCAGTAAACCGCCAAAAACTAAGGTTCACAAATGCACTGCCCGTAGGAAAAAAAAAAAACCACTCAACTTTAACCCG
Mmp1 HCR-B2/FLARIM-sB3-2	CCTCGTAAATCCTCATCAATCATCCAGTAAACCGCCAAAAAAATCGGGCGTCATGGAATCTGTAGTACTTGTAAAAAAAAAAAACCACTCAACTTTAACCCG
Mmp1 HCR-B2/FLARIM-sB3-3	CCTCGTAAATCCTCATCAATCATCCAGTAAACCGCCAAAAAAGCCGAACTGGGACAGGTAGATCTCTGAAAAAAAAAAAACCACTCAACTTTAACCCG
Mmp1 HCR-B2/FLARIM-sB3-4	CCTCGTAAATCCTCATCAATCATCCAGTAAACCGCCAAAAACGACTATGAACACTGAACTTTGGCAGTTTGTCAAAAAAAAAAAACCACTCAACTTTAACCCG
Mmp1 HCR-B2/FLARIM-sB3-5	CCTCGTAAATCCTCATCAATCATCCAGTAAACCGCCAAAAAGATCTTGGTGGTTAGATAAGGCGGGCAAAGTCAAAAAAAAAAAACCACTCAACTTTAACCCG
Mmp1 HCR-B2/FLARIM-sB3-6	CCTCGTAAATCCTCATCAATCATCCAGTAAACCGCCAAAAATATATAGTCACTATCACTTGGGCGAATTTGGCAAAAAAAAAAAACCACTCAACTTTAACCCG
Mmp1 HCR-B2/FLARIM-sB3-7	CCTCGTAAATCCTCATCAATCATCCAGTAAACCGCCAAAAACAGGGCACTATCCACACTCTACACTCAAAAAAAAAAAACCACTCAACTTTAACCCG
Mmp1 HCR-B2/FLARIM-sB3-8	CCTCGTAAATCCTCATCAATCATCCAGTAAACCGCCAAAAAGGCTAGCACAGCTCCCAGTTTCCAAGAAAAAAAAAAACCACTCAACTTTAACCCG
Mmp1 HCR-B2/FLARIM-sB3-9	CCTCGTAAATCCTCATCAATCATCCAGTAAACCGCCAAAAAGAGCTCCTTTCCCATGTGCCGACATTAAAAAAAAAAACCACTCAACTTTAACCCG
Mmp1 HCR-B2/FLARIM-sB3-10	CCTCGTAAATCCTCATCAATCATCCAGTAAACCGCCAAAAATTTGGAAACTTTACTCGAGTGGCTAGCGTTGAAAAAAAAAAAACCACTCAACTTTAACCCG
Mmp1 HCR-B2/FLARIM-sB3-11	CCTCGTAAATCCTCATCAATCATCCAGTAAACCGCCAAAAAGCTGGTATCTCTTAGCTCTTTTAGCTAACGAAAAAAAAAAACCACTCAACTTTAACCCG
Mmp1 HCR-B2/FLARIM-sB3-12	CCTCGTAAATCCTCATCAATCATCCAGTAAACCGCCAAAAAGGCTGCGTCAAAGTCATCACCGTTGCAAAAAAAAAAAACCACTCAACTTTAACCCG
Mmp1 HCR-B2/FLARIM-sB3-13	CCTCGTAAATCCTCATCAATCATCCAGTAAACCGCCAAAAAGTTCGAACTCGTTGTCCGAGCCTTCGACAAAAAAAAAAAACCACTCAACTTTAACCCG
Mmp1 HCR-B2/FLARIM-sB3-14	CCTCGTAAATCCTCATCAATCATCCAGTAAACCGCCAAAAATATTACCTGTGGACGAGGGCGTGTTCTTGAAAAAAAAAAAACCACTCAACTTTAACCCG
Mmp1 HCR-B2/FLARIM-sB3-15	CCTCGTAAATCCTCATCAATCATCCAGTAAACCGCCAAAAAGAATGCCCGTGAAGCCCTCGCTGATTAAAAAAAAAAAACCACTCAACTTTAACCCG
Mmp1 HCR-B2/FLARIM-sB3-16	CCTCGTAAATCCTCATCAATCATCCAGTAAACCGCCAAAAACTTAGGGTAGACGCCGTCCATCTGACGAAAAAAAAAAAACCACTCAACTTTAACCCG
Mmp1 HCR-B2/FLARIM-sB3-17	CCTCGTAAATCCTCATCAATCATCCAGTAAACCGCCAAAAAGAAGAAGTACGTCTTGCCGTTCTTGTAGGTGAAAAAAAAAAAACCACTCAACTTTAACCCG
Mmp1 HCR-B2/FLARIM-sB3-18	CCTCGTAAATCCTCATCAATCATCCAGTAAACCGCCAAAAACTTGGAGTCCTTGCAGATGGAGTCGTCTAAAAAAAAAAAACCACTCAACTTTAACCCG
Mmp1 HCR-B2/FLARIM-sB3-19	CCTCGTAAATCCTCATCAATCATCCAGTAAACCGCCAAAAATCAGCTGGTTTGTTTTGCGCCCATACAGAAAAAAAAAAACCACTCAACTTTAACCCG
Mmp1 HCR-B2/FLARIM-sB3-20	CCTCGTAAATCCTCATCAATCATCCAGTAAACCGCCAAAAACGCCTTGTCGTCCTCGTCCAACTTGAAAAAAAAAAAACCACTCAACTTTAACCCG
Mmp1 HCR-B2/FLARIM-sB3-21	CCTCGTAAATCCTCATCAATCATCCAGTAAACCGCCAAAAATCAGAGCGGAGCTCTGATCTGAGTGGGAAAAAAAAAAAACCACTCAACTTTAACCCG
Mmp1 HCR-B2/FLARIM-sB3-22	CCTCGTAAATCCTCATCAATCATCCAGTAAACCGCCAAAAACCACCTGGAACAGATTGGTGCCTCGAGAAAAAAAAAAAACCACTCAACTTTAACCCG
Mmp1 HCR-B2/FLARIM-sB3-23	CCTCGTAAATCCTCATCAATCATCCAGTAAACCGCCAAAAACCATGCTCGCTCTCCACGAACTTGATAAAAAAAAAAAACCACTCAACTTTAACCCG
Mmp1 HCR-B2/FLARIM-sB3-24	CCTCGTAAATCCTCATCAATCATCCAGTAAACCGCCAAAAAGATCTTGTAGGTGAGGTTCTTCACACGCCAAAAAAAAAAAACCACTCAACTTTAACCCG
Mmp1 HCR-B2/FLARIM-sB3-25	CCTCGTAAATCCTCATCAATCATCCAGTAAACCGCCAAAAACGCGAAGCTTTGGAACTCCTCGATGGCAAAAAAAAAAAACCACTCAACTTTAACCCG
Mmp1 HCR-B2/FLARIM-sB3-26	CCTCGTAAATCCTCATCAATCATCCAGTAAACCGCCAAAATGTGTGGTGGTGGAAACGGGTGCCGATTGAAAAAAAAAAAACCACTCAACTTTAACCCG
Mmp1 HCR-B2/FLARIM-sB3-27	CCTCGTAAATCCTCATCAATCATCCAGTAAACCGCCAAAAAAGGCTCGTCTATTTGTCATGTGGTTCCACAAAAAAAAAAAACCACTCAACTTTAACCCG
Mmp1 HCR-B2/FLARIM-sB3-28	CCTCGTAAATCCTCATCAATCATCCAGTAAACCGCCAAAAAGCCGCTGGCACTTTGAACTTTATATCACAAAAAAAAAAAACCACTCAACTTTAACCCG
Mmp1 HCR-B2/FLARIM-sB3-29	CCTCGTAAATCCTCATCAATCATCCAGTAAACCGCCAAAAATCTTTAGTTTCTTCACAGGGCTGTTTCGAACTAAAAAAAAAAAACCACTCAACTTTAACCCG
Mmp1 HCR-B2/FLARIM-sB3-30	CCTCGTAAATCCTCATCAATCATCCAGTAAACCGCCAAAAATGCTGCCCTTGAAGAAGTATATCTTGCCAAAAAAAAAAAACCACTCAACTTTAACCCG
Mmp1 HCR-B2/FLARIM-sB3-31	CCTCGTAAATCCTCATCAATCATCCAGTAAACCGCCAAAAACCCTGCGCCGAGTTGAAGAGTGTGTCTAAAAAAAAAAAACCACTCAACTTTAACCCG
Mmp1 HCR-B2/FLARIM-sB3-32	CCTCGTAAATCCTCATCAATCATCCAGTAAACCGCCAAAAAGAAGGGGGGCGTGGCCGAGTCAACAGAAAAAAAAAAAACCACTCAACTTTAACCCG
Mmp1 HCR-B2/FLARIM-sB3-33	CCTCGTAAATCCTCATCAATCATCCAGTAAACCGCCAAAAACCCTTGAAGAAGTACGTGTAGCCATTGGTGTAAAAAAAAAAAACCACTCAACTTTAACCCG
Mmp1 HCR-B2/FLARIM-sB3-34	CCTCGTAAATCCTCATCAATCATCCAGTAAACCGCCAAAAACTCTTGGCCGGATCGAAGCGCCAGAAAAAAAAAAAACCACTCAACTTTAACCCG
Mmp1 HCR-B2/FLARIM-sB3-35	CCTCGTAAATCCTCATCAATCATCCAGTAAACCGCCAAAAACCCAAACCATTGCGGCGTCCAGATGGAAAAAAAAAAAACCACTCAACTTTAACCCG
Mmp1 HCR-B2/FLARIM-sB3-36	CCTCGTAAATCCTCATCAATCATCCAGTAAACCGCCAAAACGGGTTCAAAGCCGCGATAGAAGGGCGCAAAAAAAAAAAACCACTCAACTTTAACCCG
Mmp1 HCR-B2/FLARIM-sB3-37	CCTCGTAAATCCTCATCAATCATCCAGTAAACCGCCAAAAAAAATGCGCGACCGATCTCCGCGTCGAAAAAAAAAAAACCACTCAACTTTAACCCG
Mmp1 HCR-B2/FLARIM-sB3-38	CCTCGTAAATCCTCATCAATCATCCAGTAAACCGCCAAAAACAGCGGGGCAGGGACATCAGCTTCATAAAAAAAAAAAACCACTCAACTTTAACCCG
Mmp1 HCR-B2/FLARIM-sB3-39	CCTCGTAAATCCTCATCAATCATCCAGTAAACCGCCAAAAATATTTTTGTTTGGTTCTCTCCAATTCCTTGCAAAAAAAAAAAACCACTCAACTTTAACCCG
Mmp1 HCR-B2/FLARIM-sB3-40	CCTCGTAAATCCTCATCAATCATCCAGTAAACCGCCAAAAATTTGGATTTCCTCTCATCGTATTCGATATGATAAAAAAAAAAAACCACTCAACTTTAACCCG
Mmp1 HCR-B2/FLARIM-sB3-41	CCTCGTAAATCCTCATCAATCATCCAGTAAACCGCCAAAAAGCTGGTATCTCTTAGCTCTTTTAGCTAACGAAAAAAAAAAAACCACTCAACTTTAACCCG

Full initiator sequence (B2)
Gene-specific probe sequence (Mmp-1)
Split initiator sequence (B3)
Spacer

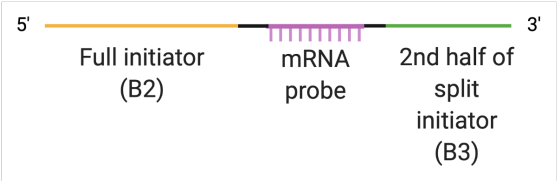

Supplementary Table 3: mmp-1 HCR B2 FLARIM split B3 probe sequences
mmp-1 gene-specific sequences (magenta), B3 split initiator sequence (green; Choi *et al.,* 2014(223)), and full B2 initiator sequence (orange; Choi *et al.,* 2014(223)).

Discussion

In this study, we have modified HCR and FLARIM methods to develop a novel dual probeset strategy to visualize single mRNA transcripts and their associated ribosomes *in vivo*(214, 223, 225). Specifically, we have applied this approach to visualize *mmp-1* transcripts in ensheathing glial cells responding to acute axon injury in adult *Drosophila*. It is becoming increasingly clear that directed transport of select mRNAs and local translation are essential for a wide range of cellular responses, including glial cell function in both the developing and mature brain(235-238). Thus, we propose that this novel methodology to visualize and quantify transcripts and, notably, ribosome association in whole tissue will be broadly valuable.

The mechanisms of mRNA localization and local translation are highly conserved and provide cells with the ability to restrict responses to subcellular compartments, conserve energy, and localize responses to specific stimuli(213, 230). Directed transport/translation of transcripts has been well described in neurons(239-243). More recently, the importance of local translation has been explored in glial cells. Local transcriptomes and translatomes have been characterized within astrocyte peripheral processes at the tripartite synapse, as well as astrocytic endfeet at the gliovascular interface(211, 212). In oligodendrocytes, myelin basic protein (*mbp*) mRNA is localized to oligodendrocyte sheaths and is required for proper myelin and axon development, while radial glia transport and locally translate mRNAs in their distal processes during development(209, 236). Research has also focused on how specific stimuli activate such mechanisms. Peripheral processes in astrocytes induce local translation in response to fear conditioning in mice, while neuronal activity may control myelination by oligodendrocytes through the induction of local protein synthesis(210, 213).

Here, we show that that our *mmp-1* FLARIM v2.0 approach can reliably detect significant *mmp-1* upregulation in glia following olfactory nerve injury and that this strategy allows us to monitor changes in the spatial distribution of mmp-1 transcripts, as well as association with ribosomes within one day after axotomy. We propose that our detection of transcript/ribosome

association indicates that local translation of secreted Mmp-1 protein occurs at the distal process of glial cells as they invade injury sites (Fig. 3). We observe markers for both ER and GA in fine distal processes of ensheathing glia under both basal and injury conditions, suggesting that this glial subtype is equipped with organelles to locally translate and secrete a released factor such as Mmp-1 (Fig. 5). Given the ramified morphology of ensheathing glia, and the well-known role of Mmp-1 in ECM remodeling, rapid, local production of Mmp-1 is likely important for proper extension of glial processes within the deeper regions of the antennal lobes. As a result, this would aid phagocytic engulfment of degenerating olfactory neurons.

From a technical standpoint, FLARIM v2.0 offers a number of important features and, notably, some key advantages over the original FLARIM approach (Fig. 2). Fewer probes are required to monitor association of ribosomes and transcripts of interest. Transcripts and ribosomes are visualized as diffraction-limited spots and can be quantified to assess relative changes in gene expression and ribosome association in discrete cell types. Moreover, this method allows for flexible fluorescent labeling within samples. Finally, the generation of probes ordered as oPools is very cost effective. This and related protocols also offer the obvious benefit of greater spatial resolution to quantify gene upregulation in discrete cell types in heterogenous tissue, as opposed to cruder approaches (e.g., quantitative-PCR on crushed tissue).

More broadly, this approach offers a novel experimental readout for a component of glial immunity that has not yet been explored in flies and minimally in other model organisms, namely local translation of immune genes at injury sites. Our results now offer a new platform to explore future questions to investigate how mRNA transcripts are transported, translated, and eventually degraded once an immune response is no longer required. Previous work from our lab has shown that insulin-like signaling (ILS) pathways are acutely activated in ensheathing glial cells responding to olfactory nerve axotomy(132). Because ILS cascades are known to promote protein translation via mammalian target of rapamycin (mTOR), this offers an intriguing candidate by which immune gene translation is locally enhanced within glia in response to

neurodegeneration(244). Future screening efforts will reveal how select immune gene transcripts are shuttled throughout glial processes to support proper innate immune reactions to acute trauma and perhaps also chronic neurodegenerative conditions.

Methods

Probe design & Synthesis

Probes to the transcript of interest were designed using Oligostan in R Studio(224, 245). The probes were compared to a database of noncoding RNAs (http://flybase.org(246): http://ftp.flybase.net/genomes/Drosophila_melanogaster/dmel_r6.37_FB2020_06/fasta/; dmel-all-miRNA-r6.37.fasta.gz, dmel-all-miscRNA-r6.37.fasta.gz, dmel-all-ncRNA-r6.37.fasta.gz) for sequence similarity using Geneious (Biomatters). Any probes similar to ncRNAs (miRNA, snoRNA, lncRNA) were discarded from the probeset. The remaining probes were used to make up the gene-specific probesets. B2 and split B3 initiator sequences were added to the probes to allow for HCR amplification and FLARIM detection, which have been previously described(214, 223). Probes were synthesized in 96-well plates or as 50 pmol oPools (Integrated DNA Technologies). Probe sequences can be found in Supplementary tables 1-3.

ORN Injury Assay & Dissection

Third antennal segments and maxillary palps were removed bilaterally using forceps, as previously described(120). Flies were raised at 25˚ C and returned to this temperature following injury, until dissection at 20 hpi. Fly lines containing the tubulin-Gal80ts transgene were raised at 18˚C and moved to 30˚C for 7 days to induce Mmp-1 RNAi expression. These flies were then injured and moved back to 30˚C until dissection. Fly heads were pulled and fixed in 4% paraformaldehyde (PFA; Electron Microscopy Sciences, #19210) + Triton X-100 (TX; 0.1%; MP Biomedicals, 04807426-CF) for 20 min at room temperature (RT) on a rocker. Then, heads were washed in 1X phosphate buffered saline (PBS; Invitrogen, AM9624) + TX (0.01%) on a rocker at

RT (3 x 2 min). Brains were dissected in 1X PBS-TX (0.01%). Brains were then fixed in 4% PFA + 0.1% TX for 20min at RT on a rocker and washed with 1X PBS-TX (0.1%) on a rocker at RT (3 x 2 min). To increase probe penetration, brains were also permeabilized for 20 min in 1X PBS-TX (0.5%), while rocking at RT. Brains for immunostaining were not additionally permeabilized.

smiFISH

The smiFISH reagents, flap hybridization, and protocol have been described previously(221, 224). The smiFISH protocol has been adapted as follows: After dissection, fixation, and permeabilization, brains were placed in hybridization buffer(224) with the Mmp-1 smiFISH ATTO 550 (Integrated DNA Technologies) probeset and hybridized overnight in a thermal cycler at 37˚C. The following day, brains were washed in 1X saline-sodium citrate (SSC; Invitrogen, AM9763)/10% formamide (Sigma, F9037)/0.1% TX/0.1% Tween-20 (Calbiochem, #655204) at 50˚C (2 x 30 min) in a thermal cycler. Brains were then mounted in Vectashield (Vector Labs) under #1.5 coverslips and imaged.

Probe Hybridization & Signal Amplification

The HCR v3.0 hybridization and amplification protocol has been described previously for whole-mount fruit fly embryos(225, 247) (https://www.molecularinstruments.com/hcr-rnafish-protocols). The protocol was utilized in adult fruit fly brains as follows: After permeabilization, brains were pre-hybridized for 20 min at 37˚C in probe hybridization buffer (Molecular Instruments), which had already been heated to 37˚C. Brains were then hybridized overnight (16-18 hrs) with the gene-specific and 18S FLARIM probes in a thermal cycler at 37˚C. The following day, brains were washed in probe wash buffer (Molecular Instruments) at 37˚C in the thermal cycler (4 x 15 min). During the washes, HCR hairpins (Molecular Instruments) were snap-cooled, and the amplification buffer (Molecular Instruments) was moved to RT. Brains were washed again in 5X SSC/0.1% Tween-20 at RT (2 x 5min). Brains were pre-amplified with amplification buffer at RT

for 10 min. Then, hairpins were added to the amplification buffer and the HCR and FLARIM signals were amplified. Amplification times were empirically determined for each probeset in this paper (*mmp-1* HCR B2 FLARIM split B3 Alexa Fluor 546: 1 hr; 18S FLARIM B3 Alexa Fluor 647: 6 hrs). Following amplification, brains were washed in 5X SSC/0.1% Tween-20 at RT (5 min, 2 x 30 min, 5 min), and then mounted in Vectashield (Vector Labs) under #1.5 coverslips and imaged.

Immunostaining

Antibodies were diluted in 1X PBS-TX (0.1%), and brains were incubated in primary antibodies overnight on a shaker at 4˚C. Brains were washed in PBS-TX (0.1%) at RT (3 x 30 min) and incubated in secondary antibodies in 1X PBS-TX (0.1%) for 2 hrs at RT on a shaker. Brains were then washed again in 1X PBS-TX (0.1%) at RT (3 x 30 min) and mounted in Vectashield (Vector Labs) under #1.5 coverslips and imaged.

Antibodies

The following primary antibodies were used: mouse beta-galactosidase 40-1a (Developmental Studies Hybridoma Bank) at 1:100, chicken anti-GFP (ThermoFisher, #A10262) at 1:1000, mouse anti-nc82 (Bruchpilot; Developmental Studies Hybridoma Bank) at 1:50, goat anti-GMAP (Developmental Studies Hybridoma Bank) at 1:800, mouse anti-Cnx99A 6-2-1 (Developmental Studies Hybridoma Bank) at 1:400. All secondary antibodies (Jackson Immunoresearch 703-545-155, 715-295-150, and 705-295-147) were used at a 1:400 dilution.

Microscopy & Analysis

Samples were imaged on a Zeiss LSM 700 with a Zeiss 40X 1.4 NA oil immersion plan-apochromatic lens. Samples with Golgi and ER staining were imaged using a Zeiss Elyra 7 with lattice SIM with a Zeiss 63X 1.4 NA oil immersion plan-apochromatic lens at the OHSU Advanced Light Microscopy Core (ALMC). Samples for high resolution quantification and DAPI staining were

imaged using a Zeiss LSM 900 with Airyscan 2 with a Zeiss 63X 1.4 NA oil immersion plan-apochromatic lens at the OHSU ALMC. Brains within the same experiment were imaged on the same day, using the same microscope settings. Images were processed in Zen (Zeiss). Volocity 3D Image Analysis Software (Quorum Technologies) was used for fluorescence and puncta quantification, while Imaris Cell Imaging Software (Andor Technology) at the OHSU ALMC was used for super-resolution image processing, 3D rendering, and colocalization analysis. GraphPad Prism 8 (Graphpad Software) was used for statistical analysis: Student's t-test, Mann-Whitney test, one-way ANOVA. Normality was tested using the D'Agostino-Pearson normality test. Outliers were identified using the ROUT method. Experiments were not blinded. For *mmp-1* FLARIM v2.0 quantifications, 5 µm was removed from the top of each z-stack to exclude ensheathing glial cell bodies from the analysis, and only quantify *mmp-1* mRNA and ribosome-association signals within the ensheathing glial processes of the ALs. A circular ROI was defined in each AL, where the total fluorescence for each signal was calculated. For maxillary palp injury quantifications, OR85e GFP+ glomeruli were selected as ROIs and segmented, and total fluorescence intensity for *mmp-1* mRNA and ribosome-association signals was calculated. For high-resolution image analysis, GFP+ membranes were segmented, and the sum of mRNA and ribosome-association puncta were calculated.

MARCM clones

MARCM clones were generated as previously described with the following moderations(248): Fly crosses were allowed to lay eggs for 48 hours at RT and were then heat shocked at 37°C for 45 minutes before being raised at room temperature. Once eclosed, flies were aged for 10-12 days before brains were dissected and immunolabeled.

Drosophila Stocks

Adult flies between 4-14 days old were used for experiments. The following lines were used: w1118 (BDSC 5905), UAS-mCD8::GFP (BDSC 5137), UAS-LacZ::NLS (BDSC 3956), TIFR-Gal4(249), repo-Gal4(70), tubulin-Gal80ts (BDSC 7108), UAS-Mmp-1 RNAi(250).

Acknowledgements

We acknowledge expert technical assistance by staff in the Advanced Light Microscopy Core, supported by grant P30NS061800. We thank Jolanda Muenzel for ensheathing glial MARCM images and Alexandra Houser for help with smiFISH experiments. We would also like to thank Dirk Bohmann, Bloomington *Drosophila* Stock Center at Indiana University, and the Developmental Studies Hybridoma Bank at the University of Iowa for flies and antibodies.

Funding

This work was supported by National Institutes of Health grants (R21 NS084112, R21 NS107771, and R01 NS117934), the Ken and Ginger Term Professor Award (M.A.L.), and the Tartar Trust Fellowship at Oregon Health and Sciences University (P.R.).

Conflict of Interest

The authors declare that no competing interests exist.

CHAPTER 4: DISCUSSION AND FUTURE DIRECTIONS

Glial responses to neuronal injury

Glial activation, characterized by changes in morphology, motility, gene expression, phagocytic function, is a cellular response observed in a variety of injury models and pathogenic contexts. Activated glia are found in TBI, ischemic injury, peripheral nerve injury, neurodegenerative disease, and in the aging brain. Research has focused on uncovering the changes in glial function, and the pathways that mediate them, in order to tease apart consequences for brain health, which range from neuroprotective to neurotoxic. A novel component of the glial response is highlighted in this dissertation, whereby immune transcript localization and local translation may play a role in proper glial function after axotomy. These findings raise numerous questions, including whether specific neuronal signals might regulate these new components of the glial response. A number of neuronal injury signals have been elucidated, including ATP signaling and PtdSer exposure; however, this dissertation presents evidence for DCVs as a neuronal injury signal.

Do neuronal DCVs carry and release glial activation signals?

In Chapter 2, I detailed our findings implicating neuronal DCV release in the glial injury response. Building on work by Musashe and colleagues (2016), I established a time course of DCV reduction through static imaging in the *Drosophila* ORN system (Fig. 2.1)(132). Beginning as soon as 30 mpi, DCVs are reduced from ORN projections, and this reduction persists up to 8 hpi. To complement these findings, I was able to show that DCV movement was halted in wing projections immediately following injury, and this stoppage of movement lasted at least until 1 hpi (Fig. 2.3). This could suggest that DCVs are docked and primed for the release of their contents in the minutes after an axotomy.

From previous work, we also know that in the ILS pathway, glial signaling is activated by Ilps, the ligands of the InR(128). However, it is unclear what other endogenous cargo might be released from DCVs in response to neuronal injury. DCVs traffic diverse cargo, which can differ

across cell types(134). Therefore, it is likely that DCV exocytosis could have varied downstream effects on surrounding cells. In the context of injury and our *Drosophila* model, it would be interesting to determine the cargo of ORN DCVs. This could give us new candidates for injury signals that neurons might use to signal to glia and uncover pathways that act together or in parallel to ones we have already described.

Ca^{2+} plays a number of roles in neurons, including the regulation of several intracellular signaling cascades. Moreover, it plays a vital role in regulating vesicular release(251). While the role of Ca^{2+} in SV release is well established, we have also learned that DCV exocytosis is reliant on Ca^{2+}(162, 252). Caps is part of the DCV Ca^{2+}-sensing release machinery, which has been found to mediate docking and fusion of vesicles at the plasma membrane(157, 159). Additionally, Ca^{2+} is particularly relevant in the context of injury, as its entry into the axon is necessary and sufficient for Wallerian degeneration(106). Studies have shown that significant rises of Ca^{2+} are observed in neurons immediately following axotomy (in zebrafish and *Drosophila*) and just before fragmentation of the axon (in zebrafish)(105, 106). It would be important for future experiments to determine whether a second Ca^{2+} wave is observed in *Drosophila* models, especially in the adult fly. The wing would serve as a particularly amenable system, where live Ca^{2+} imaging can be performed using GCaMPs, and a laser injury can be induced. Such an experiment could be combined with more direct measures of DCV behavior, such as DCV trafficking velocity, compared with intra-axonal Ca^{2+} changes. Finally, it would be interesting to determine whether perturbation of the Ca^{2+} sensing machinery (by Caps RNAi or expression of TeTXLC) or the chelation of Ca^{2+} at either stage would affect DCV release or trafficking.

Our TeTXLC findings suggest that blocking both SV and DCV release have an impact on both Draper and Mmp-1 upregulation in glia following injury (Fig. 2.8). This experiment does not tease apart potentially distinct contributions of the vesicle types; however, previous work has hinted at neurotransmitters (NTs) as injury signals. Aberrant action potentials can be hallmarks of neuronal injury, and this has been demonstrated in instances of TBI, where neurons release

excess glutamate(253). Moreover, glial cells have been demonstrated to express N-methyl-D-aspartate (NMDA) receptors and respond to neuronal glutamate signaling(4, 254, 255). In a murine cell culture model, microglia were shown to adopt a pro-inflammatory phenotype following NMDA activation(256).

ILS pathway regulation of Mmp-1

The first half of Chapter 2 examined neuronal events after axotomy; however, I was also interested in determining how DCV release might impact downstream glial responses. We know from previous work that perturbation of neuropeptide processing and DCV release lead to attenuated InR phosphorylation and Draper upregulation; however, I wanted to determine if the ILS pathway, and DCV release, had a role in the recently described Mmp-1 response. I found that expressing the dominant negative InR or perturbing DCV exocytosis resulted in a significantly attenuated Mmp-1 response in glia (Fig. 2.6, 2.7). This further strengthens the link between neuron to glia signaling via DCVs to initiate injury responses. Also, disrupting DCV release had a functional consequence, as ensheathing glia were unable to adequately clear degenerating projections over the 6 days following injury (Fig. 2.9).

Signaling from an injured neuron sets off a cascade of events in the responding glial cell; a complex mechanism with many steps that ultimately leads to upregulation of genes, cytoskeletal rearrangements, motility of processes, and phagocytic activity(16, 257). These steps are coordinated by various signaling pathways. In our model, DCV exocytosis occurs in injured neurons to release cargo, among them Ilps, which bind to the InR on surrounding glial cells. In *Drosophila*, following insulin-like peptide activation of the InR, the receptor signals through phosphatidylinositol-3-kinase (PI3K) and Akt(258, 259). Downstream of Akt and the target of rapamycin (TOR), the ribosomal protein p-70-S6 (S6K) is activated and regulates protein synthesis and ribosome biogenesis(128, 260). This suggests that the InR pathway could regulate distinct steps of transcription and translation in glial cells following neuronal injury. As a result, I

was interested in examining whether DCV release might differentially regulate transcription versus translation of immune genes.

To approach this question, I used smiFISH, a technique described in Chapter 3, to visualize *mmp-1* transcripts in brains where I had perturbed DCV release using Caps RNAi. In preliminary experiments, I found that uninjured brains had relatively low levels of *mmp-1* transcripts, while injured brains upregulated *mmp-1* mRNA at 5 hpi. It was especially surprising that control and ORN>Caps RNAi brains had comparable levels of *mmp-1*, especially when they differed significantly in protein expression at 24 hpi (Fig. 2.7, 4.1A). Interestingly, uninjured ORN>Caps RNAi brains had significantly higher levels of *mmp-1* transcript at basal levels than controls. Although Caps RNAi expression was temporally restricted, as described in Chapter 2, it is possible that leaky expression of the construct in ORNs, and therefore the disruption of DCV release, could have resulted in glial *mmp-1* expression even in uninured brains (Fig. 4.1B). To account for this, I normalized the *mmp-1* smiFISH signal to uninjured controls, which diminished the *mmp-1* mRNA upregulation observed by eye in the ORN>Caps RNAi brains (Fig. 4.1C). A caveat of fluorescence quantification as a readout for *mmp-1* transcript abundance is the inability to accurately assess *mmp-1* signal within the nucleus of ensheathing glia, since they often appear as very bright puncta. As a result, I turned to quantitative PCR to determine whether immune transcripts are still upregulated when DCV release is blocked from neurons. In a preliminary experiment, I assayed three genes: *drpr-I, mmp-1, and ets21C* in uninjured brains and in brains at 5 hpi. Overall, I found that immune genes were upregulated to similar levels in controls and Caps RNAi expressing brains (Fig. 4.1D). These experiments will need to be repeated and further substantiated; however, it is interesting to consider that neuronal DCV release following axotomy might preferentially regulate translation of immune genes.

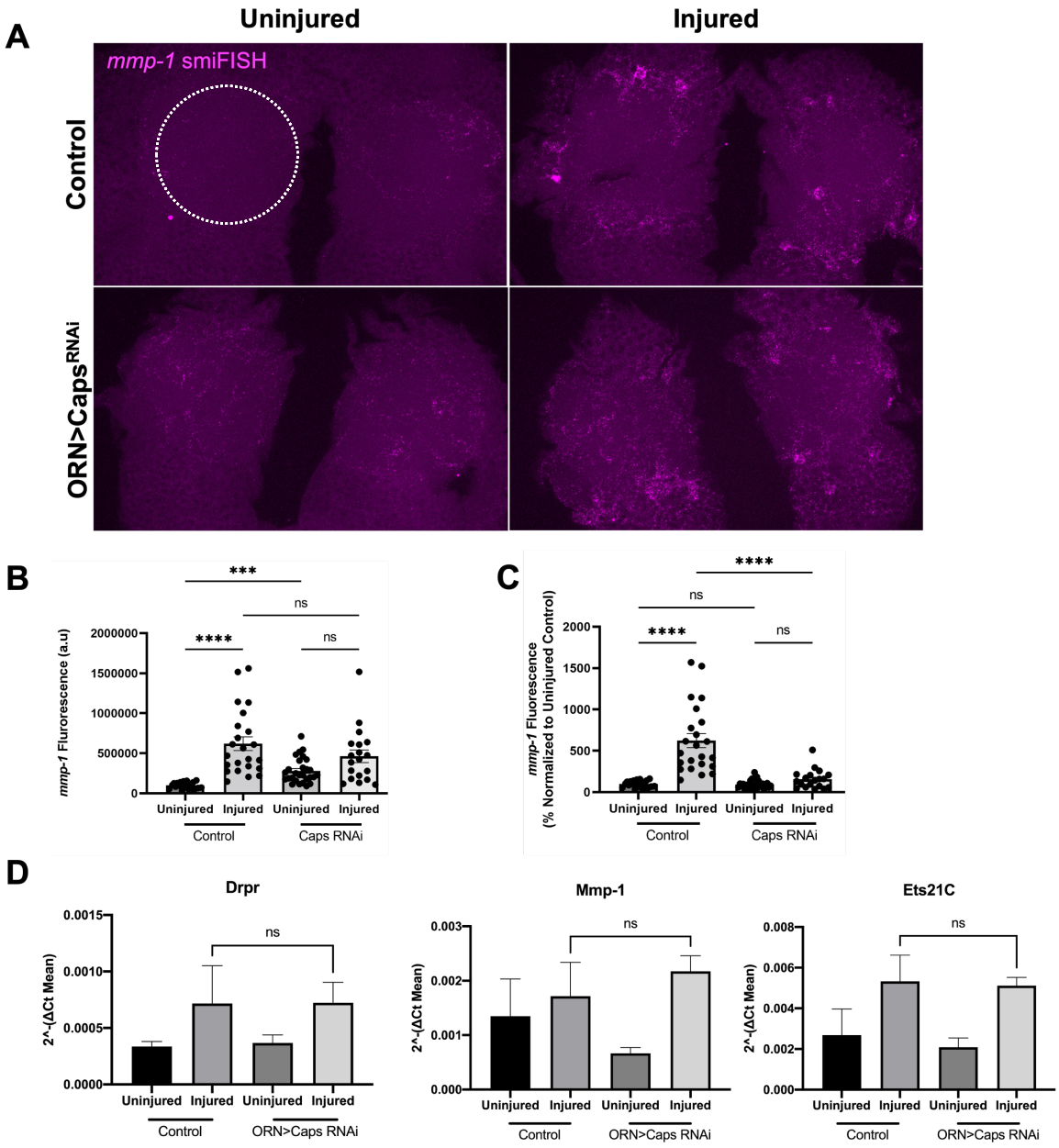

Figure 1: Immune genes are upregulated in ORN>Caps RNAi brains

(A) Representative images of *mmp-1* smiFISH probes in uninjured and injured (5 hpi) brains. Control genotype: pebbled/+;;tub-Gal80ts, UAS-DCR2/+. Caps RNAi genotype: pebbled/+;UAS-Caps RNAi/+;tub-Gal80ts, UAS-DCR2/+ **(B)** Quantification of *mmp-1* fluorescence within ALs (white dotted circle). Control uninjured (n=19), control injured (n=23), Caps RNAi uninjured (n=28), Caps RNAi injured (n=19). Mean ± SEM. Kruskal-Wallis test (Dunn's *post hoc* test). Ns: non-significant, ***(p<0.001), ****(p<0.0001). **(C)** Quantification *mmp-1* fluorescence normalized to uninjured controls. Control uninjured (n=19), control injured (n=23), Caps RNAi uninjured (n=28), Caps RNAi injured (n=19). Mean ± SEM. Kruskal-Wallis test (Dunn's *post hoc* test). Ns: non-significant, ****(p<0.0001). **(D)** Quantitative PCR analysis of immune genes: *drpr-I, mmp-1, ets21C*. Control genotype: pebbled/+;;tub-Gal80ts, UAS-DCR2/+. Caps RNAi genotype: pebbled/+;UAS-Caps RNAi/+;tub-Gal80ts, UAS-DCR2/+. Drpr-I: Control uninjured (n=2), control injured (n=3), Caps RNAi uninjured (n=3), Caps RNAi injured (n=3). Mmp-1: Control uninjured (n=3), control injured (n=3), Caps RNAi uninjured (n=3), Caps RNAi injured (n=3). Ets21C: Control uninjured (n=3), control injured (n=3), Caps RNAi uninjured (n=3), Caps RNAi injured (n=3). Mean ± SEM. One-way ANOVA (Sidak's *post hoc* test). Ns: non-significant.

Future directions

Although we were not able to conclusively show DCV release in our experiments, and tools to do this in the *in vivo* brain are scarce, we began developing a novel split GFP (spGFP) tool to quantify DCV release after an injury event. I have detailed the current progress of this project in the Appendix of this dissertation, as well as some alternative approaches to directly assay DCV release in the fruit fly brain, such as the use of a transgenic fluorogen activating protein (FAP) line, which is targeted to DCVs and could serve as a tool to indicate DCV fusion in the brain(261, 262). This will be a vital experiment to determine whether there is a direct link between neuronal injury and DCV release.

The summary of the neuronal and glial findings from this dissertation are summarized in Fig. 4.2. We propose that DCV exocytosis from injured neurons plays a role in regulating the translation of immune genes, while in preliminary experiments we find that transcription is not affected. Future experiments should utilize the FLARIM v2.0 probeset described in Chapter 3 to examine whether ribosome occupancy on the *mmp-1* transcript is altered in an ORN>Caps RNAi background. Such an experiment could examine the contribution of neuronal DCV signaling to the translation control of immune transcripts.

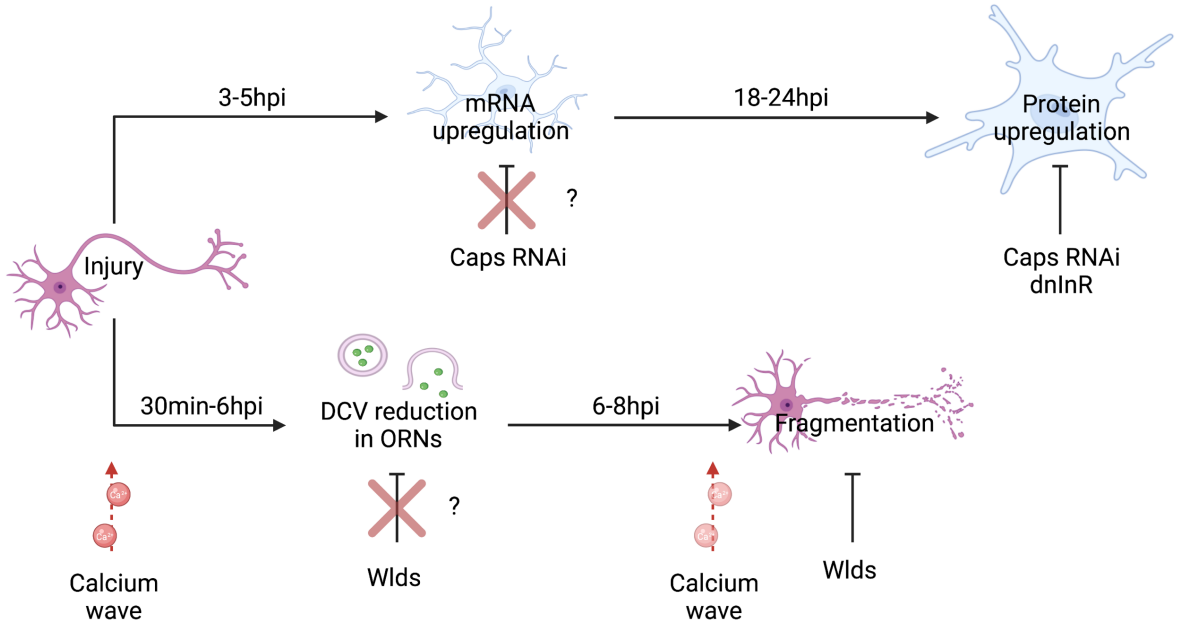

Figure 2: Summary of neuronal and glial events following axotomy
In neurons, DCVs are reduced starting at 30 minutes post-injury. This reduction is not blocked immediately following injury or close to fragmentation by the expression of Wlds in neurons. DCV release from neurons is required for the phosphorylation of the glial InR and the upregulation of Draper and Mmp-1 protein products to clear degenerating projections. Perturbation of DCV release may not affect immune gene mRNA upregulation, suggesting that DCVs may differentially regulate mRNA and protein upregulation of immune genes. Question marks represent results that will need further validation.

Glial immune genes are localized to ensheathing glial processes following injury

In Chapter 3, I described a novel method that we adapted for *in vivo* use to study injury-mediated mechanisms in *Drosophila*(204). We named this technique FLARIM v2.0, as it adapts HCR and FLARIM technology in two probesets to label individual mRNA transcripts and their associated ribosomes (Fig. 3.2)(214, 223). We tested our 18S ribosome and *mmp-1* specific probesets in the *Drosophila* brain, confirming that our signal was specific, produced minimal background, and was quantifiable. Although we initially adapted various smFISH methods to examine effects of neuronal DCV release on glial activation, through our validation experiments, we made an interesting observation regarding *mmp-1* transcripts in ensheathing glia.

Following ORN injury, *mmp-1* transcripts appeared to be distributed to distal glial processes. Ensheathing glial cell bodies reside at the outskirts of the ALs, and they do not invade this region after an injury, which could suggest that mRNAs associated with the glial immune response are being transported to processes that infiltrate the ALs (Fig. 4.3). In separate preliminary experiments, we also observed that *drpr* transcripts were visible in GFP+ ensheathing glial processes within the neuropil (data not shown). Additional work will need to be done to validate these results and determine if other known immune genes are detected in distal projections. mRNA localization has been demonstrated in other glia, such as oligodendrocytes, astrocytes, and radial glia; however, it has been most extensively studied in neurons(209, 211, 236). Given the complex and ramified morphology of many glial cells, it is likely that this mechanism is also employed by glia in response to specific stimuli. However, to our knowledge, this has not yet been demonstrated in the context of injury in glial cells. mRNA localization has several advantages for the cell since expression can be restricted to a specific region, where local stimuli can have an effect(235). Moreover, translation can occur multiple times in a localized area, as opposed to continued protein transport from the cell body.

Currently, there is no clear consensus on a general localization sequence that is associated with all targeted transcripts. Previous research suggests that the 3' untranslated region

(UTR) and even the 5'UTR of the RNA might be recognized by RNA binding proteins(263). Nuclear events have also been proposed, whereby splicing and alternative polyadenylation site selection could play role in targeting(264). Additionally, following transcript production RNA transport granules have been observed, which are transported by motor proteins across microtubules and actin filaments to their destination within the cell(265-268). Many questions remain regarding which mechanisms are utilized by glia to specify transport: Do cis-acting RNA elements play a role in *mmp-1* localization? Do distinct neuronal injury signals contribute to transcript upregulation and initiation of mRNA transport of immune genes? Is *mmp-1* transported along with other immune genes in an RNA granule? Does cytoskeletal rearrangement in glia following injury play a role in immune gene localization?

Local translation in distal glial processes as a response to acute neuronal injury

A relatively new feature of our probeset is the ability to detect ribosomes associated with a transcript of interest. The FLARIM method was first described by Burke *et al*., in 2017 in cell culture(214). We adapted this technique for use *in vivo* and demonstrated that ribosomes associated with the *mmp-1* transcript can be visualized. We also showed that there is a significant increase in the ribosome-association signal following ORN injury within ensheathing glial processes, and that ribosomes also appear to be localized to regions deep in the AL neuropil. Previous work in astrocytes had demonstrated that rough endoplasmic reticulum can be observed in end feet under electron microscopy, and the capture of ribosome-bound mRNAs from this region revealed a distinct "endfeetome", with specific roles for mRNAs in peripheral processes (*e.g.,* glutamate transport, metabolism, cytoskeletal proteins)(211, 212). It is unclear whether ribosomes are locally present in ensheathing glial processes, or if they are potentially transported along with immune genes to their sites of action.

We are also aware that neurons can initiate local translation in response to synaptic activity. This is especially vital to provide synapses with newly synthesized proteins for the

maintenance of synaptic function and plasticity(230, 231). However, the presence of astrocytes at the tripartite synapse and their ability to respond to neuronal signaling, raises the question as to whether neuronal stimuli can influence translation in astrocyte processes. Recently, changes to local translation have been demonstrated in astrocyte perisynaptic processes in response to fear conditioning in mice. Mazaré *et al*., 2020 performed translating ribosome affinity purification (TRAP), and found that a pool of distinct mRNAs are enriched in perisynaptic processes of hippocampal astrocytes(213). Moreover, following a behavioral task where mice undergo foot shocks researchers observed changes in ribosome binding to enriched transcripts. Finally, a recent preprint mirrored these findings in astrocytes in response to acute seizures. Sapkota *et al*., 2021 observed changes in ribosome occupancy via TRAP in astrocytes in response to neuronal activity(269). The researchers also performed proteomics in the context of fear conditioning and demonstrated that translation occurs in peripheral astrocyte processes. It will be interesting to examine how, and which, neuronal signals may contribute to ensheathing glial local translation following injury.

Future directions

In Chapter 3, I described the observations made using the *mmp*-1 probeset; however, there is evidence that a repertoire of immune genes are upregulated in glia after neuronal injury(77). It will be interesting to assess whether other glial genes are localized and locally translated in distal processes, and whether this has a functional consequence for proper glial clearance of degenerating projections. Also, although we have demonstrated transcript-ribosome association in our injury model, it is clear that this is not direct evidence for active translation. Future experiments could provide a stronger link by feeding flies puromycin to label the growing polypeptide chain, which would hint at active translation of immune transcripts in distal ensheathing glial processes.

In order to address the questions about *mmp-1* localization, and whether this is a directed process (active transport of immune genes versus glial membrane extension after injury), it would be interesting to generate mutations in the 3'- or 5'- UTR of *mmp-1* to see if there is an effect on transport. Furthermore, studies have demonstrated that Annexins are involved in RNA granule transport and docking(270). In a recent study, Annexin A11 was shown to tether RNA granules to lysosomes for transport in axons, allowing them to "hitchhike" to their destination(271). Annexin 9 and 11 were also upregulated in the VNC injury screen conducted by Purice *et al*. (2017)(77). We could determine whether *mmp-1* transport is inhibited by Annexin KD, and if this has an impact on timely clearance of ORN projections. A caveat to this experiment would be the non-specific effects on other essential RNA transport that may be required for glial cell homeostasis or clearance functions. Further work will be needed to elucidate the glial signaling and transport pathways that are involved in immune gene transport and translation at subcellular compartments.

Finally, although not included in this dissertation, there is ongoing work to use a variety of translation inhibitors to determine if the ribosome-association signal can be disrupted *in vivo*. This is a vital control experiment for the validation of our probeset and we are currently testing different experimental paradigms. Translation inhibitors that are of interest to us are harringtonine, which results in ribosomal runoff from the transcript, puromycin, which incorporates into the polypeptide chain and terminates translation, as well as rapamycin, which acts through the TOR pathway to inhibit translation(272-274).

Conclusions

In this dissertation, I utilized *Drosophila* as a model to further characterize DCVs as a neuronal injury signal. Additionally, I described a role for DCV exocytosis in the regulation of Mmp-1 through the InR. Future work will be needed to continue the development of the spGFP tool as a historical reporter of DCV release; however, it could serve as a helpful method to study DCVs *in vivo* in the adult brain. Finally, findings presented using the adapted FLARIM v2.0 method may

point to a role for directed RNA transport and local translation of immune genes in glial cells in response to injury, a biological function that remains understudied in glia.

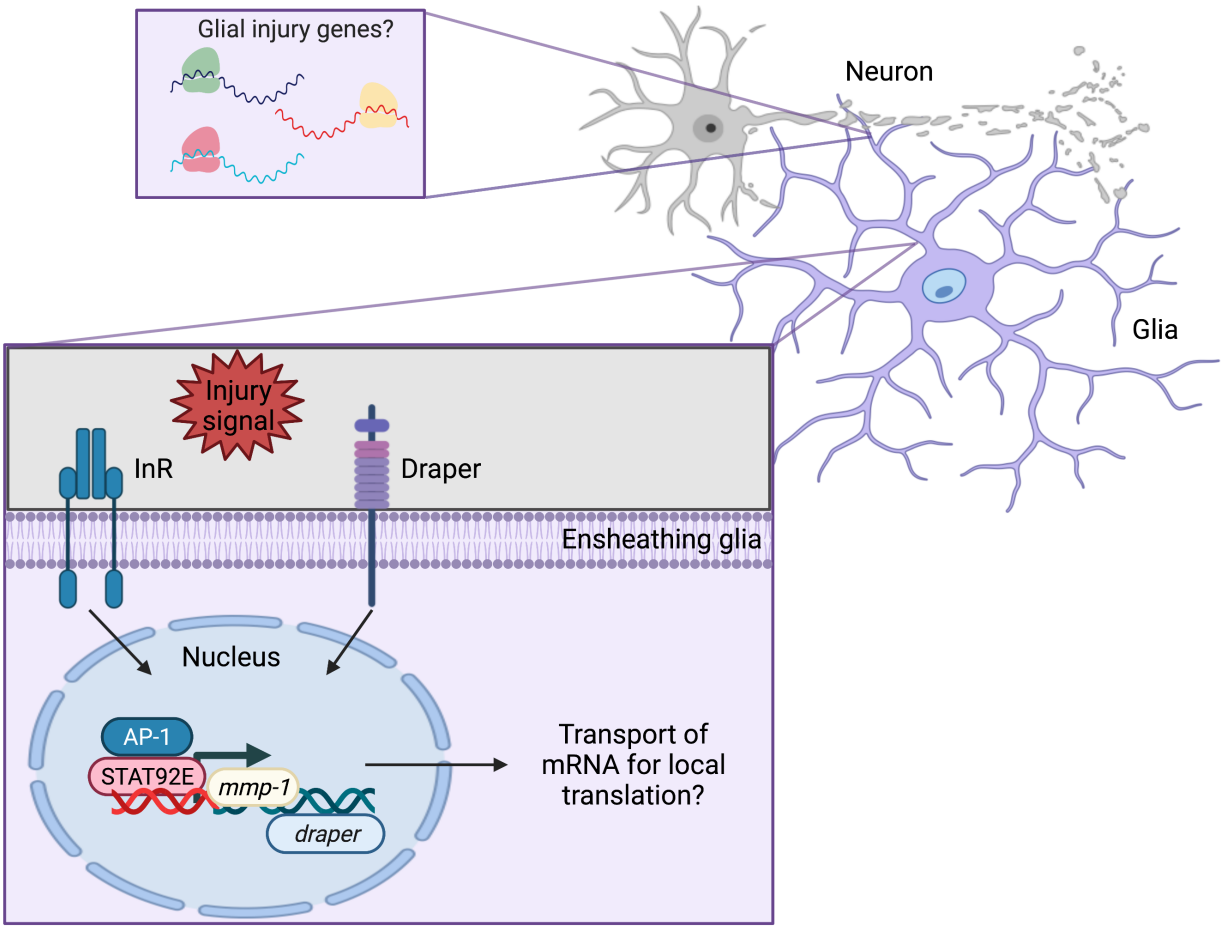

Figure 3: mRNA localization and local translation in glia following neuronal injury
Using our novel probeset, FLARIM v2.0, we demonstrate that the immune transcript *mmp-1* is localized to distal ensheathing glial processes after antennal and/or maxillary palp injury. Moreover, mRNAs are associated with ribosomes deep in the neuropil regions of the ALs, hinting at local translation. We hypothesize that following an injury signal from neurons, potentially DCVs, glial signaling is kicked off through the InR and Draper receptors to upregulate glial immune genes. It is still unclear how transcripts are transported to their sites of action, and whether different signaling mechanisms might control distinct stages of mRNA localization and translation at distal sites in glial cells. Our probeset will allow us to answer some of these questions in the future.

Materials and Methods

smiFISH

As described in Chapter 3. Flies were injured (3rd antennal segments and maxillary palps) and dissected 5 hpi.

Quantitative RT-PCR

Sample preparation was performed as previously described(77). RNA was quantified using a Nanodrop Spectrophotometer and cDNA was synthesized using the qScript cDNA SuperMix (QuantaBio). qPCR was done using TaqMan gene expression assays (ThermoFischer) and TaqMan Fast Advanced MasterMix (ThermoFischer) on a QuantStudio 3 system (ThermoFischer). Ribosomal protein 5 (Rpl5; Dm03420863_m1) was used as a control housekeeping gene. The other TaqMan assays used were: Drpr-I (custom assay; previously published), Mmp-1 (Dm01820359_m1), and Ets21C (Dm01814140_g1).

Microscopy & Analysis

Samples were imaged on a Zeiss LSM 700 with a Zeiss 40X 1.4 NA oil immersion plan-apochromatic lens. Images were processed in Zen (Zeiss). Volocity 3D Image Analysis Software (Quorum Technologies) was used for fluorescence quantification. GraphPad Prism 8 (Graphpad Software) was used for statistical analysis: One-way ANOVA and Kruskal-Wallis test. Normality was tested using the D'Agostino-Pearson normality test. Outliers were identified using the ROUT method.

APPENDIX: DEVELOPING A SPLIT GFP TOOL TO MEASURE DCV RELEASE *IN VIVO*

Introduction

Our static and live imaging experiments examining DCV dynamics following neuronal injury have demonstrated that DCVs are diminished in injured ORNs, while DCV movement is halted in wing axonal projections after axotomy. These experiments, in combination with the data presented in Chapter 2, led us to conclude that DCVs are released from neurons as an injury signal to glia; unfortunately, limited tools exist to directly examine DCV release *in vivo*. Fluorescent markers have been described as a tool; however, these indicators have been mainly validated at the larval NMJ(149, 275). This preparation allows for researchers to fillet the *Drosophila* larva, exposing the central brain and the motoneurons innervating the segmented musculature to accessible manipulation and imaging. These tools are not compatible with the olfactory injury assay, an intact *in vivo* system.

As a result, we aimed to develop a new genetically encoded tool for the field to use as an *in vivo* indicator of DCV exocytosis. This method adapted the split GFP (spGFP) system, which has been previously described to identify synaptic partners in the *Drosophila* brain(276, 277). Macpherson *et al*., 2015 demonstrated that GFP reconstitution across synaptic partners (GRASP) could utilize spGFP, targeted to SVs and the postsynaptic membrane, to label active synaptic connections(278). We decided to adapt this method for the measurement of DCV release. In our system, spGFP11 would be targeted to DCVs in neurons, while spGFP1-10 would be membrane tethered on the surrounding glial cells (Fig. 1). The 2 spGFPs on their own are not fluorescent, but when they come into close proximity, fluorescence is reconstituted as the full GFP is able to re-fold(279). In the event of an injury, if DCV exocytosis occurs, spGFP11 would be released from vesicles and would be reconstituted with spGFP1-10 (Fig. 1). This could serve as a historical reporter of DCV exocytosis, and we would be able to evaluate injury-induced release within the brain. In this appendix, I will describe the current progress towards the development of this tool, and the future work that will be required to validate it as a method to measure DCV exocytosis.

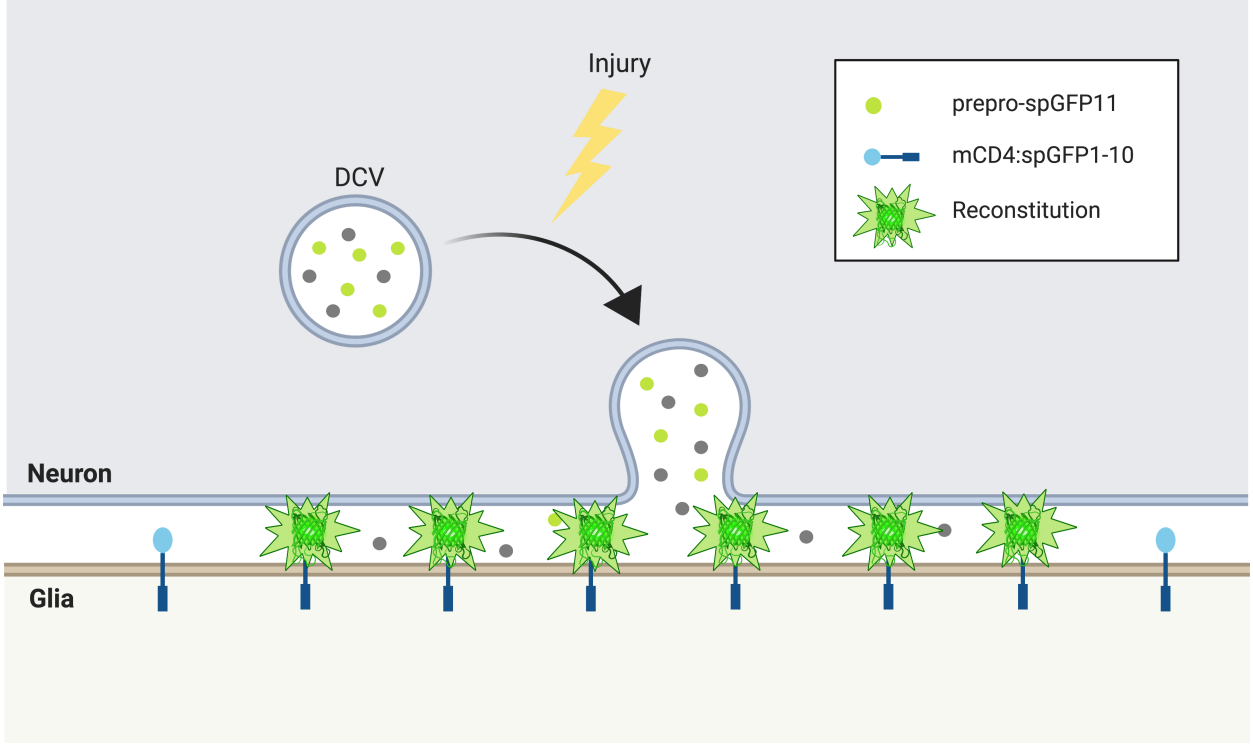

Figure 1: An adapted split GFP method to measure DCV release *in vivo*
Theoretical schematic of split GFP/GRASP method adapted from Macpherson *et al*., 2015 (GRASP: GFP reconstitution across synaptic partners)(278). Split GFP 11 (spGFP11) is targeted to DCVs in a subset of ORNs using the prepro-Dilp2 targeting sequence, while membrane tethered (mCD4) spGFP1-10 is targeted to surrounding ensheathing glial membranes. If DCV cargos are indeed release upon injury, spGFP11 is released and GFP reconstitution provides a historical record of DCV release in the *Drosophila* brain. Created using BioRender.

Results

Split GFP as a method to measure DCV release in *Drosophila*

To create our spGFP11 construct that is targeted to DCVs, we decided to use the prepro-Dilp2-GFP sequence. The Ilp2-GFP transgene is a well characterized DCV marker and was utilized in Chapter 2. The prepro-Dilp2-GFP construct was made by placing Emerald GFP, flanked by linkers and cleavage sites, into the C-peptide sequence of Ilp2 (Fig. 2A)(147). Through peptide processing at the Golgi and cleavage in the DCV, GFP becomes DCV cargo and serves as a fluorescent marker for detection. For our spGFP11 construct to achieve proper targeting to DCVs, we placed spGFP11 and a myc tag within the C-peptide sequence of prepro-Dip2-GFP as well, in place of Emerald GFP (Fig. 2A, Supp. Fig. 1A). Moreover, we generated various lengths of spGFP11 tandem repeats (2x, 4x, and 6x) to test which length of construct would be efficiently released from DCVs. Furthermore, there was evidence to suggest that increased tandem repeats of spGFP11 increase the reconstituted fluorescence intensity by clustering spGFP1-10 at the opposing membrane(279).

Flies were generated in the UAS/Gal-4 and LexA/Aop systems to allow for flexible expression of spGFP constructs in various cell types. To test whether our construct was correctly targeted to DCVs, we turned to the larval NMJ system. Here, we were able to express the spGFP11-myc transgene in motoneurons, in conjunction with the already validated Ilp2-GFP marker (Fig. 2B). When examining boutons at the NMJ, we observed that spGFP11-myc constructs were co-localized with the Ilp2-GFP marker (Fig. 2b’’’’), which would suggest that our spGFP11 constructs are correctly targeted to DCVs.

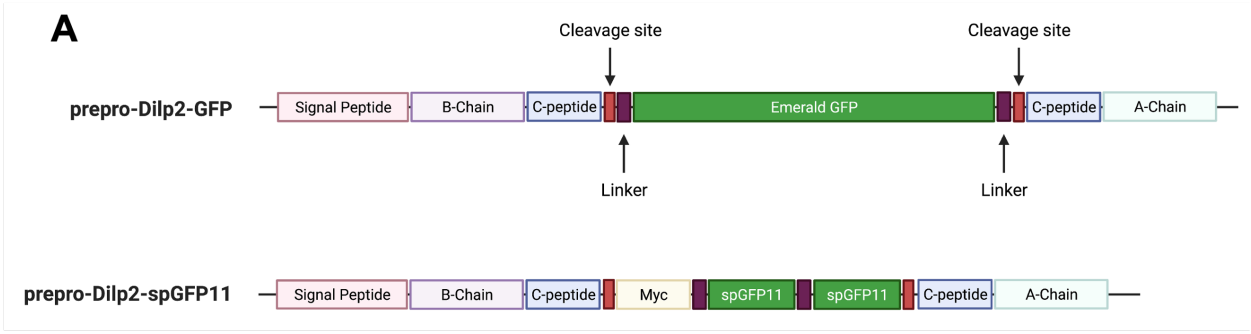

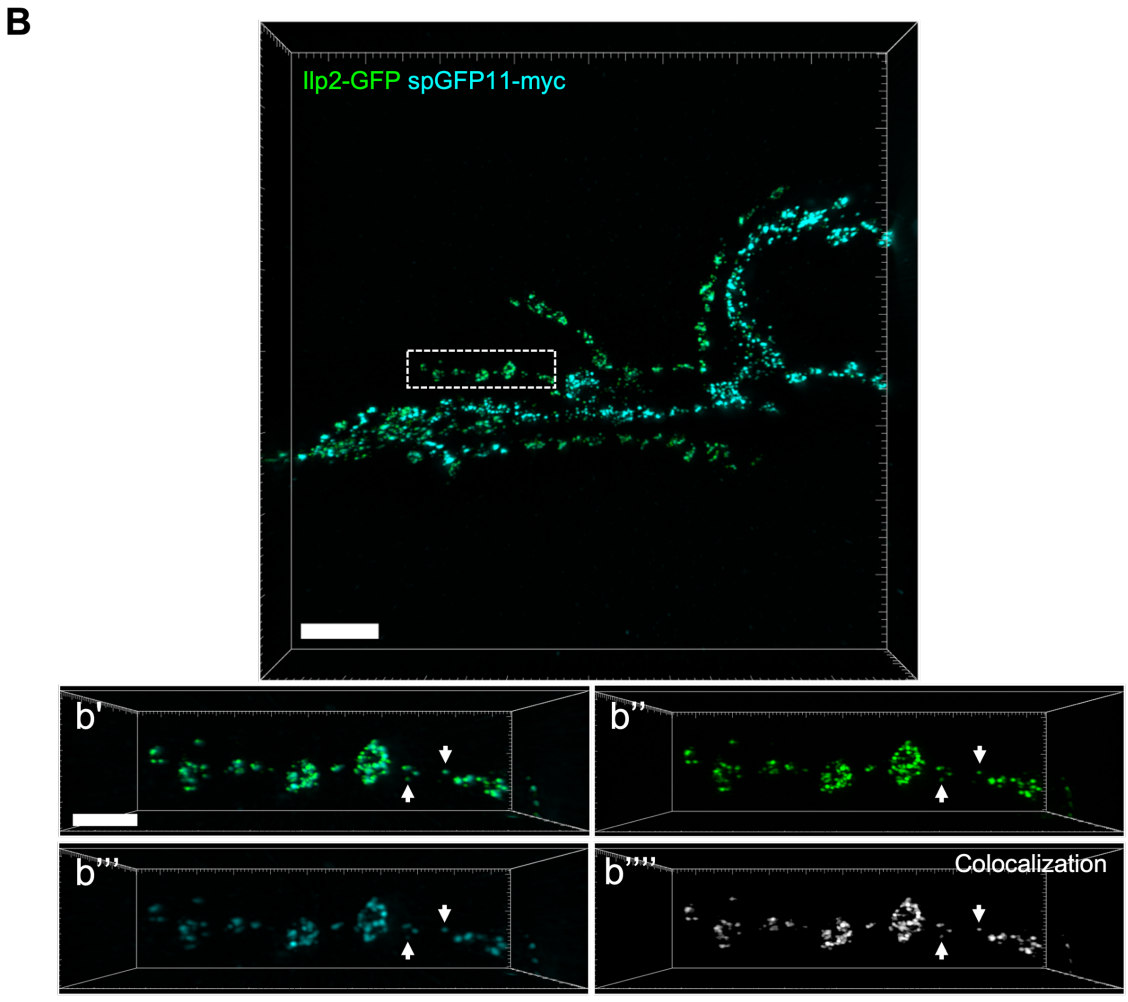

Figure 2: The spGFP11 construct is targeted to DCVs
(A) Schematic of prepro-Dilp2-GFP and prepro-Dilp2-spGFP11 constructs. The spGFP11 constructs were based on the original *Drosophila* Ilp2 (Dilp2) emerald GFP construct (provided by E. Levitan). The emerald GFP portion of the construct was replaced with various lengths of spGFP11 tandem repeats (2, 4, 6x), and an additional myc tag was added to allow for localization. Created using BioRender. **(B)** High resolution image of DCVs labeled with Ilp2-GFP and myc-tagged spGFP11 constructs at larval motoneurons. MIPs: 10.2 µm. Scale bar: 10 µm. Genotype: ;OK371-Gal4, UAS-Ilp2-GFP, 10X-UAS-myr-tdTomato/+; UAS-2x-spGFP11-myc/+ **(b')** High magnification inset from dotted rectangle. Merge of GFP and myc in boutons. Arrows indicate co-localization of channels. Scale bar: 2 µm. **(b''-b''')** GFP and myc, respectively. **(b'''')** Co-localization channel.

The spGFP construct at the larval NMJ

To test whether GFP would be reconstituted following DCV release, we expressed spGFP11 in glutamatergic motoneurons and spGFP1-10 on muscle membranes in the larva (Fig. 3A). We find that when both spGFP components are expressed, GFP reconstitution is observed around HRP-stained motoneurons (Fig. 3B). Importantly, a GFP signal is not observed when only spGFP11 or spGFP1-10 are present in motoneurons or on the muscle, respectively (Fig. 3B). These results suggest that GFP fluorescence is reconstitution-specific and depends on the presence of both components of spGFP. It also demonstrates that basal DCV release occurs from larval motoneurons through the life of the animal, which has been shown with other markers of DCV release at the NMJ(280). This control experiment was conducted with the 4x-spGFP11 construct, but we were interested in examining the reconstituted fluorescence signal generated by all our constructs.

Based on a previous study of tandem spGFP11 in cells, we hypothesized that upon release, the 6x-spGFP11 construct would yield the greatest fluorescence intensity when reconstituted(279). Indeed, we found that increasing the number of tandem spGFP11 resulted in an increase in reconstituted fluorescence intensity (Fig. 4A). 2x-spGFP had the dimmest GFP fluorescence, with a faint halo around HRP-stained boutons, while 4x-spGFP and 6x-spGFP generated a brighter signal surrounding the motoneurons (Fig. 4B). Our control experiments demonstrated that GFP fluorescence is reconstitution-specific and increases with the number of spGFP11 repeats.

The observations and measurements from the previous experiments represent GFP reconstitution from basal DCV release, over the course of the larva's life. As our ultimate goal is to use this as a tool to measure injury induced DCV release, we wanted to test whether the spGFP method has adequate dynamic range to detect an increase in DCV release. The larval NMJ allows for various stimulation paradigms, whereby motoneurons can be stimulated chemically or electrically. We used these methods to elicit DCV release from motoneurons and measure GFP

reconstitution. We hypothesized that elevated DCV, and thus spGFP11, exocytosis would result in an increase in reconstituted GFP fluorescence, above basal levels.

The first paradigm we tested was high K+ stimulation. In this experiment, high K+ HL-3 was bath applied to the filleted larva(281). The same NMJ was imaged before stimulation, 30 minutes post-stimulation (mps), and 60 mps, at segment A3 (muscles 6/7) and segment A4 (muscles 6/7) (Fig. 5A, B). Surprisingly, we found that NMJs had the greatest GFP fluorescence intensity before high K+ stimulation, and fluorescence was markedly diminished 30 and 60 mps. When our collaborators in the Levitan lab electrically stimulated DCV release from motoneurons, they also did not detect a change in GFP fluorescence at 20mps (data not shown). This suggested to us that our current spGFP system would not be able to detect changes in DCV exocytosis at the larval NMJ.

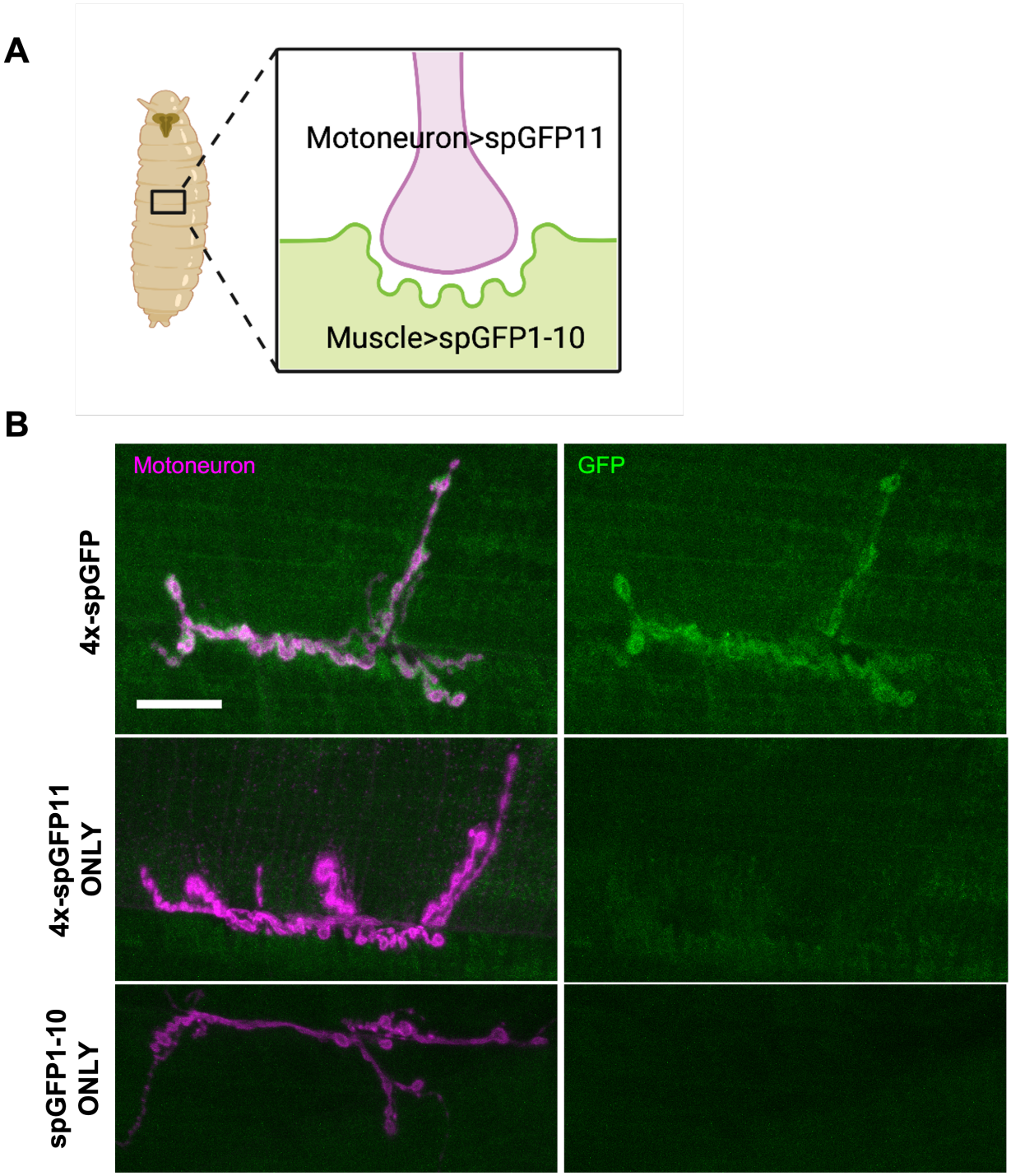

Figure 3: GFP fluorescence is reconstitution-specific
(A) Schematic of the larval NMJ model to test spGFP constructs. spGFP11 constructs are expressed in motoneurons, while spGFP1-10 is expressed on the muscle membranes that motoneurons innervate. Created using BioRender. **(B) I**mages from motoneurons innervating muscles 6/7. GFP reconstitution is only observed when both spGFP11 and spGFP1-10 are present. Images are MIPs. Scale bar: 20 μm. 4x-spGFP genotype: ;Vglut-LexA/Aop-4x-spGFP11-myc; MHC-Gal4/UAS-mCD4-spGFP1-10. 4x-spGFP11 ONLY genotype: ;Vglut-LexA/Aop-4x-spGFP11-myc; MHC-Gal4/+. spGFP1-10 genotype: ;Vglut-LexA/+; MHC-Gal4/UAS-mCD4-spGFP1-10.

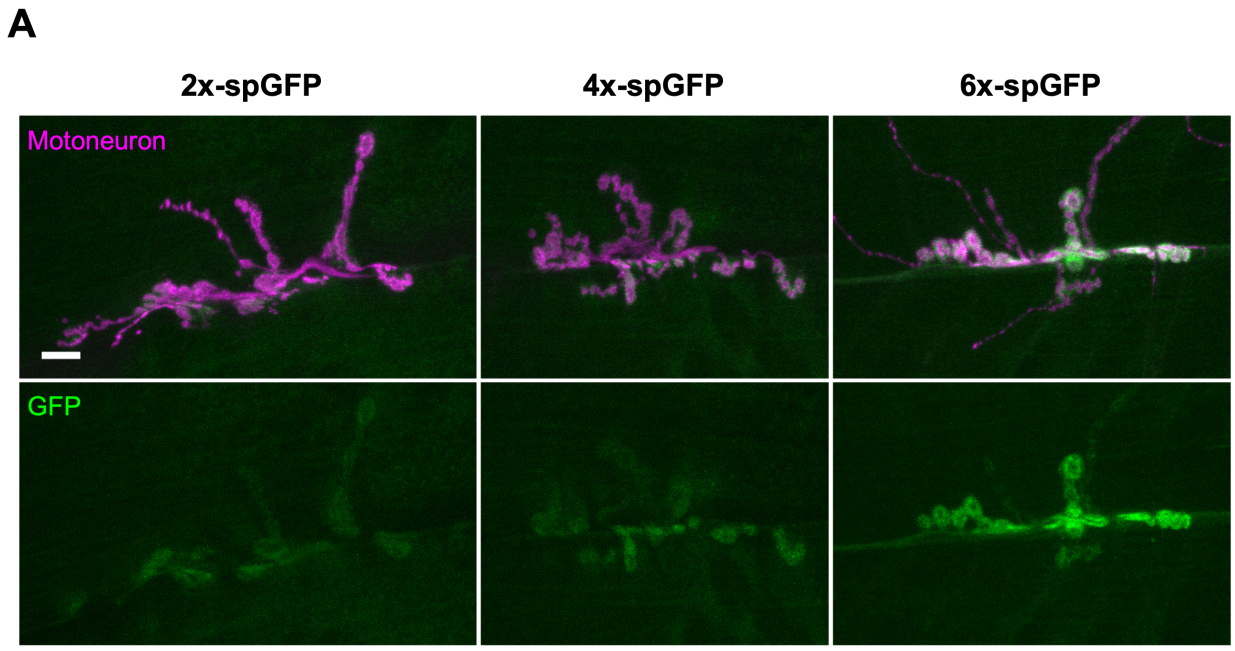

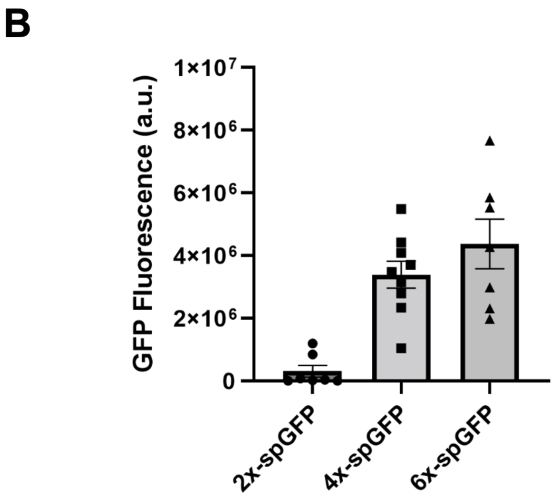

	2x-spGFP	4x-spGFP	6x-spGFP
Mean	311793	3390265	4371895

Figure 4: Tandem spGFP11s increase reconstitution fluorescence intensity
(A) Representative images of motoneurons innervating muscles 6/7 and reconstituted GFP signals from increasing tandem spGFP11 lengths (2, 4, 6x). MIPs: 21µm. Scale bar: 10 µm. Genotypes: ;Vglut-LexA/Aop-2x or 4x or 6x-spGFP11-myc; MHC-Gal4/UAS-mCD4-spGFP1-10. **(B)** Quantification of GFP fluorescence associated with HRP 647-labeled motoneurons. 2x-spGFP (n=7), 4x-spGFP (n=9), 6x-spGFP (n=7). Mean ± SEM.

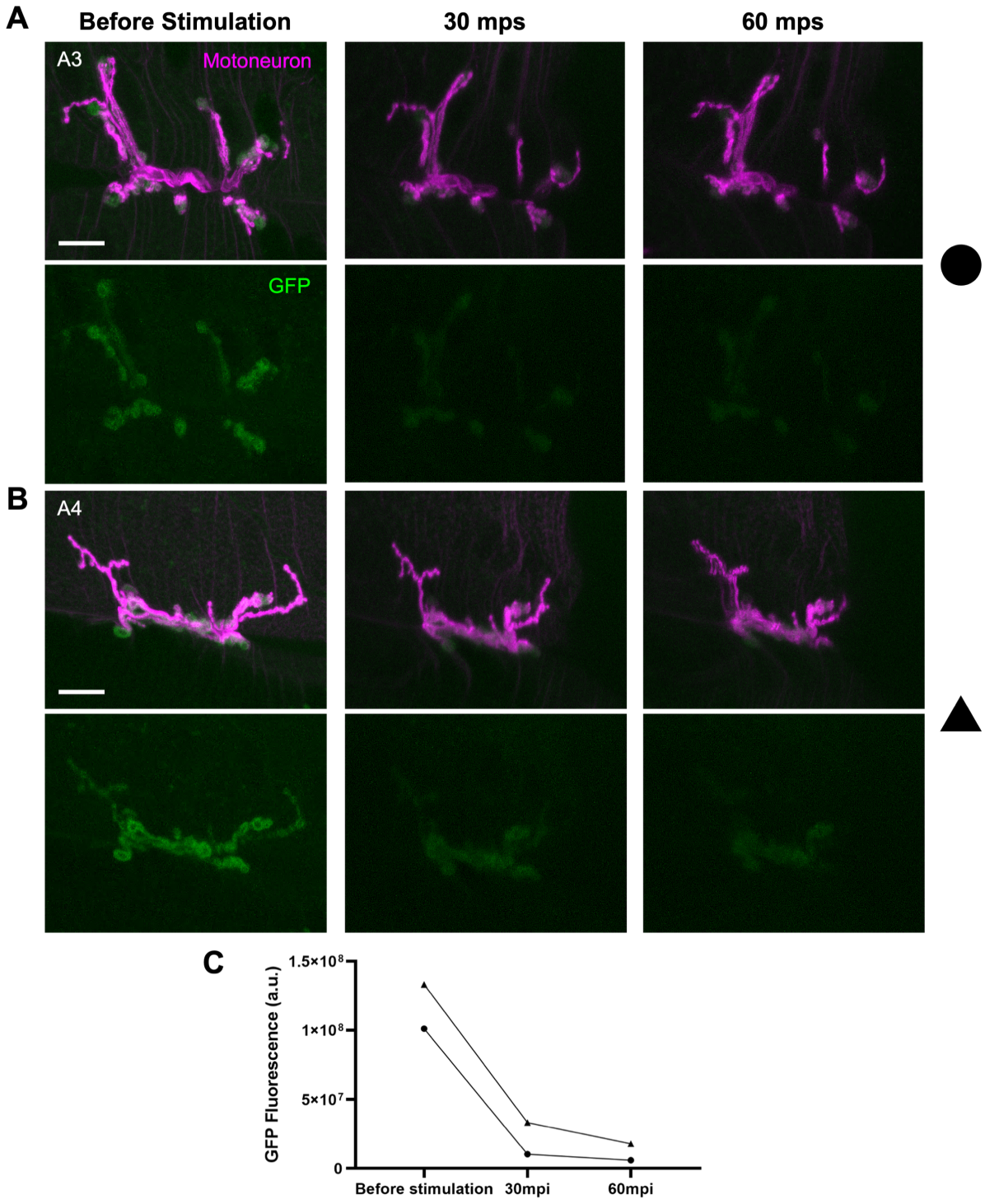

Figure 5: High K+ stimulation does not result in increased GFP fluorescence
(A) Images of the same NMJ imaged before, 30 mps, and 60 mps at segment A3, muscles 6/7. MIPs: 14 µm. Scale bar: 20 µm. Genotypes: ;Vglut-LexA/Aop-4x-spGFP11-myc; MHC-Gal4/UAS-mCD4-spGFP1-10. **(B)** Images of the same NMJ imaged before, 30mps, and 60mps at segment A4, muscles 6/7. MIPs: 14 µm. Scale bar: 20 µm. Genotypes: ;Vglut-LexA/Aop-4x-spGFP11-myc; MHC-Gal4/UAS-mCD4-spGFP1-10. **(C)** Quantification of GFP fluorescence associated with HRP 647-labeled motoneurons. Individual data points. A3 (circle); A4 (triangle)

The spGFP construct in the adult brain

In parallel with our larval experiments, we began testing our construct in the brain of the adult fly. In this system, we expressed the shorter fragment, spGFP11, in a subset of ORNs, while spGFP1-10 was expressed on glial membranes (Fig. 6A). In the uninjured brain, our larval results were recapitulated: increases in tandem spGFP11 number resulted in increased GFP fluorescence, while expressing constructs alone did not generate a fluorescent signal within ALs (Fig. 6B, C). The pattern of basal DCV release, and thus GFP reconstitution, was present around the ALs in an ensheathing glial-like pattern. This demonstrates that spGFP11 is released from ORNs and is reconstituted with spGFP1-10 across a broad area of the ALs, where ensheathing glial membranes are present.

To assess whether GFP fluorescence increases following injury, with our hypothesized increase in DCV release, we turned to the ORN assay. In order to limit the amount of basal GFP reconstitution that our system was detecting, we introduced tub-Gal80ts to restrict expression of our construct to just before the time of injury (Fig. 7A). This required raising the flies at 18˚C and moving them to 30˚C for 48hrs before the injury to elicit spGFP expression (Fig. 7B). Following ORN axotomy, brains were dissected at various timepoints after antennal injury: 1, 2, 4, 6 hpi (Fig. 7C). However, we found that uninjured brains had the greatest GFP fluorescence intensity. Moreover, as time after injury elapsed, GFP intensity was progressively diminished in ALs (Fig. 7C, D). Taken together, these results indicate that our current system, and attempts to restrict construct expression, do not adequately prevent the detection of basal release. This is evident by the widespread fluorescent signal in uninjured brains and suggests that injury-induced DCV exocytosis may not be captured due to the saturation of spGFP1-10 on glial membranes from basal release.

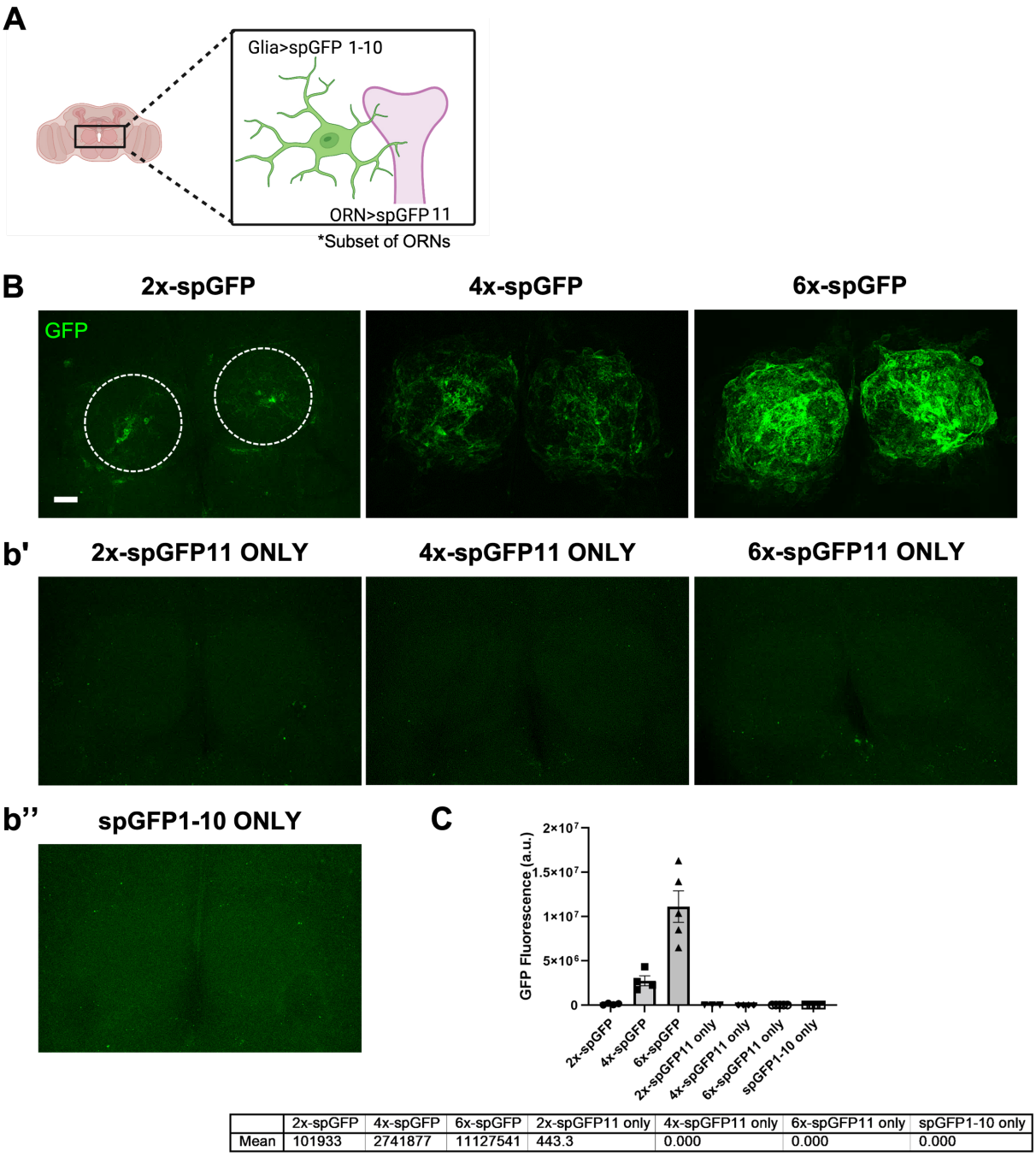

	2x-spGFP	4x-spGFP	6x-spGFP	2x-spGFP11 only	4x-spGFP11 only	6x-spGFP11 only	spGFP1-10 only
Mean	101933	2741877	11127541	443.3	0.000	0.000	0.000

Figure 6: GFP reconstitution in the adult *Drosophila* brain
(A) Schematic of expression in the adult fly brain to test spGFP constructs. spGFP11 constructs are expressed in a subset of ORNs, while spGFP1-10 is expressed on glial membranes. Created using BioRender. **(B)** Reconstituted GFP at the ALs. White dotted circles used as ROIs for quantification. MIPs: 31 µm. Scale bar: 20 µm. Genotypes: ;Or22a-LexA/Aop-2x or 4x or 6x-spGFP11-myc; repo-Gal4/UAS-mCD4-spGFP1-10. **(b')** Expression of only spGFP11 constructs. Genotypes: ;Or22a-LexA/Aop-2x or 4x or 6x-spGFP11-myc; repo-Gal4/+. **(b'')** Expression of only the spGFP1-10 construct. Genotype: ;Or22a-LexA/+; repo-Gal4/UAS-mCD4-spGFP1-10. (C) Quantification of GFP fluorescence in ALs. 2x-spGFP (n=4), 4x-spGFP (n=4), 6x-spGFP (n=5), 2x-spGFP ONLY (n=3), 4x-spGFP ONLY (n=4), 6x-spGFP ONLY (n=5), spGFP1-10 ONLY (n=4). Mean ± SEM.

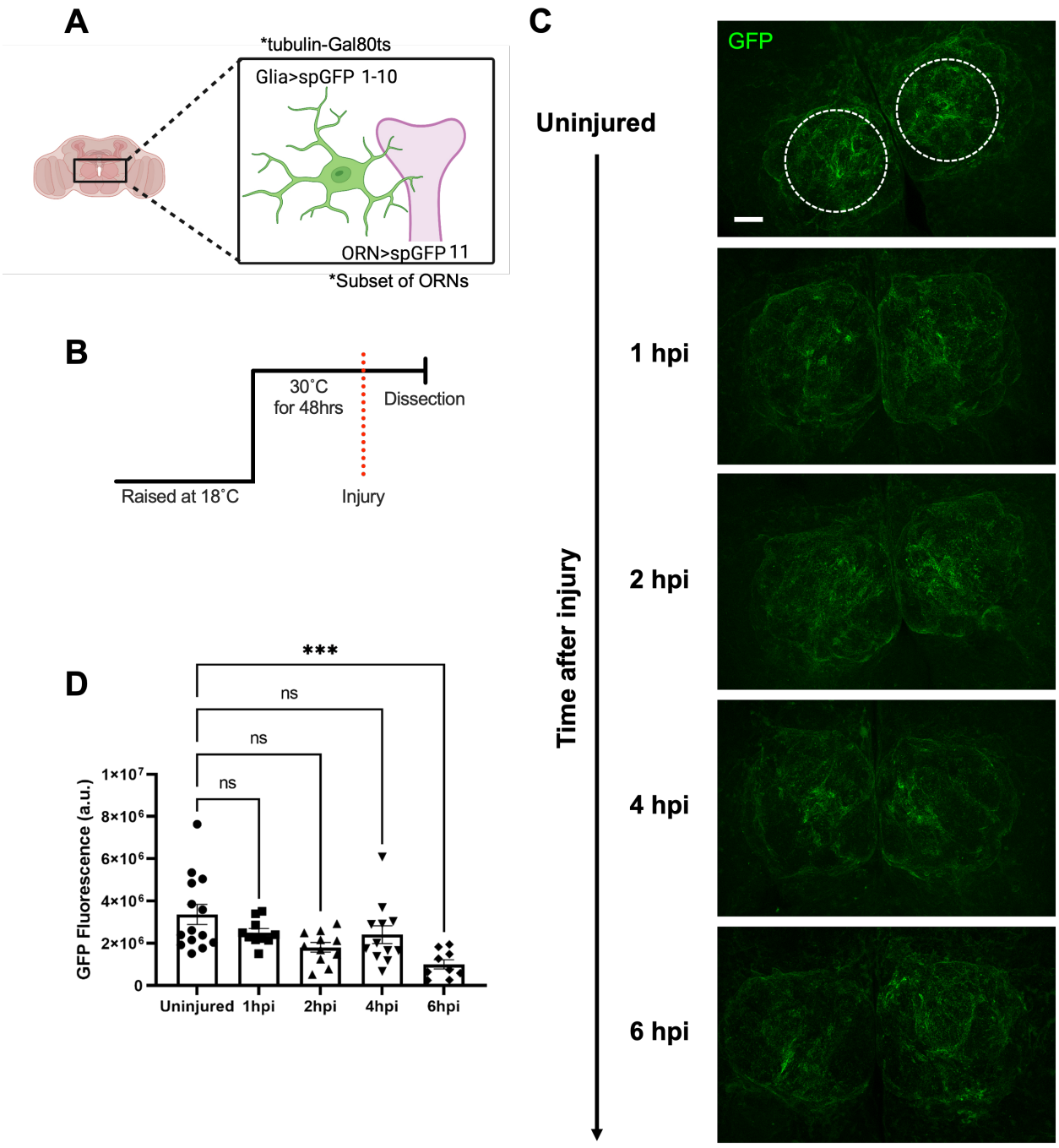

Figure 7: GFP reconstitution following ORN injury
(A) Schematic of expression in the adult fly brain to test spGFP constructs. spGFP11 constructs are expressed in a subset of ORNs, while spGFP1-10 is expressed on glial membranes. A temperature sensitive tubulin-Gal80 was used in this experiment to restrict construct expression and avoid detection of basal DCV release. Created using BioRender. **(B)** Schematic of experimental set-up and temperature shift to induce construct expression. **(C)** Reconstituted GFP at the ALs. White dotted circles used as ROIs for quantification. MIPs: 15 µm. Scale bar: 20 µm. Genotype: ;Or82a-GAD-LexA/Aop-4x-spGFP11-myc; repo-Gal4, tub-Gal80ts/UAS-mCD4-spGFP1-10. **(D)** Quantification of GFP fluorescence in ALs. Uninjured (n=14), 1hpi (n=10), 2hpi (n=11), 4hpi (n=12), 6hpi (n=9). Mean ± SEM. Kruskal-Wallis test (Dunn's *post hoc* test). ns: non-significant; ***p<0.001.

Discussion

This appendix has detailed the work completed to develop a spGFP system to measure DCV exocytosis. With our current constructs, we are only able to detect a historical record of DCV release over the life of the animal, at both the larval and adult stage. The spGFP method does not have the dynamic range necessary to indicate a change in DCV release in the context of injury, or other paradigms that this tool could be used for. We hypothesize that spGFP1-10 on muscle or glial membranes in the larva or adult brain, respectively, become saturated as spGFP11 is released upon basal DCV exocytosis. This is evident by the fluorescence detected surrounding unstimulated motoneurons and uninjured brains. Moreover, the decrease in fluorescence following motoneuron stimulation or ORN injury may suggest that reconstituted GFP is turned over at the membrane and degraded over time.

To address the pitfalls of our approach, we propose re-designing the spGFP1-10 construct. Originally published by Feinberg *et al*., in 2008, spGFP1-10 is membrane tethered and has been used for the identification of synaptic partners(276-278). We utilized this already available transgenic line in our experiments. We posit that designing a membrane tethered spGFP1-10 with a destabilizing domain would allow for turnover during the life of the animal as DCV exocytosis occurs(282, 283). This approach may allow for the removal of reconstituted GFP that is not relevant to the stimulus being studied, in our case, injury. Additionally, in the context of our current spGFP model, or using newly designed constructs, a vital control experiment that will need to be carried out is the expression of a DCV release inhibitor, such as Caps RNAi or TeTXLC. We have demonstrated that the GFP signal in the spGFP system is reconstitution specific and a greater number of tandem spGFP11 repeats increases reconstituted fluorescence; however, it would be important to test whether blocking of DCV release abolishes the GFP signal.

Although the current spGFP system cannot yet be used as a tool to measure DCV release *in vivo* as we had hoped, much of the preliminary work has been completed in validating the targeting of spGFP11 to DCVs and confirming the reconstitution specific GFP signal following

DCV exocytosis. We aim to modify the spGFP1-10 construct so that this method can be a valuable tool for the field of DCV research. Two current genetically encoded indicators exist to study DCV release in the *Drosophila* brain. The first utilizes a fluorogen activating protein (FAP) approach, whereby Ilp2-FAP is targeted to DCVs, and the brain is incubated in malachite green (MG) dye(261, 262). Fluorescence occurs when the FAP comes in contact with MG and signifies DCV fusion. While the second method uses a genetically encoded Ca^{2+} indicator (GCaMP) to signal DCV release(275). The first method requires *ex vivo* dissection of the brain to apply the dye, while the second method requires live imaging of the brain. Our method aims to provide an improved tool to examine DCV release in the intact *Drosophila* brain. When fully developed and tested, it could serve as a helpful system to study DCV release beyond the scope of this project, as DCVs have been implicated in cognitive and mood disorders and are known to regulate brain development and plasticity.

Supplementary Information

A

CAGGCGGCCGCTCGACCCGGCTCGACCCAACTTAATCCATTTGATCGTAAAGCAACCTAA
GCAGTAAACCCATAACCATGAGCAAGCCTTTGTCCTTCATCTCGATGGTGGCCGTGATTTT
GCTGGCCAGCTCCACAGTGAAGTTGGCCCAAGGAACGCTCTGCAGTGAAAAGCTCAACG
AGGTGCTGAGTATGGTGTGCGAGGAGTATAATCCCGTGATTCCACACAAGCGCGAACAAA
AACTCATATCCGAAGAGGATCTGGGCTCCGGTGGCGGACGAGACCATATGGTTCTTCACG
AGTACGTTAATGCCGCTGGTATCACCGGTTCCGGTAGTGGCGGACGCGATCACATGGTG
TTGCACGAATATGTTAACGCAGCGGGCATCACGGGTGGAGGCTCGGGGCGTGACCATAT
GGTCCTGCATGAGTATGTGAATGCCGCCGGTATTACAGGATCCGGTGGCGGTCGTGACC
ATATGGTTTTGCACGAATACGTTAACGCCGCAGGTATTACGGGCAGTGGTGGCGGACGG
GACCATATGGTGCTCCACGAATATGTTAATGCCGCTGGCATCACTGGTGGTAGCGGCGGA
CGCGACCACATGGTATTGCATGAGTACGTAAACGCTGCAGGCATCACGAGGCGAACTCG
CCAACGGCAAGGAATCGTGGAGAGGTGCTGCAAAAAGTCCTGTGATATGAAGGCTCTGC
GGGAGTACTGCTCCGTGGTCAGAAATTAGGCCTCCTAATGCGAAAATCATTGACCCCAAC
TGACCTGGTCGACGCGATTATCTCTGGATCTGGTTCCAAACCAACCATGTGCATATATACT
ACAATCGATGTTTTTTACAGCTTGTTGCATGTTACTCTTTACGAATGATCGAAATGGATTAA
ATATATATTCTGCTTTAAGCTTGGGCAAACAATCTCTAGACAG

Restriction sites: NotI, XbaI
UTR
Signal peptide
B-chain
C-peptide
Myc tag
Linker
spGFP11
A-chain

Supplementary Figure 1: prepro-Dilp2-myc-6x-spGFP11 sequence
(A) spGFP11 was inserted into the prepro-Dilp2-EGFP C-peptide sequence, in place of Emerald GFP (sequence provided by E. Levitan;(147)).

Materials and Methods

Split GFP11 Constructs

Tandem spGFP11 sequences (2x, 4x, 6x), along with a myc tag, were inserted into the prepro-Dilp2-EGFP C-peptide sequence, in the place of Emerald GFP (see Fig. 2A/Supp. Fig. 1A). The sequence was provided by E. Levitan. Prepro-Dilp2-spGFP11 was cloned into 5XUAS and 13XLexAop2 vectors using the NotI and XbaI sites with the help of A. Sheehan in the Freeman lab. Transgenic flies were generated by BestGene.

Fly husbandry & Temperature shift

Crosses were set up and flies were raised in 25˚C humidity-controlled incubators. Experiments requiring temporally restricted expression of transgenes contained tub-Gal80ts in their genetic background. These crosses were set up and raised at 18˚C. See figures and figure legends for details about specific experimental paradigms.

Larval Dissection & Immunostaining

3rd instar larvae were dissected as previously described in HL-3 saline or Schneider's solution(281). For myc immunostaining, larvae were filleted and then fixed in 4% PFA+0.1% TX for 20 min at RT, permeabilized in 0.5% PBS-TX for 20 min at RT, and stained with primary antibody diluted in 0.1% PBS-TX overnight at 4˚C. Following staining, larvae were washed in 0.1% PBS-TX at RT (3 x 30 min); secondary antibody was applied for 2 hrs, and larvae were washed again (3 x 30 min). Larvae were then mounted in Vectashield under #1.5 coverslips and imaged. For HRP staining, larvae were filleted and then fixed in 4% PFA+0.1% TX for 15min at RT, permeabilized in 0.2% PBS-TX for 5min at RT, and stained with primary antibody diluted in HL-3 or Schneider's for 10 min at RT. Following 3 quick washes with HL-3 or Schneider's, larvae were mounted and imaged.

High K+ Stimulation

3rd instar larvae were filleted in RT Schneider's solution and stretched out using magnetic pins as previously described(82). Larvae were then glued down to the imaging chamber using dental glue. Larvae were stained for 5 min with HRP-RRX in Schneider's to locate NMJs. Baseline fluorescence was imaged. Glue was removed from posterior end of the larvae to allow for muscle contractions. Schneider's was washed out with RT HL-3 ($[Ca^{2+}]$: 1.5 mM) for 5 min. HL-3 was exchanged with high K+ HL-3 ($[Ca^{2+}]$: 1.5 mM) for 3 min and then washed out with Schneider's. Larvae were glued down again and kept in darkness for 20 min to allow for GFP folding and maturation to occur. The same NMJs were then imaged at 30 and 60 mps.

ORN Axotomy Assay & Brain Dissection

Antennal injuries and dissections were performed as described in Chapter 2.

Microscopy & Analysis

Brain samples were imaged on a Zeiss LSM 700 with a Zeiss 40X 1.4NA oil immersion plan-apochromatic lens, while larval NMJ samples were imaged using a Zeiss 63X 1.3NA water immersion plan-neofluar lens. Larval samples examining spGFP11 and Ilp2-GFP co-localization were imaged using a Zeiss Elyra 7 with lattice SIM with a Zeiss 63X 1.4NA oil immersion plan-apochromatic lens at the OHSU ALMC. Samples within the same experiment were imaged on the same day, using the same microscope settings. Volocity 3D Image Analysis Software (Quorum Technologies) was used for GFP total fluorescence quantification. Imaris Cell Imaging Software (Andor Technology) at the OHSU ALMC was used for colocalization analysis at the larval NMJ. GraphPad Prism 8 (Graphpad Software) was used for statistical analysis: Kruskal-Wallis test (Dunn's *post hoc* test); see figure legends for details. Outliers were identified using the ROUT method (Q=1%). Normality of datasets was determined using the D'Agostino-Pearson normality test.

Antibodies

The following antibodies were used: goat anti-HRP-RRX (123-295-021; Jackson Immunoresearch) at 1:50, mouse anti-c-Myc (9E10, DSHB) at 1:50. All secondary antibodies (Jackson ImmunoResearch: 715-605-150) were used at a 1:400 dilution.

Drosophila stocks

OK371-Gal4 (II; BDSC 26160), UAS-Ilp2-GFP (II; gift from E. Levitan and D. Deitcher), 10X-UAS-myr-tdTomato (II; BDSC 32222), Vglut-LexA (II; BDSC 84442), MHC-Gal4 (III; (284)), UAS-mCD4-spGFP1-10 (III; gift from K. Scott), Or22a-LexA (II; BDSC 80543), repo-Gal4 (III; BDSC 7415), Or82a-GAD-LexA (II; gift from G. Struhl), repo-Gal4, tubulin-Gal80ts (III; gift from K. Colodner).

References

1. Ndubaku U, de Bellard ME. Glial cells: old cells with new twists. Acta Histochem. 2008;110(3):182-95. 10.1016/j.acthis.2007.10.003
2. Allen NJ, Barres BA. Neuroscience: Glia - more than just brain glue. Nature. 2009;457(7230):675-7. 10.1038/457675a
3. Freeman MR. Drosophila Central Nervous System Glia. Cold Spring Harb Perspect Biol. 2015;7(11). 10.1101/cshperspect.a020552
4. Khakh BS, Sofroniew MV. Diversity of astrocyte functions and phenotypes in neural circuits. Nat Neurosci. 2015;18(7):942-52. 10.1038/nn.4043
5. Matejuk A, Ransohoff RM. Crosstalk Between Astrocytes and Microglia: An Overview. Front Immunol. 2020;11:1416. 10.3389/fimmu.2020.01416
6. Halassa MM, Fellin T, Haydon PG. The tripartite synapse: roles for gliotransmission in health and disease. Trends Mol Med. 2007;13(2):54-63. 10.1016/j.molmed.2006.12.005
7. Poskanzer KE, Molofsky AV. Dynamism of an Astrocyte In Vivo: Perspectives on Identity and Function. Annu Rev Physiol. 2018;80:143-57. 10.1146/annurev-physiol-021317-121125
8. Poskanzer KE, Yuste R. Astrocytes regulate cortical state switching in vivo. Proc Natl Acad Sci U S A. 2016;113(19):E2675-84. 10.1073/pnas.1520759113
9. Panickar KS, Norenberg MD. Astrocytes in cerebral ischemic injury: morphological and general considerations. Glia. 2005;50(4):287-98. 10.1002/glia.20181
10. Abbott NJ, Ronnback L, Hansson E. Astrocyte-endothelial interactions at the blood-brain barrier. Nat Rev Neurosci. 2006;7(1):41-53. 10.1038/nrn1824
11. Bazargani N, Attwell D. Astrocyte calcium signaling: the third wave. Nat Neurosci. 2016;19(2):182-9. 10.1038/nn.4201
12. Freeman MR, Doherty J. Glial cell biology in Drosophila and vertebrates. Trends Neurosci. 2006;29(2):82-90. 10.1016/j.tins.2005.12.002
13. Limmer S, Weiler A, Volkenhoff A, Babatz F, Klambt C. The Drosophila blood-brain barrier: development and function of a glial endothelium. Front Neurosci. 2014;8:365. 10.3389/fnins.2014.00365
14. Tremblay ME, Stevens B, Sierra A, Wake H, Bessis A, Nimmerjahn A. The role of microglia in the healthy brain. J Neurosci. 2011;31(45):16064-9. 10.1523/JNEUROSCI.4158-11.2011
15. Nimmerjahn A, Kirchhoff F, Helmchen F. Resting microglial cells are highly dynamic surveillants of brain parenchyma in vivo. Science. 2005;308(5726):1314-8. 10.1126/science.1110647

16. Vainchtein ID, Molofsky AV. Astrocytes and Microglia: In Sickness and in Health. Trends Neurosci. 2020;43(3):144-54. 10.1016/j.tins.2020.01.003
17. Davalos D, Grutzendler J, Yang G, Kim JV, Zuo Y, Jung S, Littman DR, Dustin ML, Gan WB. ATP mediates rapid microglial response to local brain injury in vivo. Nat Neurosci. 2005;8(6):752-8. 10.1038/nn1472
18. Donat CK, Scott G, Gentleman SM, Sastre M. Microglial Activation in Traumatic Brain Injury. Front Aging Neurosci. 2017;9:208. 10.3389/fnagi.2017.00208
19. Paolicelli RC, Bolasco G, Pagani F, Maggi L, Scianni M, Panzanelli P, Giustetto M, Ferreira TA, Guiducci E, Dumas L, Ragozzino D, Gross CT. Synaptic pruning by microglia is necessary for normal brain development. Science. 2011;333(6048):1456-8. 10.1126/science.1202529
20. Logan MA, Freeman MR. The scoop on the fly brain: glial engulfment functions in Drosophila. Neuron Glia Biol. 2007;3(1):63-74. 10.1017/S1740925X07000646
21. Hartenstein V. Morphological diversity and development of glia in Drosophila. Glia. 2011;59(9):1237-52. 10.1002/glia.21162
22. Simons M, Nave KA. Oligodendrocytes: Myelination and Axonal Support. Cold Spring Harb Perspect Biol. 2015;8(1):a020479. 10.1101/cshperspect.a020479
23. O'Rourke M, Gasperini R, Young KM. Adult myelination: wrapping up neuronal plasticity. Neural Regen Res. 2014;9(13):1261-4. 10.4103/1673-5374.137571
24. Bergles DE, Richardson WD. Oligodendrocyte Development and Plasticity. Cold Spring Harb Perspect Biol. 2015;8(2):a020453. 10.1101/cshperspect.a020453
25. Mirsky R, Jessen KR. The neurobiology of Schwann cells. Brain Pathol. 1999;9(2):293-311. 10.1111/j.1750-3639.1999.tb00228.x
26. Schafer DP, Stevens B. Phagocytic glial cells: sculpting synaptic circuits in the developing nervous system. Curr Opin Neurobiol. 2013;23(6):1034-40. 10.1016/j.conb.2013.09.012
27. Brosius Lutz A, Chung WS, Sloan SA, Carson GA, Zhou L, Lovelett E, Posada S, Zuchero JB, Barres BA. Schwann cells use TAM receptor-mediated phagocytosis in addition to autophagy to clear myelin in a mouse model of nerve injury. Proc Natl Acad Sci U S A. 2017;114(38):E8072-E80. 10.1073/pnas.1710566114
28. Yildirim K, Petri J, Kottmeier R, Klambt C. Drosophila glia: Few cell types and many conserved functions. Glia. 2019;67(1):5-26. 10.1002/glia.23459

29. Awasaki T, Lai SL, Ito K, Lee T. Organization and postembryonic development of glial cells in the adult central brain of Drosophila. J Neurosci. 2008;28(51):13742-53. 10.1523/JNEUROSCI.4844-08.2008
30. Pereanu W, Spindler S, Cruz L, Hartenstein V. Tracheal development in the Drosophila brain is constrained by glial cells. Dev Biol. 2007;302(1):169-80. 10.1016/j.ydbio.2006.09.022
31. Hanani M, Spray DC. Emerging importance of satellite glia in nervous system function and dysfunction. Nat Rev Neurosci. 2020;21(9):485-98. 10.1038/s41583-020-0333-z
32. Zhang Y, Chen K, Sloan SA, Bennett ML, Scholze AR, O'Keeffe S, Phatnani HP, Guarnieri P, Caneda C, Ruderisch N, Deng S, Liddelow SA, Zhang C, Daneman R, Maniatis T, Barres BA, Wu JQ. An RNA-sequencing transcriptome and splicing database of glia, neurons, and vascular cells of the cerebral cortex. J Neurosci. 2014;34(36):11929-47. 10.1523/JNEUROSCI.1860-14.2014
33. Holtman IR, Noback M, Bijlsma M, Duong KN, van der Geest MA, Ketelaars PT, Brouwer N, Vainchtein ID, Eggen BJ, Boddeke HW. Glia Open Access Database (GOAD): A comprehensive gene expression encyclopedia of glia cells in health and disease. Glia. 2015;63(9):1495-506. 10.1002/glia.22810
34. Boisvert MM, Erikson GA, Shokhirev MN, Allen NJ. The Aging Astrocyte Transcriptome from Multiple Regions of the Mouse Brain. Cell Rep. 2018;22(1):269-85. 10.1016/j.celrep.2017.12.039
35. Erickson EK, Blednov YA, Harris RA, Mayfield RD. Glial gene networks associated with alcohol dependence. Sci Rep. 2019;9(1):10949. 10.1038/s41598-019-47454-4
36. Galloway DA, Phillips AEM, Owen DRJ, Moore CS. Phagocytosis in the Brain: Homeostasis and Disease. Front Immunol. 2019;10:790. 10.3389/fimmu.2019.00790
37. Frost JL, Schafer DP. Microglia: Architects of the Developing Nervous System. Trends Cell Biol. 2016;26(8):587-97. 10.1016/j.tcb.2016.02.006
38. Filipello F, Morini R, Corradini I, Zerbi V, Canzi A, Michalski B, Erreni M, Markicevic M, Starvaggi-Cucuzza C, Otero K, Piccio L, Cignarella F, Perrucci F, Tamborini M, Genua M, Rajendran L, Menna E, Vetrano S, Fahnestock M, Paolicelli RC, Matteoli M. The Microglial Innate Immune Receptor TREM2 Is Required for Synapse Elimination and Normal Brain Connectivity. Immunity. 2018;48(5):979-91 e8. 10.1016/j.immuni.2018.04.016
39. Schafer DP, Lehrman EK, Kautzman AG, Koyama R, Mardinly AR, Yamasaki R, Ransohoff RM, Greenberg ME, Barres BA, Stevens B. Microglia sculpt postnatal neural circuits in an activity and complement-dependent manner. Neuron. 2012;74(4):691-705. 10.1016/j.neuron.2012.03.026

40. Allen NJ, Lyons DA. Glia as architects of central nervous system formation and function. Science. 2018;362(6411):181-5. 10.1126/science.aat0473
41. Bialas AR, Stevens B. TGF-beta signaling regulates neuronal C1q expression and developmental synaptic refinement. Nat Neurosci. 2013;16(12):1773-82. 10.1038/nn.3560
42. Chung WS, Clarke LE, Wang GX, Stafford BK, Sher A, Chakraborty C, Joung J, Foo LC, Thompson A, Chen C, Smith SJ, Barres BA. Astrocytes mediate synapse elimination through MEGF10 and MERTK pathways. Nature. 2013;504(7480):394-400. 10.1038/nature12776
43. Lemke G. Phosphatidylserine Is the Signal for TAM Receptors and Their Ligands. Trends Biochem Sci. 2017;42(9):738-48. 10.1016/j.tibs.2017.06.004
44. Iram T, Ramirez-Ortiz Z, Byrne MH, Coleman UA, Kingery ND, Means TK, Frenkel D, El Khoury J. Megf10 Is a Receptor for C1Q That Mediates Clearance of Apoptotic Cells by Astrocytes. J Neurosci. 2016;36(19):5185-92. 10.1523/JNEUROSCI.3850-15.2016
45. Reemst K, Noctor SC, Lucassen PJ, Hol EM. The Indispensable Roles of Microglia and Astrocytes during Brain Development. Front Hum Neurosci. 2016;10:566. 10.3389/fnhum.2016.00566
46. Clarke LE, Barres BA. Emerging roles of astrocytes in neural circuit development. Nat Rev Neurosci. 2013;14(5):311-21. 10.1038/nrn3484
47. Kozlov AS, Angulo MC, Audinat E, Charpak S. Target cell-specific modulation of neuronal activity by astrocytes. Proc Natl Acad Sci U S A. 2006;103(26):10058-63. 10.1073/pnas.0603741103
48. Tambuyzer BR, Ponsaerts P, Nouwen EJ. Microglia: gatekeepers of central nervous system immunology. J Leukoc Biol. 2009;85(3):352-70. 10.1189/jlb.0608385
49. Karve IP, Taylor JM, Crack PJ. The contribution of astrocytes and microglia to traumatic brain injury. Br J Pharmacol. 2016;173(4):692-702. 10.1111/bph.13125
50. Anderson KV. Toll signaling pathways in the innate immune response. Curr Opin Immunol. 2000;12(1):13-9. 10.1016/s0952-7915(99)00045-x
51. Luo C, Jian C, Liao Y, Huang Q, Wu Y, Liu X, Zou D, Wu Y. The role of microglia in multiple sclerosis. Neuropsychiatr Dis Treat. 2017;13:1661-7. 10.2147/NDT.S140634
52. Yamasaki R, Lu H, Butovsky O, Ohno N, Rietsch AM, Cialic R, Wu PM, Doykan CE, Lin J, Cotleur AC, Kidd G, Zorlu MM, Sun N, Hu W, Liu L, Lee JC, Taylor SE, Uehlein L, Dixon D, Gu J, Floruta CM, Zhu M, Charo IF, Weiner HL, Ransohoff RM. Differential roles of microglia and monocytes in the inflamed central nervous system. J Exp Med. 2014;211(8):1533-49. 10.1084/jem.20132477

53. Healy LM, Perron G, Won SY, Michell-Robinson MA, Rezk A, Ludwin SK, Moore CS, Hall JA, Bar-Or A, Antel JP. MerTK Is a Functional Regulator of Myelin Phagocytosis by Human Myeloid Cells. J Immunol. 2016;196(8):3375-84. 10.4049/jimmunol.1502562
54. Poliani PL, Wang Y, Fontana E, Robinette ML, Yamanishi Y, Gilfillan S, Colonna M. TREM2 sustains microglial expansion during aging and response to demyelination. J Clin Invest. 2015;125(5):2161-70. 10.1172/JCI77983
55. Cantoni C, Bollman B, Licastro D, Xie M, Mikesell R, Schmidt R, Yuede CM, Galimberti D, Olivecrona G, Klein RS, Cross AH, Otero K, Piccio L. TREM2 regulates microglial cell activation in response to demyelination in vivo. Acta Neuropathol. 2015;129(3):429-47. 10.1007/s00401-015-1388-1
56. Sadigh-Eteghad S, Sabermarouf B, Majdi A, Talebi M, Farhoudi M, Mahmoudi J. Amyloid-beta: a crucial factor in Alzheimer's disease. Med Princ Pract. 2015;24(1):1-10. 10.1159/000369101
57. Brion JP, Couck AM, Passareiro E, Flament-Durand J. Neurofibrillary tangles of Alzheimer's disease: an immunohistochemical study. J Submicrosc Cytol. 1985;17(1):89-96.
58. Lee CY, Landreth GE. The role of microglia in amyloid clearance from the AD brain. J Neural Transm (Vienna). 2010;117(8):949-60. 10.1007/s00702-010-0433-4
59. Condello C, Yuan P, Schain A, Grutzendler J. Microglia constitute a barrier that prevents neurotoxic protofibrillar Abeta42 hotspots around plaques. Nat Commun. 2015;6:6176. 10.1038/ncomms7176
60. Bylicky MA, Mueller GP, Day RM. Mechanisms of Endogenous Neuroprotective Effects of Astrocytes in Brain Injury. Oxid Med Cell Longev. 2018;2018:6501031. 10.1155/2018/6501031
61. Hsu JY, Bourguignon LY, Adams CM, Peyrollier K, Zhang H, Fandel T, Cun CL, Werb Z, Noble-Haeusslein LJ. Matrix metalloproteinase-9 facilitates glial scar formation in the injured spinal cord. J Neurosci. 2008;28(50):13467-77. 10.1523/JNEUROSCI.2287-08.2008
62. Chen Y, Swanson RA. Astrocytes and brain injury. J Cereb Blood Flow Metab. 2003;23(2):137-49. 10.1097/01.WCB.0000044631.80210.3C
63. Silver J, Miller JH. Regeneration beyond the glial scar. Nat Rev Neurosci. 2004;5(2):146-56. 10.1038/nrn1326
64. Hong S, Beja-Glasser VF, Nfonoyim BM, Frouin A, Li S, Ramakrishnan S, Merry KM, Shi Q, Rosenthal A, Barres BA, Lemere CA, Selkoe DJ, Stevens B. Complement and microglia mediate early synapse loss in Alzheimer mouse models. Science. 2016;352(6286):712-6. 10.1126/science.aad8373

65. Terry RD, Masliah E, Salmon DP, Butters N, DeTeresa R, Hill R, Hansen LA, Katzman R. Physical basis of cognitive alterations in Alzheimer's disease: synapse loss is the major correlate of cognitive impairment. Ann Neurol. 1991;30(4):572-80. 10.1002/ana.410300410
66. Orre M, Kamphuis W, Osborn LM, Melief J, Kooijman L, Huitinga I, Klooster J, Bossers K, Hol EM. Acute isolation and transcriptome characterization of cortical astrocytes and microglia from young and aged mice. Neurobiol Aging. 2014;35(1):1-14. 10.1016/j.neurobiolaging.2013.07.008
67. Brand AH, Perrimon N. Targeted gene expression as a means of altering cell fates and generating dominant phenotypes. Development. 1993;118(2):401-15.
68. Potter CJ, Tasic B, Russler EV, Liang L, Luo L. The Q system: a repressible binary system for transgene expression, lineage tracing, and mosaic analysis. Cell. 2010;141(3):536-48. 10.1016/j.cell.2010.02.025
69. Lai SL, Lee T. Genetic mosaic with dual binary transcriptional systems in Drosophila. Nat Neurosci. 2006;9(5):703-9. 10.1038/nn1681
70. MacDonald JM, Beach MG, Porpiglia E, Sheehan AE, Watts RJ, Freeman MR. The Drosophila cell corpse engulfment receptor Draper mediates glial clearance of severed axons. Neuron. 2006;50(6):869-81. 10.1016/j.neuron.2006.04.028
71. Hoopfer ED, McLaughlin T, Watts RJ, Schuldiner O, O'Leary DD, Luo L. Wlds protection distinguishes axon degeneration following injury from naturally occurring developmental pruning. Neuron. 2006;50(6):883-95. 10.1016/j.neuron.2006.05.013
72. Macdonald JM, Doherty J, Hackett R, Freeman MR. The c-Jun kinase signaling cascade promotes glial engulfment activity through activation of draper and phagocytic function. Cell Death Differ. 2013;20(9):1140-8. 10.1038/cdd.2013.30
73. Doherty J, Logan MA, Tasdemir OE, Freeman MR. Ensheathing glia function as phagocytes in the adult Drosophila brain. J Neurosci. 2009;29(15):4768-81. 10.1523/JNEUROSCI.5951-08.2009
74. Doherty J, Sheehan AE, Bradshaw R, Fox AN, Lu TY, Freeman MR. PI3K signaling and Stat92E converge to modulate glial responsiveness to axonal injury. PLoS Biol. 2014;12(11):e1001985. 10.1371/journal.pbio.1001985
75. Neukomm LJ, Burdett TC, Gonzalez MA, Zuchner S, Freeman MR. Rapid in vivo forward genetic approach for identifying axon death genes in Drosophila. Proc Natl Acad Sci U S A. 2014;111(27):9965-70. 10.1073/pnas.1406230111
76. Court R, Namiki S, Armstrong JD, Borner J, Card G, Costa M, Dickinson M, Duch C, Korff W, Mann R, Merritt D, Murphey RK, Seeds AM, Shirangi T, Simpson JH, Truman JW,

Tuthill JC, Williams DW, Shepherd D. A Systematic Nomenclature for the Drosophila Ventral Nerve Cord. Neuron. 2020;107(6):1071-9 e2. 10.1016/j.neuron.2020.08.005
77. Purice MD, Ray A, Munzel EJ, Pope BJ, Park DJ, Speese SD, Logan MA. A novel Drosophila injury model reveals severed axons are cleared through a Draper/MMP-1 signaling cascade. Elife. 2017;6. 10.7554/eLife.23611
78. Menon KP, Carrillo RA, Zinn K. Development and plasticity of the Drosophila larval neuromuscular junction. Wiley Interdiscip Rev Dev Biol. 2013;2(5):647-70. 10.1002/wdev.108
79. Koh YH, Gramates LS, Budnik V. Drosophila larval neuromuscular junction: molecular components and mechanisms underlying synaptic plasticity. Microsc Res Tech. 2000;49(1):14-25. 10.1002/(SICI)1097-0029(20000401)49:1<14::AID-JEMT3>3.0.CO;2-G
80. Rooney TM, Freeman MR. Drosophila models of neuronal injury. ILAR J. 2014;54(3):291-5. 10.1093/ilar/ilt057
81. Brent JR, Werner KM, McCabe BD. Drosophila larval NMJ dissection. J Vis Exp. 2009(24). 10.3791/1107
82. Ramachandran P, Budnik V. Dissection of Drosophila larval body-wall muscles. Cold Spring Harb Protoc. 2010;2010(8):pdb prot5469. 10.1101/pdb.prot5469
83. Freeman MR. Signaling mechanisms regulating Wallerian degeneration. Curr Opin Neurobiol. 2014;27:224-31. 10.1016/j.conb.2014.05.001
84. Waller A. Experiments on the Section of the Glossopharyngeal and Hypoglossal Nerves of the Frog, and Observations of the Alterations Produced Thereby in the Structure of Their Primitive Fibres. Phil Trans R Soc Lond. 1850;140:423-9.
85. Finn JT, Weil M, Archer F, Siman R, Srinivasan A, Raff MC. Evidence that Wallerian degeneration and localized axon degeneration induced by local neurotrophin deprivation do not involve caspases. J Neurosci. 2000;20(4):1333-41.
86. Rotshenker S. Wallerian degeneration: the innate-immune response to traumatic nerve injury. J Neuroinflammation. 2011;8:109. 10.1186/1742-2094-8-109
87. Conforti L, Gilley J, Coleman MP. Wallerian degeneration: an emerging axon death pathway linking injury and disease. Nat Rev Neurosci. 2014;15(6):394-409. 10.1038/nrn3680
88. Beirowski B, Adalbert R, Wagner D, Grumme DS, Addicks K, Ribchester RR, Coleman MP. The progressive nature of Wallerian degeneration in wild-type and slow Wallerian degeneration (WldS) nerves. BMC Neurosci. 2005;6:6. 10.1186/1471-2202-6-6
89. Sta M, Cappaert NL, Ramekers D, Baas F, Wadman WJ. The functional and morphological characteristics of sciatic nerve degeneration and regeneration after crush injury in rats. J Neurosci Methods. 2014;222:189-98. 10.1016/j.jneumeth.2013.11.012

90. Freeman MR, Delrow J, Kim J, Johnson E, Doe CQ. Unwrapping glial biology: Gcm target genes regulating glial development, diversification, and function. Neuron. 2003;38(4):567-80. 10.1016/s0896-6273(03)00289-7
91. Xiong X, Hao Y, Sun K, Li J, Li X, Mishra B, Soppina P, Wu C, Hume RI, Collins CA. The Highwire ubiquitin ligase promotes axonal degeneration by tuning levels of Nmnat protein. PLoS Biol. 2012;10(12):e1001440. 10.1371/journal.pbio.1001440
92. Ji H, Sapar ML, Sarkar A, Wang B, Han C. Phagocytosis and self-destruction break down dendrites of Drosophila sensory neurons at distinct steps of Wallerian degeneration. Proc Natl Acad Sci U S A. 2022;119(4). 10.1073/pnas.2111818119
93. Zhai RG, Rizzi M, Garavaglia S. Nicotinamide/nicotinic acid mononucleotide adenylyltransferase, new insights into an ancient enzyme. Cell Mol Life Sci. 2009;66(17):2805-18. 10.1007/s00018-009-0047-x
94. Sporny M, Guez-Haddad J, Khazma T, Yaron A, Dessau M, Shkolnisky Y, Mim C, Isupov MN, Zalk R, Hons M, Opatowsky Y. Structural basis for SARM1 inhibition and activation under energetic stress. Elife. 2020;9. 10.7554/eLife.62021
95. Gerdts J, Brace EJ, Sasaki Y, DiAntonio A, Milbrandt J. SARM1 activation triggers axon degeneration locally via NAD(+) destruction. Science. 2015;348(6233):453-7. 10.1126/science.1258366
96. Ma M, Ferguson TA, Schoch KM, Li J, Qian Y, Shofer FS, Saatman KE, Neumar RW. Calpains mediate axonal cytoskeleton disintegration during Wallerian degeneration. Neurobiol Dis. 2013;56:34-46. 10.1016/j.nbd.2013.03.009
97. Lunn ER, Perry VH, Brown MC, Rosen H, Gordon S. Absence of Wallerian Degeneration does not Hinder Regeneration in Peripheral Nerve. Eur J Neurosci. 1989;1(1):27-33. 10.1111/j.1460-9568.1989.tb00771.x
98. Coleman MP, Conforti L, Buckmaster EA, Tarlton A, Ewing RM, Brown MC, Lyon MF, Perry VH. An 85-kb tandem triplication in the slow Wallerian degeneration (Wlds) mouse. Proc Natl Acad Sci U S A. 1998;95(17):9985-90. 10.1073/pnas.95.17.9985
99. Perry VH, Brown MC, Lunn ER. Very Slow Retrograde and Wallerian Degeneration in the CNS of C57BL/Ola Mice. Eur J Neurosci. 1991;3(1):102-5. 10.1111/j.1460-9568.1991.tb00815.x
100. Loring HS, Thompson PR. Emergence of SARM1 as a Potential Therapeutic Target for Wallerian-type Diseases. Cell Chem Biol. 2020;27(1):1-13. 10.1016/j.chembiol.2019.11.002
101. Schlaepfer WW. Calcium-induced degeneration of axoplasm in isolated segments of rat peripheral nerve. Brain Res. 1974;69(2):203-15. 10.1016/0006-8993(74)90002-x

102. George EB, Glass JD, Griffin JW. Axotomy-induced axonal degeneration is mediated by calcium influx through ion-specific channels. J Neurosci. 1995;15(10):6445-52.
103. Mishra B, Carson R, Hume RI, Collins CA. Sodium and potassium currents influence Wallerian degeneration of injured Drosophila axons. J Neurosci. 2013;33(48):18728-39. 10.1523/JNEUROSCI.1007-13.2013
104. Knoferle J, Koch JC, Ostendorf T, Michel U, Planchamp V, Vutova P, Tonges L, Stadelmann C, Bruck W, Bahr M, Lingor P. Mechanisms of acute axonal degeneration in the optic nerve in vivo. Proc Natl Acad Sci U S A. 2010;107(13):6064-9. 10.1073/pnas.0909794107
105. Vargas ME, Yamagishi Y, Tessier-Lavigne M, Sagasti A. Live Imaging of Calcium Dynamics during Axon Degeneration Reveals Two Functionally Distinct Phases of Calcium Influx. J Neurosci. 2015;35(45):15026-38. 10.1523/JNEUROSCI.2484-15.2015
106. Adalbert R, Morreale G, Paizs M, Conforti L, Walker SA, Roderick HL, Bootman MD, Siklos L, Coleman MP. Intra-axonal calcium changes after axotomy in wild-type and slow Wallerian degeneration axons. Neuroscience. 2012;225:44-54. 10.1016/j.neuroscience.2012.08.056
107. Yang J, Weimer RM, Kallop D, Olsen O, Wu Z, Renier N, Uryu K, Tessier-Lavigne M. Regulation of axon degeneration after injury and in development by the endogenous calpain inhibitor calpastatin. Neuron. 2013;80(5):1175-89. 10.1016/j.neuron.2013.08.034
108. Fields RD, Stevens B. ATP: an extracellular signaling molecule between neurons and glia. Trends Neurosci. 2000;23(12):625-33. 10.1016/s0166-2236(00)01674-x
109. Fields RD, Burnstock G. Purinergic signalling in neuron-glia interactions. Nat Rev Neurosci. 2006;7(6):423-36. 10.1038/nrn1928
110. Sapar ML, Ji H, Wang B, Poe AR, Dubey K, Ren X, Ni JQ, Han C. Phosphatidylserine Externalization Results from and Causes Neurite Degeneration in Drosophila. Cell Rep. 2018;24(9):2273-86. 10.1016/j.celrep.2018.07.095
111. Leventis PA, Grinstein S. The distribution and function of phosphatidylserine in cellular membranes. Annu Rev Biophys. 2010;39:407-27. 10.1146/annurev.biophys.093008.131234
112. Segawa K, Nagata S. An Apoptotic 'Eat Me' Signal: Phosphatidylserine Exposure. Trends Cell Biol. 2015;25(11):639-50. 10.1016/j.tcb.2015.08.003
113. Mazaheri F, Breus O, Durdu S, Haas P, Wittbrodt J, Gilmour D, Peri F. Distinct roles for BAI1 and TIM-4 in the engulfment of dying neurons by microglia. Nat Commun. 2014;5:4046. 10.1038/ncomms5046

114. Furuta Y, Pena-Ramos O, Li Z, Chiao L, Zhou Z. Calcium ions trigger the exposure of phosphatidylserine on the surface of necrotic cells. PLoS Genet. 2021;17(2):e1009066. 10.1371/journal.pgen.1009066
115. Nomura-Komoike K, Saitoh F, Fujieda H. Phosphatidylserine recognition and Rac1 activation are required for Muller glia proliferation, gliosis and phagocytosis after retinal injury. Sci Rep. 2020;10(1):1488. 10.1038/s41598-020-58424-6
116. Chiu H, Zou Y, Suzuki N, Hsieh YW, Chuang CF, Wu YC, Chang C. Engulfing cells promote neuronal regeneration and remove neuronal debris through distinct biochemical functions of CED-1. Nat Commun. 2018;9(1):4842. 10.1038/s41467-018-07291-x
117. Logan MA. Glial contributions to neuronal health and disease: new insights from Drosophila. Curr Opin Neurobiol. 2017;47:162-7. 10.1016/j.conb.2017.10.008
118. Ziegenfuss JS, Doherty J, Freeman MR. Distinct molecular pathways mediate glial activation and engulfment of axonal debris after axotomy. Nat Neurosci. 2012;15(7):979-87. 10.1038/nn.3135
119. Logan MA, Hackett R, Doherty J, Sheehan A, Speese SD, Freeman MR. Negative regulation of glial engulfment activity by Draper terminates glial responses to axon injury. Nat Neurosci. 2012;15(5):722-30. 10.1038/nn.3066
120. Purice MD, Speese SD, Logan MA. Delayed glial clearance of degenerating axons in aged Drosophila is due to reduced PI3K/Draper activity. Nat Commun. 2016;7:12871. 10.1038/ncomms12871
121. Chung WS, Barres BA. The role of glial cells in synapse elimination. Curr Opin Neurobiol. 2012;22(3):438-45. 10.1016/j.conb.2011.10.003
122. Ziegenfuss JS, Biswas R, Avery MA, Hong K, Sheehan AE, Yeung YG, Stanley ER, Freeman MR. Draper-dependent glial phagocytic activity is mediated by Src and Syk family kinase signalling. Nature. 2008;453(7197):935-9. 10.1038/nature06901
123. Awasaki T, Tatsumi R, Takahashi K, Arai K, Nakanishi Y, Ueda R, Ito K. Essential role of the apoptotic cell engulfment genes draper and ced-6 in programmed axon pruning during Drosophila metamorphosis. Neuron. 2006;50(6):855-67. 10.1016/j.neuron.2006.04.027
124. Lu TY, Doherty J, Freeman MR. DRK/DOS/SOS converge with Crk/Mbc/dCed-12 to activate Rac1 during glial engulfment of axonal debris. Proc Natl Acad Sci U S A. 2014;111(34):12544-9. 10.1073/pnas.1403450111
125. Murphy G, Nagase H. Progress in matrix metalloproteinase research. Mol Aspects Med. 2008;29(5):290-308. 10.1016/j.mam.2008.05.002

126. Shapiro SD. Matrix metalloproteinase degradation of extracellular matrix: biological consequences. Curr Opin Cell Biol. 1998;10(5):602-8. 10.1016/s0955-0674(98)80035-5
127. van der Heide LP, Ramakers GM, Smidt MP. Insulin signaling in the central nervous system: learning to survive. Prog Neurobiol. 2006;79(4):205-21. 10.1016/j.pneurobio.2006.06.003
128. Garofalo RS. Genetic analysis of insulin signaling in Drosophila. Trends Endocrinol Metab. 2002;13(4):156-62. 10.1016/s1043-2760(01)00548-3
129. Miltiadous P, Stamatakis A, Stylianopoulou F. Neuroprotective effects of IGF-I following kainic acid-induced hippocampal degeneration in the rat. Cell Mol Neurobiol. 2010;30(3):347-60. 10.1007/s10571-009-9457-4
130. Guan J, Williams C, Gunning M, Mallard C, Gluckman P. The effects of IGF-1 treatment after hypoxic-ischemic brain injury in adult rats. J Cereb Blood Flow Metab. 1993;13(4):609-16. 10.1038/jcbfm.1993.79
131. Carro E, Trejo JL, Spuch C, Bohl D, Heard JM, Torres-Aleman I. Blockade of the insulin-like growth factor I receptor in the choroid plexus originates Alzheimer's-like neuropathology in rodents: new cues into the human disease? Neurobiol Aging. 2006;27(11):1618-31. 10.1016/j.neurobiolaging.2005.09.039
132. Musashe DT, Purice MD, Speese SD, Doherty J, Logan MA. Insulin-like Signaling Promotes Glial Phagocytic Clearance of Degenerating Axons through Regulation of Draper. Cell Rep. 2016;16(7):1838-50. 10.1016/j.celrep.2016.07.022
133. Persoon CM, Moro A, Nassal JP, Farina M, Broeke JH, Arora S, Dominguez N, van Weering JR, Toonen RF, Verhage M. Pool size estimations for dense-core vesicles in mammalian CNS neurons. EMBO J. 2018;37(20). 10.15252/embj.201899672
134. Gondre-Lewis MC, Park JJ, Loh YP. Cellular mechanisms for the biogenesis and transport of synaptic and dense-core vesicles. Int Rev Cell Mol Biol. 2012;299:27-115. 10.1016/B978-0-12-394310-1.00002-3
135. Gronke S, Clarke DF, Broughton S, Andrews TD, Partridge L. Molecular evolution and functional characterization of Drosophila insulin-like peptides. PLoS Genet. 2010;6(2):e1000857. 10.1371/journal.pgen.1000857
136. Garelli A, Gontijo AM, Miguela V, Caparros E, Dominguez M. Imaginal discs secrete insulin-like peptide 8 to mediate plasticity of growth and maturation. Science. 2012;336(6081):579-82. 10.1126/science.1216735
137. Kim T, Gondre-Lewis MC, Arnaoutova I, Loh YP. Dense-core secretory granule biogenesis. Physiology (Bethesda). 2006;21:124-33. 10.1152/physiol.00043.2005

138. Dikeakos JD, Di Lello P, Lacombe MJ, Ghirlando R, Legault P, Reudelhuber TL, Omichinski JG. Functional and structural characterization of a dense core secretory granule sorting domain from the PC1/3 protease. Proc Natl Acad Sci U S A. 2009;106(18):7408-13. 10.1073/pnas.0809576106
139. Orci L, Ravazzola M, Amherdt M, Perrelet A, Powell SK, Quinn DL, Moore HP. The trans-most cisternae of the Golgi complex: a compartment for sorting of secretory and plasma membrane proteins. Cell. 1987;51(6):1039-51. 10.1016/0092-8674(87)90590-3
140. Sobota JA, Back N, Eipper BA, Mains RE. Inhibitors of the V0 subunit of the vacuolar H+-ATPase prevent segregation of lysosomal- and secretory-pathway proteins. J Cell Sci. 2009;122(Pt 19):3542-53. 10.1242/jcs.034298
141. Garcia AL, Han SK, Janssen WG, Khaing ZZ, Ito T, Glucksman MJ, Benson DL, Salton SR. A prohormone convertase cleavage site within a predicted alpha-helix mediates sorting of the neuronal and endocrine polypeptide VGF into the regulated secretory pathway. J Biol Chem. 2005;280(50):41595-608. 10.1074/jbc.M509122200
142. Gorr SU, Jain RK, Kuehn U, Joyce PB, Cowley DJ. Comparative sorting of neuroendocrine secretory proteins: a search for common ground in a mosaic of sorting models and mechanisms. Mol Cell Endocrinol. 2001;172(1-2):1-6. 10.1016/s0303-7207(00)00342-7
143. Tooze SA, Flatmark T, Tooze J, Huttner WB. Characterization of the immature secretory granule, an intermediate in granule biogenesis. J Cell Biol. 1991;115(6):1491-503. 10.1083/jcb.115.6.1491
144. Wu MM, Grabe M, Adams S, Tsien RY, Moore HP, Machen TE. Mechanisms of pH regulation in the regulated secretory pathway. J Biol Chem. 2001;276(35):33027-35. 10.1074/jbc.M103917200
145. Kwinter DM, Lo K, Mafi P, Silverman MA. Dynactin regulates bidirectional transport of dense-core vesicles in the axon and dendrites of cultured hippocampal neurons. Neuroscience. 2009;162(4):1001-10. 10.1016/j.neuroscience.2009.05.038
146. Stucchi R, Plucinska G, Hummel JJA, Zahavi EE, Guerra San Juan I, Klykov O, Scheltema RA, Altelaar AFM, Hoogenraad CC. Regulation of KIF1A-Driven Dense Core Vesicle Transport: Ca(2+)/CaM Controls DCV Binding and Liprin-alpha/TANC2 Recruits DCVs to Postsynaptic Sites. Cell Rep. 2018;24(3):685-700. 10.1016/j.celrep.2018.06.071
147. Wong MY, Zhou C, Shakiryanova D, Lloyd TE, Deitcher DL, Levitan ES. Neuropeptide delivery to synapses by long-range vesicle circulation and sporadic capture. Cell. 2012;148(5):1029-38. 10.1016/j.cell.2011.12.036

148. Moughamian AJ, Holzbaur EL. Synaptic vesicle distribution by conveyor belt. Cell. 2012;148(5):849-51. 10.1016/j.cell.2012.02.007
149. Wong MY, Cavolo SL, Levitan ES. Synaptic neuropeptide release by dynamin-dependent partial release from circulating vesicles. Mol Biol Cell. 2015;26(13):2466-74. 10.1091/mbc.E15-01-0002
150. Tallent MK. Presynaptic inhibition of glutamate release by neuropeptides: use-dependent synaptic modification. Results Probl Cell Differ. 2008;44:177-200. 10.1007/400_2007_037
151. Matsuda N, Lu H, Fukata Y, Noritake J, Gao H, Mukherjee S, Nemoto T, Fukata M, Poo MM. Differential activity-dependent secretion of brain-derived neurotrophic factor from axon and dendrite. J Neurosci. 2009;29(45):14185-98. 10.1523/JNEUROSCI.1863-09.2009
152. Zhou H, Wei Z, Wang S, Yao D, Zhang R, Ma C. Structural and Functional Analysis of the CAPS SNARE-Binding Domain Required for SNARE Complex Formation and Exocytosis. Cell Rep. 2019;26(12):3347-59 e6. 10.1016/j.celrep.2019.02.064
153. Sollner TH. Regulated exocytosis and SNARE function (Review). Mol Membr Biol. 2003;20(3):209-20. 10.1080/0968768031000104953
154. Farina M, van de Bospoort R, He E, Persoon CM, van Weering JR, Broeke JH, Verhage M, Toonen RF. CAPS-1 promotes fusion competence of stationary dense-core vesicles in presynaptic terminals of mammalian neurons. Elife. 2015;4. 10.7554/eLife.05438
155. van Keimpema L, Kooistra R, Toonen RF, Verhage M. CAPS-1 requires its C2, PH, MHD1 and DCV domains for dense core vesicle exocytosis in mammalian CNS neurons. Sci Rep. 2017;7(1):10817. 10.1038/s41598-017-10936-4
156. Renden R, Berwin B, Davis W, Ann K, Chin CT, Kreber R, Ganetzky B, Martin TF, Broadie K. Drosophila CAPS is an essential gene that regulates dense-core vesicle release and synaptic vesicle fusion. Neuron. 2001;31(3):421-37.
157. Lin XG, Ming M, Chen MR, Niu WP, Zhang YD, Liu B, Jiu YM, Yu JW, Xu T, Wu ZX. UNC-31/CAPS docks and primes dense core vesicles in C. elegans neurons. Biochem Biophys Res Commun. 2010;397(3):526-31. 10.1016/j.bbrc.2010.05.148
158. Speese S, Petrie M, Schuske K, Ailion M, Ann K, Iwasaki K, Jorgensen EM, Martin TF. UNC-31 (CAPS) is required for dense-core vesicle but not synaptic vesicle exocytosis in Caenorhabditis elegans. J Neurosci. 2007;27(23):6150-62. 10.1523/JNEUROSCI.1466-07.2007
159. Berwin B, Floor E, Martin TF. CAPS (mammalian UNC-31) protein localizes to membranes involved in dense-core vesicle exocytosis. Neuron. 1998;21(1):137-45. 10.1016/s0896-6273(00)80521-8

160. Hammarlund M, Watanabe S, Schuske K, Jorgensen EM. CAPS and syntaxin dock dense core vesicles to the plasma membrane in neurons. J Cell Biol. 2008;180(3):483-91. 10.1083/jcb.200708018
161. Kabachinski G, Kielar-Grevstad DM, Zhang X, James DJ, Martin TF. Resident CAPS on dense-core vesicles docks and primes vesicles for fusion. Mol Biol Cell. 2016;27(4):654-68. 10.1091/mbc.E15-07-0509
162. Kreutzberger AJB, Kiessling V, Liang B, Seelheim P, Jakhanwal S, Jahn R, Castle JD, Tamm LK. Reconstitution of calcium-mediated exocytosis of dense-core vesicles. Sci Adv. 2017;3(7):e1603208. 10.1126/sciadv.1603208
163. Jockusch WJ, Speidel D, Sigler A, Sorensen JB, Varoqueaux F, Rhee JS, Brose N. CAPS-1 and CAPS-2 are essential synaptic vesicle priming proteins. Cell. 2007;131(4):796-808. 10.1016/j.cell.2007.11.002
164. Lassmann H, Weiler R, Fischer P, Bancher C, Jellinger K, Floor E, Danielczyk W, Seitelberger F, Winkler H. Synaptic pathology in Alzheimer's disease: immunological data for markers of synaptic and large dense-core vesicles. Neuroscience. 1992;46(1):1-8. 10.1016/0306-4522(92)90003-k
165. Watanabe I, Vachal E, Tomita T. Dense core vesicles around the Lewy body in incidental Parkinson's disease: an electron microscopic study. Acta Neuropathol. 1977;39(2):173-5. 10.1007/BF00703325
166. Annangudi SP, Luszpak AE, Kim SH, Ren S, Hatcher NG, Weiler IJ, Thornley KT, Kile BM, Wightman RM, Greenough WT, Sweedler JV. Neuropeptide Release is Impaired in a Mouse Model of Fragile X Mental Retardation Syndrome. ACS Chem Neurosci. 2010;1(4):306-14. 10.1021/cn900036x
167. Landen M, Grenfeldt B, Davidsson P, Stridsberg M, Regland B, Gottfries CG, Blennow K. Reduction of chromogranin A and B but not C in the cerebrospinal fluid in subjects with schizophrenia. Eur Neuropsychopharmacol. 1999;9(4):311-5. 10.1016/s0924-977x(98)00042-x
168. Bulgari D, Deitcher DL, Levitan ES. Loss of Huntingtin stimulates capture of retrograde dense-core vesicles to increase synaptic neuropeptide stores. Eur J Cell Biol. 2017;96(5):402-6. 10.1016/j.ejcb.2017.01.001
169. Veriepe J, Fossouo L, Parker JA. Neurodegeneration in C. elegans models of ALS requires TIR-1/Sarm1 immune pathway activation in neurons. Nat Commun. 2015;6:7319. 10.1038/ncomms8319
170. Barres BA. The mystery and magic of glia: a perspective on their roles in health and disease. Neuron. 2008;60(3):430-40. 10.1016/j.neuron.2008.10.013

171. Dissing-Olesen L, LeDue JM, Rungta RL, Hefendehl JK, Choi HB, MacVicar BA. Activation of neuronal NMDA receptors triggers transient ATP-mediated microglial process outgrowth. J Neurosci. 2014;34(32):10511-27. 10.1523/JNEUROSCI.0405-14.2014
172. Hines DJ, Hines RM, Mulligan SJ, Macvicar BA. Microglia processes block the spread of damage in the brain and require functional chloride channels. Glia. 2009;57(15):1610-8. 10.1002/glia.20874
173. Hong S, Stevens B. Microglia: Phagocytosing to Clear, Sculpt, and Eliminate. Dev Cell. 2016;38(2):126-8. 10.1016/j.devcel.2016.07.006
174. Napoli I, Neumann H. Microglial clearance function in health and disease. Neuroscience. 2009;158(3):1030-8. 10.1016/j.neuroscience.2008.06.046
175. Polazzi E, Monti B. Microglia and neuroprotection: from in vitro studies to therapeutic applications. Prog Neurobiol. 2010;92(3):293-315. 10.1016/j.pneurobio.2010.06.009
176. Lee YM, Sun YH. Drosophila as a model to study the role of glia in neurodegeneration. J Neurogenet. 2015;29(2-3):69-79. 10.3109/01677063.2015.1076816
177. Cantera R, Barrio R. Do the genes of the innate immune response contribute to neuroprotection in Drosophila? J Innate Immun. 2015;7(1):3-10. 10.1159/000365195
178. Lu TY, MacDonald JM, Neukomm LJ, Sheehan AE, Bradshaw R, Logan MA, Freeman MR. Axon degeneration induces glial responses through Draper-TRAF4-JNK signalling. Nat Commun. 2017;8:14355. 10.1038/ncomms14355
179. Burgoyne RD, Morgan A. Secretory granule exocytosis. Physiol Rev. 2003;83(2):581-632. 10.1152/physrev.00031.2002
180. Huang EJ, Reichardt LF. Neurotrophins: roles in neuronal development and function. Annu Rev Neurosci. 2001;24:677-736. 10.1146/annurev.neuro.24.1.677
181. McAllister AK, Katz LC, Lo DC. Neurotrophins and synaptic plasticity. Annu Rev Neurosci. 1999;22:295-318. 10.1146/annurev.neuro.22.1.295
182. Meyer-Lindenberg A, Domes G, Kirsch P, Heinrichs M. Oxytocin and vasopressin in the human brain: social neuropeptides for translational medicine. Nat Rev Neurosci. 2011;12(9):524-38. 10.1038/nrn3044
183. Leng G, Ludwig M. Neurotransmitters and peptides: whispered secrets and public announcements. J Physiol. 2008;586(23):5625-32. 10.1113/jphysiol.2008.159103
184. Hirokawa N, Noda Y, Tanaka Y, Niwa S. Kinesin superfamily motor proteins and intracellular transport. Nat Rev Mol Cell Biol. 2009;10(10):682-96. 10.1038/nrm2774
185. Nurrish S. Dense core vesicle release: controlling the where as well as the when. Genetics. 2014;196(3):601-4. 10.1534/genetics.113.159905

186. Zhu PC, Thureson-Klein A, Klein RL. Exocytosis from large dense cored vesicles outside the active synaptic zones of terminals within the trigeminal subnucleus caudalis: a possible mechanism for neuropeptide release. Neuroscience. 1986;19(1):43-54.
187. Hartmann M, Heumann R, Lessmann V. Synaptic secretion of BDNF after high-frequency stimulation of glutamatergic synapses. EMBO J. 2001;20(21):5887-97. 10.1093/emboj/20.21.5887
188. van de Bospoort R, Farina M, Schmitz SK, de Jong A, de Wit H, Verhage M, Toonen RF. Munc13 controls the location and efficiency of dense-core vesicle release in neurons. J Cell Biol. 2012;199(6):883-91. 10.1083/jcb.201208024
189. Rao S, Lang C, Levitan ES, Deitcher DL. Visualization of neuropeptide expression, transport, and exocytosis in Drosophila melanogaster. J Neurobiol. 2001;49(3):159-72. 10.1002/neu.1072
190. Fang Y, Bonini NM. Axon degeneration and regeneration: insights from Drosophila models of nerve injury. Annu Rev Cell Dev Biol. 2012;28:575-97. 10.1146/annurev-cellbio-101011-155836
191. Fang Y, Bonini NM. Hope on the (fruit) fly: the Drosophila wing paradigm of axon injury. Neural Regen Res. 2015;10(2):173-5. 10.4103/1673-5374.152359
192. Hsu JM, Kang Y, Corty MM, Mathieson D, Peters OM, Freeman MR. Injury-Induced Inhibition of Bystander Neurons Requires dSarm and Signaling from Glia. Neuron. 2021;109(3):473-87 e5. 10.1016/j.neuron.2020.11.012
193. Avery MA, Rooney TM, Pandya JD, Wishart TM, Gillingwater TH, Geddes JW, Sullivan PG, Freeman MR. WldS prevents axon degeneration through increased mitochondrial flux and enhanced mitochondrial Ca2+ buffering. Curr Biol. 2012;22(7):596-600. 10.1016/j.cub.2012.02.043
194. Mack TG, Reiner M, Beirowski B, Mi W, Emanuelli M, Wagner D, Thomson D, Gillingwater T, Court F, Conforti L, Fernando FS, Tarlton A, Andressen C, Addicks K, Magni G, Ribchester RR, Perry VH, Coleman MP. Wallerian degeneration of injured axons and synapses is delayed by a Ube4b/Nmnat chimeric gene. Nat Neurosci. 2001;4(12):1199-206. 10.1038/nn770
195. Perry VH, Lunn ER, Brown MC, Cahusac S, Gordon S. Evidence that the Rate of Wallerian Degeneration is Controlled by a Single Autosomal Dominant Gene. Eur J Neurosci. 1990;2(5):408-13. 10.1111/j.1460-9568.1990.tb00433.x
196. Page-McCaw A. Remodeling the model organism: matrix metalloproteinase functions in invertebrates. Semin Cell Dev Biol. 2008;19(1):14-23. 10.1016/j.semcdb.2007.06.004

197. Fujioka H, Dairyo Y, Yasunaga K, Emoto K. Neural functions of matrix metalloproteinases: plasticity, neurogenesis, and disease. Biochem Res Int. 2012;2012:789083. 10.1155/2012/789083
198. Xia X, Lessmann V, Martin TF. Imaging of evoked dense-core-vesicle exocytosis in hippocampal neurons reveals long latencies and kiss-and-run fusion events. J Cell Sci. 2009;122(Pt 1):75-82. 10.1242/jcs.034603
199. Ahnert-Hilger G, Weller U, Dauzenroth ME, Habermann E, Gratzl M. The tetanus toxin light chain inhibits exocytosis. FEBS Lett. 1989;242(2):245-8. 10.1016/0014-5793(89)80478-8
200. Petrie M, Esquibel J, Kabachinski G, Maciuba S, Takahashi H, Edwardson JM, Martin TF. The Vesicle Priming Factor CAPS Functions as a Homodimer via C2 Domain Interactions to Promote Regulated Vesicle Exocytosis. J Biol Chem. 2016;291(40):21257-70. 10.1074/jbc.M116.728097
201. Lund VK, Lycas MD, Schack A, Andersen RC, Gether U, Kjaerulff O. Rab2 drives axonal transport of dense core vesicles and lysosomal organelles. Cell Rep. 2021;35(2):108973. 10.1016/j.celrep.2021.108973
202. Couto A, Alenius M, Dickson BJ. Molecular, anatomical, and functional organization of the Drosophila olfactory system. Curr Biol. 2005;15(17):1535-47. 10.1016/j.cub.2005.07.034
203. Song J, Wu L, Chen Z, Kohanski RA, Pick L. Axons guided by insulin receptor in Drosophila visual system. Science. 2003;300(5618):502-5. 10.1126/science.1081203
204. Richer P, Speese, S.D., Logan, M.A. FLARIM v2.0, an improved method to quantify transcript-ribosome interactions *in vivo* in the *Drosophila* brain. bioRxiv. 2021. https://doi.org/10.1101/2021.08.13.456301
205. Fields RD, Stevens-Graham B. New insights into neuron-glia communication. Science. 2002;298(5593):556-62. 10.1126/science.298.5593.556
206. Glezer I, Simard AR, Rivest S. Neuroprotective role of the innate immune system by microglia. Neuroscience. 2007;147(4):867-83. 10.1016/j.neuroscience.2007.02.055
207. Ray A, Speese SD, Logan MA. Glial Draper Rescues Abeta Toxicity in a Drosophila Model of Alzheimer's Disease. J Neurosci. 2017;37(49):11881-93. 10.1523/JNEUROSCI.0862-17.2017
208. Scheib JL, Sullivan CS, Carter BD. Jedi-1 and MEGF10 signal engulfment of apoptotic neurons through the tyrosine kinase Syk. J Neurosci. 2012;32(38):13022-31. 10.1523/JNEUROSCI.6350-11.2012

209. Lyons DA, Naylor SG, Scholze A, Talbot WS. Kif1b is essential for mRNA localization in oligodendrocytes and development of myelinated axons. Nat Genet. 2009;41(7):854-8. 10.1038/ng.376
210. Wake H, Lee PR, Fields RD. Control of local protein synthesis and initial events in myelination by action potentials. Science. 2011;333(6049):1647-51. 10.1126/science.1206998
211. Boulay AC, Saubamea B, Adam N, Chasseigneaux S, Mazare N, Gilbert A, Bahin M, Bastianelli L, Blugeon C, Perrin S, Pouch J, Ducos B, Le Crom S, Genovesio A, Chretien F, Decleves X, Laplanche JL, Cohen-Salmon M. Translation in astrocyte distal processes sets molecular heterogeneity at the gliovascular interface. Cell Discov. 2017;3:17005. 10.1038/celldisc.2017.5
212. Sakers K, Lake AM, Khazanchi R, Ouwenga R, Vasek MJ, Dani A, Dougherty JD. Astrocytes locally translate transcripts in their peripheral processes. Proc Natl Acad Sci U S A. 2017;114(19):E3830-E8. 10.1073/pnas.1617782114
213. Mazare N, Oudart M, Moulard J, Cheung G, Tortuyaux R, Mailly P, Mazaud D, Bemelmans AP, Boulay AC, Blugeon C, Jourdren L, Le Crom S, Rouach N, Cohen-Salmon M. Local Translation in Perisynaptic Astrocytic Processes Is Specific and Changes after Fear Conditioning. Cell Rep. 2020;32(8):108076. 10.1016/j.celrep.2020.108076
214. Burke KS, Antilla KA, Tirrell DA. A Fluorescence in Situ Hybridization Method To Quantify mRNA Translation by Visualizing Ribosome-mRNA Interactions in Single Cells. ACS Cent Sci. 2017;3(5):425-33. 10.1021/acscentsci.7b00048
215. Kosman D, Mizutani CM, Lemons D, Cox WG, McGinnis W, Bier E. Multiplex detection of RNA expression in Drosophila embryos. Science. 2004;305(5685):846. 10.1126/science.1099247
216. Pare A, Lemons D, Kosman D, Beaver W, Freund Y, McGinnis W. Visualization of individual Scr mRNAs during Drosophila embryogenesis yields evidence for transcriptional bursting. Curr Biol. 2009;19(23):2037-42. 10.1016/j.cub.2009.10.028
217. Weil TT, Parton RM, Herpers B, Soetaert J, Veenendaal T, Xanthakis D, Dobbie IM, Halstead JM, Hayashi R, Rabouille C, Davis I. Drosophila patterning is established by differential association of mRNAs with P bodies. Nat Cell Biol. 2012;14(12):1305-13. 10.1038/ncb2627
218. Abbaszadeh EK, Gavis ER. Fixed and live visualization of RNAs in Drosophila oocytes and embryos. Methods. 2016;98:34-41. 10.1016/j.ymeth.2016.01.018
219. Long X, Colonell J, Wong AM, Singer RH, Lionnet T. Quantitative mRNA imaging throughout the entire Drosophila brain. Nat Methods. 2017;14(7):703-6. 10.1038/nmeth.4309

220. Trcek T, Lionnet T, Shroff H, Lehmann R. mRNA quantification using single-molecule FISH in Drosophila embryos. Nat Protoc. 2017;12(7):1326-48. 10.1038/nprot.2017.030
221. Yang L, Titlow J, Ennis D, Smith C, Mitchell J, Young FL, Waddell S, Ish-Horowicz D, Davis I. Single molecule fluorescence in situ hybridisation for quantitating post-transcriptional regulation in Drosophila brains. Methods. 2017;126:166-76. 10.1016/j.ymeth.2017.06.025
222. Meissner GW, Nern A, Singer RH, Wong AM, Malkesman O, Long X. Mapping Neurotransmitter Identity in the Whole-Mount Drosophila Brain Using Multiplex High-Throughput Fluorescence in Situ Hybridization. Genetics. 2019;211(2):473-82. 10.1534/genetics.118.301749
223. Choi HM, Beck VA, Pierce NA. Multiplexed in situ hybridization using hybridization chain reaction. Zebrafish. 2014;11(5):488-9. 10.1089/zeb.2014.1501
224. Tsanov N, Samacoits A, Chouaib R, Traboulsi AM, Gostan T, Weber C, Zimmer C, Zibara K, Walter T, Peter M, Bertrand E, Mueller F. smiFISH and FISH-quant - a flexible single RNA detection approach with super-resolution capability. Nucleic Acids Res. 2016;44(22):e165. 10.1093/nar/gkw784
225. Choi HMT, Schwarzkopf M, Fornace ME, Acharya A, Artavanis G, Stegmaier J, Cunha A, Pierce NA. Third-generation in situ hybridization chain reaction: multiplexed, quantitative, sensitive, versatile, robust. Development. 2018;145(12). 10.1242/dev.165753
226. Ayaz D, Leyssen M, Koch M, Yan J, Srahna M, Sheeba V, Fogle KJ, Holmes TC, Hassan BA. Axonal injury and regeneration in the adult brain of Drosophila. J Neurosci. 2008;28(23):6010-21. 10.1523/JNEUROSCI.0101-08.2008
227. Vosshall LB, Amrein H, Morozov PS, Rzhetsky A, Axel R. A spatial map of olfactory receptor expression in the Drosophila antenna. Cell. 1999;96(5):725-36.
228. Kremer MC, Jung C, Batelli S, Rubin GM, Gaul U. The glia of the adult Drosophila nervous system. Glia. 2017;65(4):606-38. 10.1002/glia.23115
229. Wu B, Li J, Chou YH, Luginbuhl D, Luo L. Fibroblast growth factor signaling instructs ensheathing glia wrapping of Drosophila olfactory glomeruli. Proc Natl Acad Sci U S A. 2017;114(29):7505-12. 10.1073/pnas.1706533114
230. Dziembowska M, Wlodarczyk J. MMP9: a novel function in synaptic plasticity. Int J Biochem Cell Biol. 2012;44(5):709-13. 10.1016/j.biocel.2012.01.023
231. Dziembowska M, Milek J, Janusz A, Rejmak E, Romanowska E, Gorkiewicz T, Tiron A, Bramham CR, Kaczmarek L. Activity-dependent local translation of matrix metalloproteinase-9. J Neurosci. 2012;32(42):14538-47. 10.1523/JNEUROSCI.6028-11.2012

232. Tantale K, Mueller F, Kozulic-Pirher A, Lesne A, Victor JM, Robert MC, Capozi S, Chouaib R, Backer V, Mateos-Langerak J, Darzacq X, Zimmer C, Basyuk E, Bertrand E. A single-molecule view of transcription reveals convoys of RNA polymerases and multi-scale bursting. Nat Commun. 2016;7:12248. 10.1038/ncomms12248
233. Dermit M, Dodel M, Mardakheh FK. Methods for monitoring and measurement of protein translation in time and space. Mol Biosyst. 2017;13(12):2477-88. 10.1039/c7mb00476a
234. Biswas J, Liu Y, Singer RH, Wu B. Fluorescence Imaging Methods to Investigate Translation in Single Cells. Cold Spring Harb Perspect Biol. 2019;11(4). 10.1101/cshperspect.a032722
235. Martin KC, Ephrussi A. mRNA localization: gene expression in the spatial dimension. Cell. 2009;136(4):719-30. 10.1016/j.cell.2009.01.044
236. Pilaz LJ, Lennox AL, Rouanet JP, Silver DL. Dynamic mRNA Transport and Local Translation in Radial Glial Progenitors of the Developing Brain. Curr Biol. 2016;26(24):3383-92. 10.1016/j.cub.2016.10.040
237. Blanco-Urrejola M, Gaminde-Blasco A, Gamarra M, de la Cruz A, Vecino E, Alberdi E, Baleriola J. RNA Localization and Local Translation in Glia in Neurological and Neurodegenerative Diseases: Lessons from Neurons. Cells. 2021;10(3). 10.3390/cells10030632
238. Meservey LM, Topkar VV, Fu M-m. mRNA Transport and Local Translation in Glia. Trends in Cell Biology. 10.1016/j.tcb.2021.03.006
239. Akins MR, Berk-Rauch HE, Fallon JR. Presynaptic translation: stepping out of the postsynaptic shadow. Front Neural Circuits. 2009;3:17. 10.3389/neuro.04.017.2009
240. Kuklin EA, Alkins S, Bakthavachalu B, Genco MC, Sudhakaran I, Raghavan KV, Ramaswami M, Griffith LC. The Long 3'UTR mRNA of CaMKII Is Essential for Translation-Dependent Plasticity of Spontaneous Release in Drosophila melanogaster. J Neurosci. 2017;37(44):10554-66. 10.1523/JNEUROSCI.1313-17.2017
241. Rangaraju V, Tom Dieck S, Schuman EM. Local translation in neuronal compartments: how local is local? EMBO Rep. 2017;18(5):693-711. 10.15252/embr.201744045
242. Biever A, Donlin-Asp PG, Schuman EM. Local translation in neuronal processes. Curr Opin Neurobiol. 2019;57:141-8. 10.1016/j.conb.2019.02.008
243. Holt CE, Martin KC, Schuman EM. Local translation in neurons: visualization and function. Nat Struct Mol Biol. 2019;26(7):557-66. 10.1038/s41594-019-0263-5
244. Wang X, Proud CG. The mTOR pathway in the control of protein synthesis. Physiology (Bethesda). 2006;21:362-9. 10.1152/physiol.00024.2006

245. Team RS. R Studio: Integrated development for R. R Studio, PBC, Boston, MA2020.
246. Thurmond J, Goodman JL, Strelets VB, Attrill H, Gramates LS, Marygold SJ, Matthews BB, Millburn G, Antonazzo G, Trovisco V, Kaufman TC, Calvi BR, FlyBase C. FlyBase 2.0: the next generation. Nucleic Acids Res. 2019;47(D1):D759-D65. 10.1093/nar/gky1003
247. Choi HM, Calvert CR, Husain N, Huss D, Barsi JC, Deverman BE, Hunter RC, Kato M, Lee SM, Abelin AC, Rosenthal AZ, Akbari OS, Li Y, Hay BA, Sternberg PW, Patterson PH, Davidson EH, Mazmanian SK, Prober DA, van de Rijn M, Leadbetter JR, Newman DK, Readhead C, Bronner ME, Wold B, Lansford R, Sauka-Spengler T, Fraser SE, Pierce NA. Mapping a multiplexed zoo of mRNA expression. Development. 2016;143(19):3632-7. 10.1242/dev.140137
248. Lee T, Luo L. Mosaic analysis with a repressible cell marker for studies of gene function in neuronal morphogenesis. Neuron. 1999;22(3):451-61. 10.1016/s0896-6273(00)80701-1
249. Yao Y, Wu Y, Yin C, Ozawa R, Aigaki T, Wouda RR, Noordermeer JN, Fradkin LG, Hing H. Antagonistic roles of Wnt5 and the Drl receptor in patterning the Drosophila antennal lobe. Nat Neurosci. 2007;10(11):1423-32. 10.1038/nn1993
250. Uhlirova M, Bohmann D. JNK- and Fos-regulated Mmp1 expression cooperates with Ras to induce invasive tumors in Drosophila. EMBO J. 2006;25(22):5294-304. 10.1038/sj.emboj.7601401
251. Neher E, Sakaba T. Multiple roles of calcium ions in the regulation of neurotransmitter release. Neuron. 2008;59(6):861-72. 10.1016/j.neuron.2008.08.019
252. Voets T, Moser T, Lund PE, Chow RH, Geppert M, Sudhof TC, Neher E. Intracellular calcium dependence of large dense-core vesicle exocytosis in the absence of synaptotagmin I. Proc Natl Acad Sci U S A. 2001;98(20):11680-5. 10.1073/pnas.201398798
253. Dorsett CR, McGuire JL, DePasquale EA, Gardner AE, Floyd CL, McCullumsmith RE. Glutamate Neurotransmission in Rodent Models of Traumatic Brain Injury. J Neurotrauma. 2017;34(2):263-72. 10.1089/neu.2015.4373
254. Eroglu C, Barres BA. Regulation of synaptic connectivity by glia. Nature. 2010;468(7321):223-31. 10.1038/nature09612
255. Domercq M, Vazquez-Villoldo N, Matute C. Neurotransmitter signaling in the pathophysiology of microglia. Front Cell Neurosci. 2013;7:49. 10.3389/fncel.2013.00049
256. Raghunatha P, Vosoughi A, Kauppinen TM, Jackson MF. Microglial NMDA receptors drive pro-inflammatory responses via PARP-1/TRMP2 signaling. Glia. 2020;68(7):1421-34. 10.1002/glia.23790

257. Buhlman LM, Krishna G, Jones TB, Thomas TC. Drosophila as a model to explore secondary injury cascades after traumatic brain injury. Biomed Pharmacother. 2021;142:112079. 10.1016/j.biopha.2021.112079
258. Bateman JM, McNeill H. Temporal control of differentiation by the insulin receptor/tor pathway in Drosophila. Cell. 2004;119(1):87-96. 10.1016/j.cell.2004.08.028
259. Rambur A, Lours-Calet C, Beaudoin C, Bunay J, Vialat M, Mirouse V, Trousson A, Renaud Y, Lobaccaro JA, Baron S, Morel L, de Joussineau C. Sequential Ras/MAPK and PI3K/AKT/mTOR pathways recruitment drives basal extrusion in the prostate-like gland of Drosophila. Nat Commun. 2020;11(1):2300. 10.1038/s41467-020-16123-w
260. Dutriaux A, Godart A, Brachet A, Silber J. The insulin receptor is required for the development of the Drosophila peripheral nervous system. PLoS One. 2013;8(9):e71857. 10.1371/journal.pone.0071857
261. Klose MK, Bruchez MP, Deitcher DL, Levitan ES. Temporally and spatially partitioned neuropeptide release from individual clock neurons. Proc Natl Acad Sci U S A. 2021;118(17). 10.1073/pnas.2101818118
262. Bulgari D, Deitcher DL, Schmidt BF, Carpenter MA, Szent-Gyorgyi C, Bruchez MP, Levitan ES. Activity-evoked and spontaneous opening of synaptic fusion pores. Proc Natl Acad Sci U S A. 2019;116(34):17039-44. 10.1073/pnas.1905322116
263. Fernandopulle MS, Lippincott-Schwartz J, Ward ME. RNA transport and local translation in neurodevelopmental and neurodegenerative disease. Nat Neurosci. 2021;24(5):622-32. 10.1038/s41593-020-00785-2
264. Giorgi C, Moore MJ. The nuclear nurture and cytoplasmic nature of localized mRNPs. Semin Cell Dev Biol. 2007;18(2):186-93. 10.1016/j.semcdb.2007.01.002
265. Ainger K, Avossa D, Morgan F, Hill SJ, Barry C, Barbarese E, Carson JH. Transport and localization of exogenous myelin basic protein mRNA microinjected into oligodendrocytes. J Cell Biol. 1993;123(2):431-41. 10.1083/jcb.123.2.431
266. Kiebler MA, Hemraj I, Verkade P, Kohrmann M, Fortes P, Marion RM, Ortin J, Dotti CG. The mammalian staufen protein localizes to the somatodendritic domain of cultured hippocampal neurons: implications for its involvement in mRNA transport. J Neurosci. 1999;19(1):288-97.
267. Krichevsky AM, Kosik KS. Neuronal RNA granules: a link between RNA localization and stimulation-dependent translation. Neuron. 2001;32(4):683-96. 10.1016/s0896-6273(01)00508-6
268. Kanai Y, Dohmae N, Hirokawa N. Kinesin transports RNA: isolation and characterization of an RNA-transporting granule. Neuron. 2004;43(4):513-25. 10.1016/j.neuron.2004.07.022

269. Sapkota D, Kater. M.S.J., Sakers, K., Nygaard, K.R., Liu, Y., Lake, A.M., Khazanchi, R., Khankan, R.R., Smit, A.B., Maloney, S.E., Verheijen, M.H.G., Zhang, Y., Dougherty, J.D. Activity dependent translation in astrocytes dynamically alters the proteome of the perisynaptic astrocyte process. bioRxiv. 2021. https://doi.org/10.1101/2020.04.08.033027
270. Mickleburgh I, Burtle B, Hollas H, Campbell G, Chrzanowska-Lightowlers Z, Vedeler A, Hesketh J. Annexin A2 binds to the localization signal in the 3' untranslated region of c-myc mRNA. FEBS J. 2005;272(2):413-21. 10.1111/j.1742-4658.2004.04481.x
271. Liao YC, Fernandopulle MS, Wang G, Choi H, Hao L, Drerup CM, Patel R, Qamar S, Nixon-Abell J, Shen Y, Meadows W, Vendruscolo M, Knowles TPJ, Nelson M, Czekalska MA, Musteikyte G, Gachechiladze MA, Stephens CA, Pasolli HA, Forrest LR, St George-Hyslop P, Lippincott-Schwartz J, Ward ME. RNA Granules Hitchhike on Lysosomes for Long-Distance Transport, Using Annexin A11 as a Molecular Tether. Cell. 2019;179(1):147-64 e20. 10.1016/j.cell.2019.08.050
272. Martin I, Kim JW, Lee BD, Kang HC, Xu JC, Jia H, Stankowski J, Kim MS, Zhong J, Kumar M, Andrabi SA, Xiong Y, Dickson DW, Wszolek ZK, Pandey A, Dawson TM, Dawson VL. Ribosomal protein s15 phosphorylation mediates LRRK2 neurodegeneration in Parkinson's disease. Cell. 2014;157(2):472-85. 10.1016/j.cell.2014.01.064
273. Azzam ME, Algranati ID. Mechanism of puromycin action: fate of ribosomes after release of nascent protein chains from polysomes. Proc Natl Acad Sci U S A. 1973;70(12):3866-9. 10.1073/pnas.70.12.3866
274. Li J, Kim SG, Blenis J. Rapamycin: one drug, many effects. Cell Metab. 2014;19(3):373-9. 10.1016/j.cmet.2014.01.001
275. Ding K, Han Y, Seid TW, Buser C, Karigo T, Zhang S, Dickman DK, Anderson DJ. Imaging neuropeptide release at synapses with a genetically engineered reporter. Elife. 2019;8. 10.7554/eLife.46421
276. Gordon MD, Scott K. Motor control in a Drosophila taste circuit. Neuron. 2009;61(3):373-84. 10.1016/j.neuron.2008.12.033
277. Feinberg EH, Vanhoven MK, Bendesky A, Wang G, Fetter RD, Shen K, Bargmann CI. GFP Reconstitution Across Synaptic Partners (GRASP) defines cell contacts and synapses in living nervous systems. Neuron. 2008;57(3):353-63. 10.1016/j.neuron.2007.11.030
278. Macpherson LJ, Zaharieva EE, Kearney PJ, Alpert MH, Lin TY, Turan Z, Lee CH, Gallio M. Dynamic labelling of neural connections in multiple colours by trans-synaptic fluorescence complementation. Nat Commun. 2015;6:10024. 10.1038/ncomms10024

279. Kamiyama D, Sekine S, Barsi-Rhyne B, Hu J, Chen B, Gilbert LA, Ishikawa H, Leonetti MD, Marshall WF, Weissman JS, Huang B. Versatile protein tagging in cells with split fluorescent protein. Nat Commun. 2016;7:11046. 10.1038/ncomms11046
280. Harris KP, Littleton JT. Transmission, Development, and Plasticity of Synapses. Genetics. 2015;201(2):345-75. 10.1534/genetics.115.176529
281. Levitan ES, Lanni F, Shakiryanova D. In vivo imaging of vesicle motion and release at the Drosophila neuromuscular junction. Nat Protoc. 2007;2(5):1117-25. 10.1038/nprot.2007.142
282. Ramadurgum P, Hulleman JD. Protocol for Designing Small-Molecule-Regulated Destabilizing Domains for In Vitro Use. STAR Protoc. 2020;1(2). 10.1016/j.xpro.2020.100069
283. Banaszynski LA, Chen LC, Maynard-Smith LA, Ooi AG, Wandless TJ. A rapid, reversible, and tunable method to regulate protein function in living cells using synthetic small molecules. Cell. 2006;126(5):995-1004. 10.1016/j.cell.2006.07.025
284. Schuster CM, Davis GW, Fetter RD, Goodman CS. Genetic dissection of structural and functional components of synaptic plasticity. I. Fasciclin II controls synaptic stabilization and growth. Neuron. 1996;17(4):641-54. 10.1016/s0896-6273(00)80197-x